TEARING RESISTANCE FOR FILLET WELDS IN SHIPS EXPOSED TO GROUNDING - A FULL SCALE TEST & COST IMPLICATIONS

by

Kirko Dimitar Kirkov

B. Eng. Mechanical Engineering
University of Ottawa, Canada
(1989)

Submitted to the Department of Ocean Engineering
in partial fulfillment of the requirements
for the degrees of

MASTER OF SCIENCE
IN NAVAL ARCHITECTURE AND MARINE ENGINEERING

and

MASTER OF SCIENCE
IN OCEAN SYSTEMS MANAGEMENT

at the

MASSACHUSETTS INSTITUTE OF TECHNOLOGY ©MIT
May, 1994

Signature of Author_____
Department of Ocean Engineering
May, 1994

Certified by_____
Professor Henry Marcus
Department of Ocean Engineering, Thesis Reader

Certified by_____
Professor Frank A. McClintock
Department of Mechanical Engineering, Thesis Supervisor

Accepted by_____
Professor A. Douglas Carmichael
Department Graduate Committee, Department of Ocean Engineering

TEARING RESISTANCE FOR FILLET WELDS IN SHIPS EXPOSED TO GROUNDING - A FULL SCALE TEST & COST IMPLICATIONS

by

Kirko Dimitar Kirkov

Submitted to the Department of Ocean Engineering on May 6, 1994, in partial fulfillment of the requirements for the degrees of Master in Science of Naval Architecture and Marine Engineering and Master in Science of Ocean Systems Management

Abstract

Peeling failure of fillet welds joining shell plating to longitudinal stiffeners has been observed in some ship grounding accidents (including the *Exxon Valdez*). The peeling phenomenon is a previously unexplored avenue of ship research. In this mode of failure it is found out that limit load and tearing work per unit length are key criteria in the analysis process.

A simple model and test (the Transversely Welded Beam [TWB] test) are developed to describe the failure of a T-joint (as commonly encountered at the interface between shell plating and longitudinal stiffeners in ship bottom hull structures) when subjected to tensile tearing (tension along the vertical axis of the stiffener, orthogonal to the shell plating). After a review of the mechanics of deformation, crack initiation, and crack growth for fully plastic structures, limit loads as a function of bend angle are tabulated for welded T-joints under the loading expected in service. The tearing work is found to be important in preventing peeling of the shell plate from the stiffener in such joints. Although much larger welds (12mm weld leg length) than are in current use (6mm to 9mm leg length) would be required to prevent peeling by shifting deformation to the stiffener, it was determined that, if desired, the change can still be performed by single pass welding during (costs for a 250 000 dwt VLCC range from 30 000$ to 80 000$ in addition to existing total cost, these values are obtained from the Weldcostmdl spreadsheet developed in this paper).

Model data interpretation is based on the assumption of plane strain crack growth and a homogeneous hardness weld cross-section within the weld metal. The model is used to predict the limit load per unit length of weld (P_L), the critical steady state displacement for crack growth (u_c), and the critical tearing work (R_c) per unit length of the weld. Test results show good agreement (+/- 3% for limit load, and within the 0.4 to 1.1 mm range defined in existing literature for critical displacement) with the developed theory. The TWB test is a cost effective means for industry to test full-scale T-joint weld limit load and tearing work.

Thesis Supervisor: Frank A. McClintock
Title: Professor Emeritus

Acknowledgments

The support of several organizations is deeply appreciated: the Joint MIT-Industry Consortium on Tanker Safety, The Office of Naval Research, the MIT Departments of Aerospace Engineering, Ocean Engineering, and Mechanical Engineering.

Special acknowledgment is also made to past and present team members, Professor T. Wierzbicki for his leadership and encouragement, Professor F. McClintock for his guidance, patience, and tireless hours of support, Professor K. Masubuchi and Mr. A. T. Supple for essential help and patience during the long hours of testing.

The following individuals also deserve special consideration in view of their key contributions to the project: A. Guerra, H. A. McDonald, X.-D. Wang, R. A. Middaugh, S. Koga, M. D. Bracco, and P. E. Little.

Grateful thanks are also due to D. Sucharski and P. Lacey of ARCO marine, who arranged for the steel plate and its timely delivery

Table Of Contents

List of Figures

List of Tables

CHAPTER 1
INTRODUCTION

In March 1989 the grounding of the Exxon Valdez, with its resulting spillage of 11 million gallons of oil into Prince William sound renewed interest in the design of pollution-resistant tankers. In general, the damage resulting from a grounding involves various combinations of deformation, puncture, and tearing. Although it is certainly clear that such damage can never altogether be eliminated from grounding accidents, it is also agreed that better design of structures can allow improved performance (defined here as less leakage following a grounding).

Since the combination of damage mechanisms results in a most complex behavior of the structure (difficult to model), initial research was focused towards the study and modeling of simple parts of the process with the aim in this research group of finding possible improvements to the welded joints. Possible improvements (which must also be economically viable) are

1. weld geometry;
2. weld penetration;
3. weld overmatching;
4. resistance to cleavage fracture;
5. resistance to hole growth fracture;
6. resistance to fatigue.

The mechanism of interest in this project can best be termed as the peeling of fillet welds observed at the stiffener and shell plate interface (essentially vertical tearing separation of the stiffener from the shell plating, or vice versa). Separation of shell plating from stiffeners during a grounding opens large holes in the structure (similar to the peeling of a sardine can). This pattern has been observed on some damaged structures as a folding over of the shell plating beginning from the point of impact and running for a length along the longitudinal axis of the vessel. Under ideal circumstances, it would be desirable for these T-joints to remain intact (for the welds to hold) despite the resulting surrounding structural deformations and tearing. By remaining intact, the joints increase the localized severity of the damage but reduce the overall affected area and thus spillage.

Conventional analysis is based on the principle of equilibrium across a cross-section of the weld. It is not a lower bound to the limit load because of its failure to satisfy the equilibrium equations and the yield criterion everywhere and it is not an upper bound because it fails to provide a compatible displacement field (incompressible and compatible to the boundary condition). The study focuses on analysis of the peeling failure (tension along the cross-section of the joint in a direction parallel to the vertical axis of the stiffener web - orthogonal to the shell plate) and its mechanism as related to limit load and tearing work per unit length of the weld.

1.1 Need For a Test Quantifying Tearing Resistance (R)

Tearing resistance (R) is defined as the work per unit length necessary to induce fracture failure in the weld when the latter is subjected to web tension (along the vertical axis of the stiffener). Present joint designs do not take into account tearing failure of the joint under such tension. A need was thus identified to develop a quantitative test (full scale since the welding process does not scale) for the tearing resistance of typical T-joints. Tearing work per unit weld length R is a function of the limit load P_L and critical displacement for cracking u_c and is obtained after determination of these two factors. Determination of P_L and u_c provides a clear picture of the failure mechanism not only as function of loading but also of displacement.

A key design priority was to ensure that the test allow evaluation of full-scale welds in a laboratory sized environment with standard testing equipment (a 50 Ton load frame).

1.2. Scope of The Project

A test is proposed for measuring the limit load and tearing work of T-joints. Experimental results from the test are discussed and can be used to evaluate potential improvements in the design of joints. An analysis is also carried out on the economic feasibility (effects on capital cost of construction) of increasing weld leg length while still using single pass welding (increasing R). The discussion will focus primarily on weld geometry (leg length (d)). The analysis

assumes a homogeneous weld (Fig.1.1), confirmed by Middaugh (1994), with non-hardening material properties. This assumption was found to remain valid even for low penetration welds.

The reference weld geometry used for the study was that of a 6mm x 6mm fillet weld as found in smaller shell plate/stiffener T-joints in tankers (Fig.1.1). Results from tests with the smaller weld were then compared to results from specimen with a larger weld (9mm x 9mm).

1.3 Organization of the Paper

Chapter 2 discusses the design of the "bend" test and the Transversely Welded Beam (TWB) specimen. Detailed design calculations for Chapter 2 are found in Appendix A. Chapter 3, written as a self contained paper, develops the necessary theoretical background for interpretation of experimental results. The theoretical framework in Chapter 3 was developed by Professor F.A. McClintock (McClintock (1994)) and is presented in its entirety in Report #26 of the Joint M.I.T.-Industry Project on Tanker Safety. Appendix B contains the processed experimental data used to calculate the results presented in the chapter. The detailed theoretical framework for Chapter 3 is contained in Appendix E. Note that all experimental raw data is contained in a laboratory log book, the latter in the possession of Professor Frank A. McClintock M.I.T. Department of Mechanical Engineering. Chapter 4 provides a cost analysis based on the "Weldcostmdl" spreadsheet model. "Weldcostmodel" is a basic tool developed for the purpose of

obtaining rough estimates of increased capital costs associated with the use of larger welds (single pass). "Weldcostmdl" is contained in Appendix C. Conclusions are found in Chapter 5.

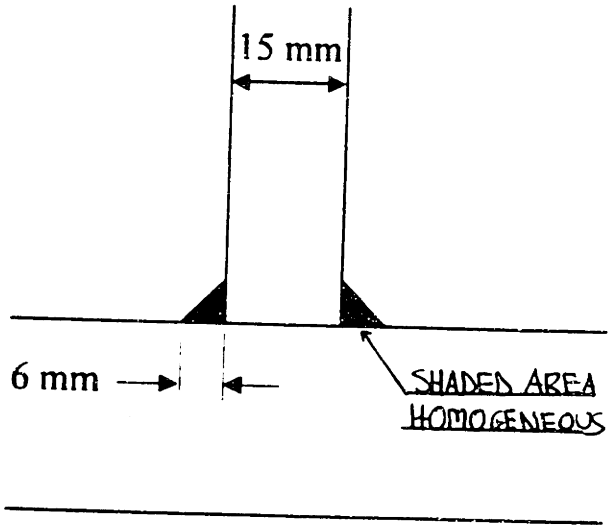

FIGURE 1.1 The Welded T-joint

CHAPTER 2

DESIGN AND SELECTION OF THE TEST RIG

The moment/curvature plot in Fig. 2.1 defines the critical considerations for the design of a suitable test specimen (these are discussed in detail in Chapter 3). Moreover, another key consideration is the stability of the test rig. Initial attempts at the design of a specimen where folding over of the shell plating would result in localized tearing at the weld required a large specimen (7 ft long and weighing approximately 350 lb). The large size of the specimen resulted in a calculated instability of the test due to the combined compliances of the specimen and the testing machine. Instability of the test occurs when compliance (the reciprocal $\left|dv/dP\right|$) of the load drop per unit specimen extension on crack growth, including arm deflection) of the welded section, exceeds compliance of the testing apparatus (load frame and associated test rig compliances - e.g. loading beams):

$$\left|\left(dv/dP\right)_{specimen}\right| \geq \left|\left(dv/dP\right)_{test.apparatus}\right| \tag{2.1}$$

An unstable test would result, upon initiation of the tearing, in uncontrolled (unstable) crack growth within the weld. A solution to the stability problem was proposed by McDonald (1994). In the proposed "beam" test consists of tensile tearing induced by the application of a bending moment to a beam containing a transverse T-joint (Fig. 2.2). The test is essentially a four point bending test

where tearing is induced on the tensile side. This specimen configuration offers two key advantages:

1. reduced size (because of no plastic deformation is induced outside of weld),

2. stability.

An analysis was carried out by the author to confirm the stability of the test. The resulting gross dimensions of the specimen obtained from the analysis pointed to an approximate length of 760 mm and a weight of 29 kg. The reduced size of the specimen also allowed use of conventional testing equipment (50 Ton MTS 410 Load Frame).

Rotation of the weld by an angle θ (Fig.2.3) causes displacement of the weld and cracking at the tensile extremity of the welded section.

2.1 Detailed Design of the Specimen

Having selected an acceptable configuration (TWB) for the specimen and its supporting rig (Fig.2.4), the following design details were then worked out (see Appendix A for relevant equations and calculations):

1. specimen configuration ,

- maximum weld dimensions (d) deformable by the test facility
- weight and scantlings
- materials
- supporting rig scantlings

2. sustainable design stresses for rig elements,

3. manufacturing details and considerations.

2.1.1. Test Rig Configuration

Figs. 2.5 depicts the specimen dimensions and geometry. Load was applied, from position up, to the specimen in the form of a displacement through the load cell to the load applying beam, in turn to the specimen through the point loading bearings, and finally to the load bearing beam. Hardened loading pads were fitted to eliminate local yielding at areas of high stress concentration (at the loading bearing contact points).

2.1.2. Configuration of the Specimen

Overall, eight specimens were manufactured with the weld parameters as indicated in table 2.1.

Specimen# 8 was poorly manufactured and was not used in the tests. Specimen# 2 models a defective weld where the leg length on the tensile stress side (9mm) is longer than that on the side

subjected to shear stress (6mm). Fig.2.6 illustrates the various weld geometries used for the tests.

Testing the 6x6mm welds was the primary objective. Four specimens were tested with this weld geometry. The four tests provided good data correlation and sufficient data points for processing of the information. For the 9x9mm weld, a narrower specimen with shorter weld length L was tested (weld length of 89mm versus 163 mm). L was reduced because the 50 Ton load frame capacity was not adequate to initiate fracture in the weld at a length of 163 mm. All eight specimen were welded using the GMAW process with E7016 electrodes.

2.1.3. Conclusions

The design calculations contained in Appendix A provided useful predictions for the performance of the specimen in the actual tests (stability). These calculations were performed using a low value of elastic modulus (E = 214,000 N/mm^2). A low value was used to be sure of accommodating the deflection and its effect on stability. Furthermore, the modulus (E) could not be obtained for the E7016 electrode and KA 36 steel at the time of design. A tensile strength range of 467-691 N/mm^2 was used for the electrode since the tensile strength of a weldment can vary within the range depending on the quality of the welding performed (size of the weld & welding speed).

Experimental results (to be discussed in Chapter 3) confirmed the validity of the calculations performed during the design stage.

Specimen	Size of Weld (mm)	Length of Weld (mm)
1	6x6	163
2	6x9	163
3	9x9	89
4	9x9	89
5	6x6	163
6	6x6	163
7	6x6	163
8	6x6	163

TABLE 2.1 Specimen Weld Characteristics

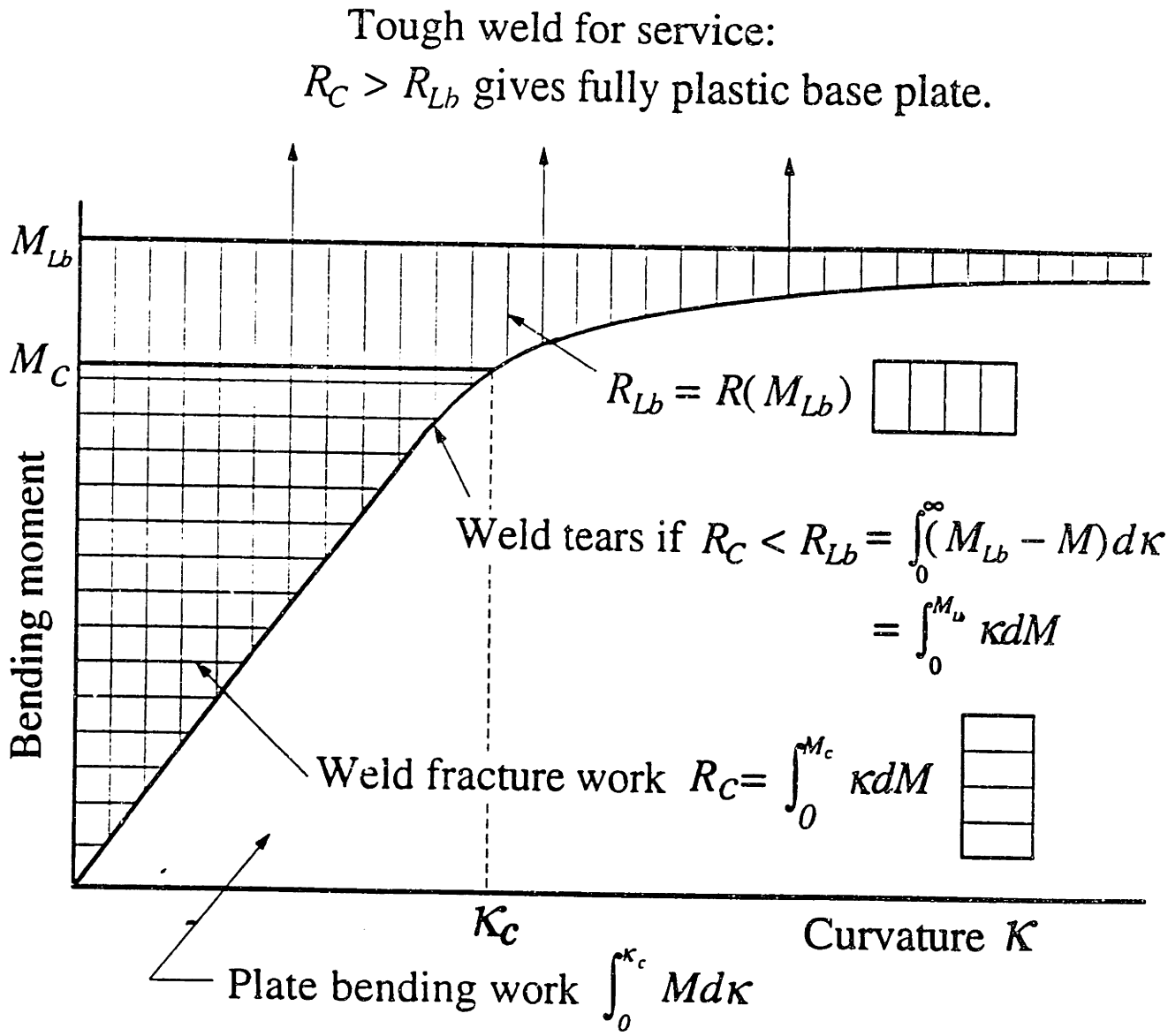

Finding the critical tearing work R_c needed to prevent a base plate from simply peeling off the stringers.

FIGURE 2.1 Moment-Curvature Relation, (McClintock (1994))

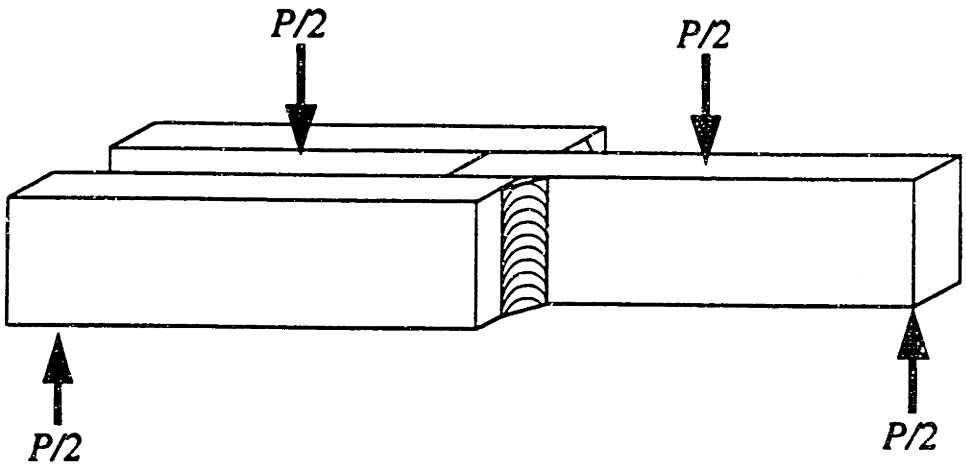

FIGURE 2.2 "TWB" Specimen

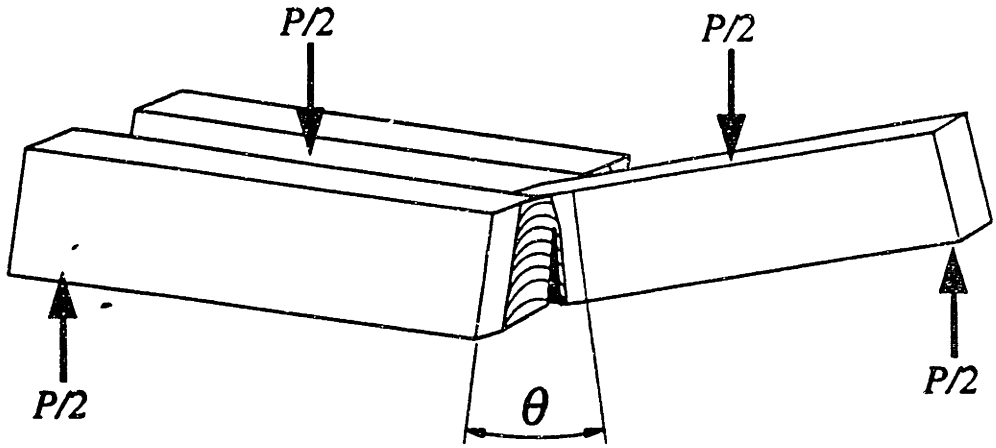

FIGURE 2.3 "TWB" Bending

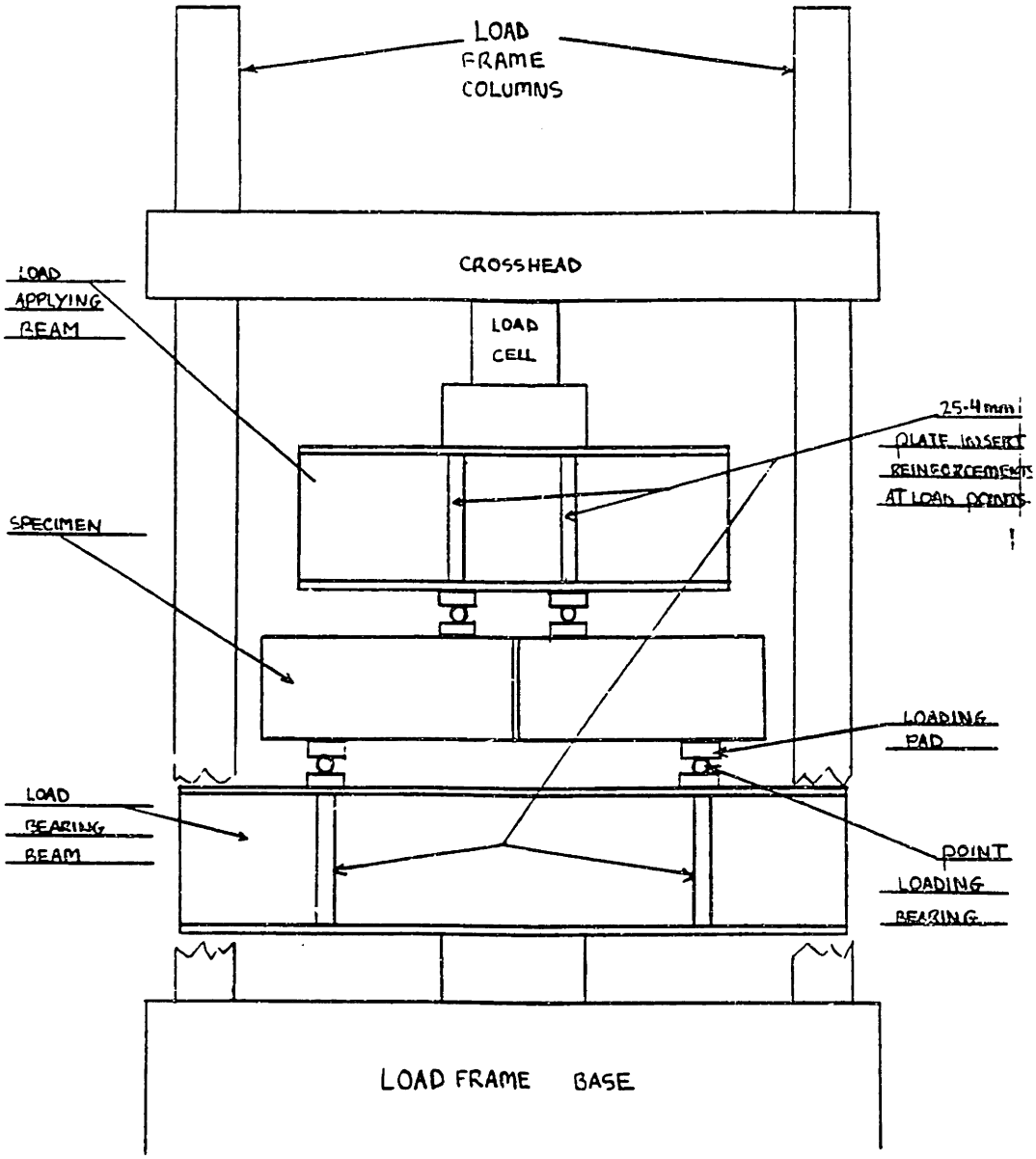

FIGURE 2.4 "TWB" Test Rig

Specimen Configuration

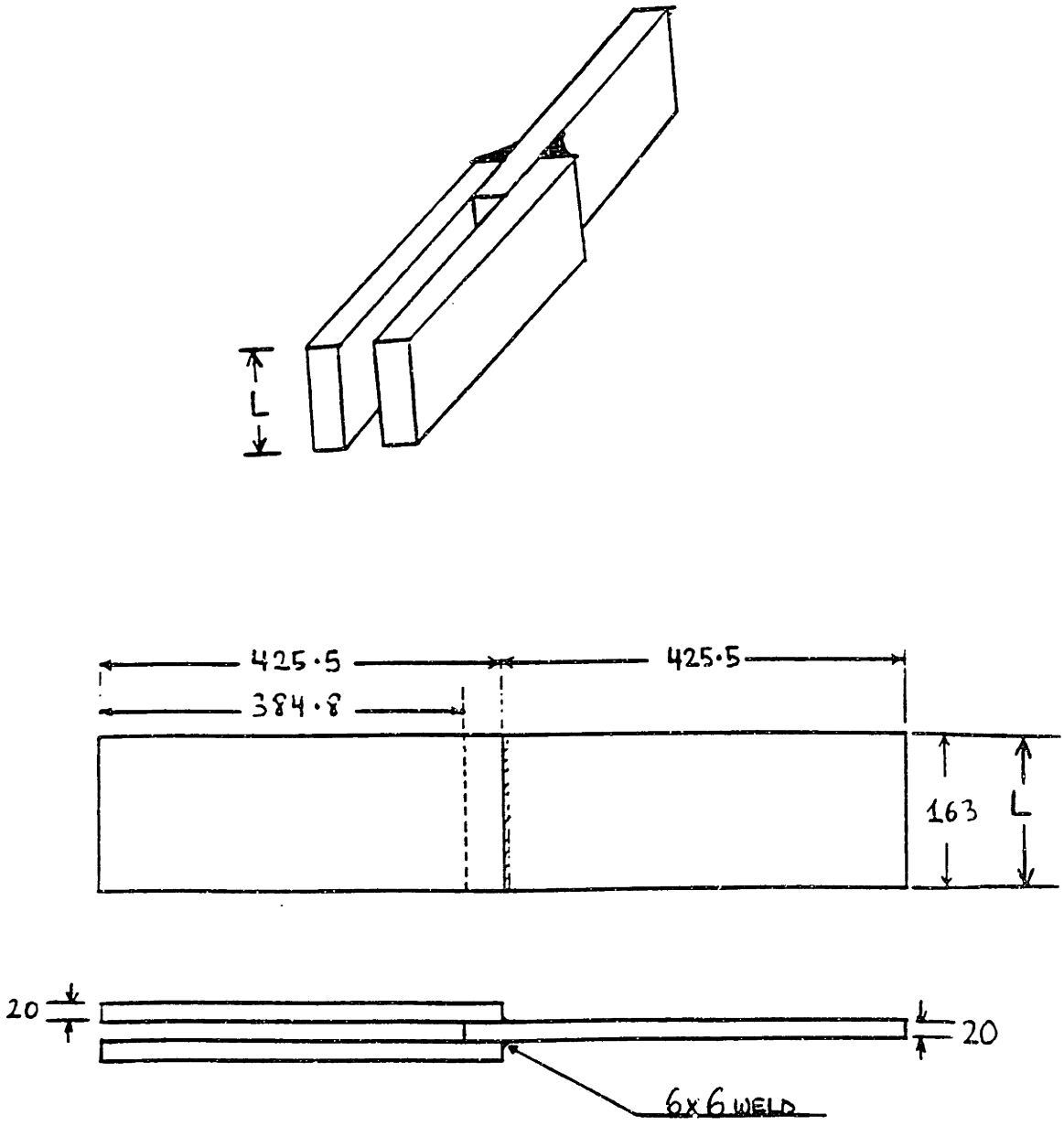

Note: 1. Tolerances: +/- 0.4 mm
2. For 9 mm x 9 mm , L = 89 mm
3. All dimensions in mm

FIGURE 2.5 Specimen Configuration

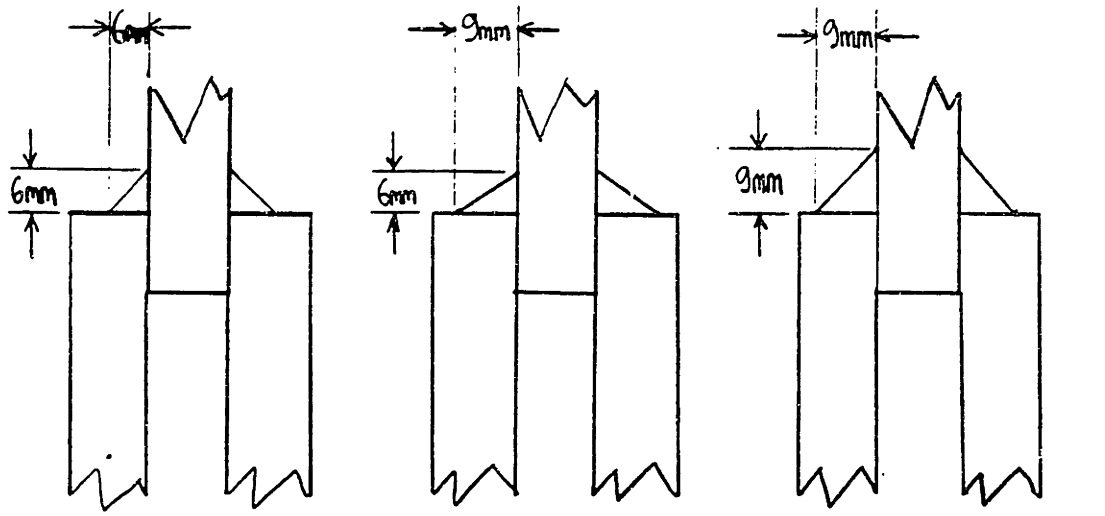

FIGURE 2.6 Specimen Weld Geometries

CHAPTER 3

A "BEND" TEST FOR TENSILE TEARING RESISTANCE OF TRANSVERSELY WELDED T-JOINTS, THE "TWB" TEST

by Kirk D. Kirkov

ABSTRACT

A simple model and test (Transversely Welded Beam [TWB] test) are developed to describe the failure of a T-joint when subjected to peeling (modeled by four point bending of the TWB specimen). Bending of the beam results in localized tensile tearing at the transverse weld (tension along the vertical axis of the longitudinal stiffener, orthogonal to the plane of the shell plating in a ship application). A review of the mechanics of deformation, crack initiation, and crack growth is given for fully plastic structures. Limit loads for welded T-joints under tensile loading during grounding were predicted within an absolute range of 3% of estimated values. The tearing work is found to be important in preventing peeling of the shell plate from the stiffener in such joints. In situations where it is desired to transfer deformation from the weld to the stiffener web limit load becomes the critical criterion. Interpretation of data is based on the assumption of plane strain crack growth and a homogeneous hardness weld cross-section. The critical steady state displacement for crack growth (experimentally determined to range from 0.72mm-0.78mm) shows good correlation with the developed theory (range for various steels from 0.4mm-1.1mm).

3.1 Introduction

In March 1989 the grounding of the Exxon Valdez, with its resulting spillage of 11 million gallons of oil into Prince William sound and the subsequent passage of OPA 90 renewed interest in the design of pollution-resistant tankers around the world In general, the damage resulting from a grounding involves various combinations of deformation, puncture, and tearing. Although it is certainly clear that such damage can never altogether be eliminated from grounding accidents, it is also agreed that better design of structures can allow improved performance (defined here as less leakage following a grounding). In general when designing welded structures, it is desired in the case of structural failure that the general surrounding and not the weld fail by plastic deformation under both normal and accidental service.

Since the combination of damage mechanisms results in a behavior of the structure that is very difficult to model, initial research was focused towards the study and modeling of simple parts of the process.

The mechanism of interest here is the peeling of fillet welds at the stiffener and shell plate interface (Fig.3.1). During a grounding, this mechanism can open large holes in the structure (similar to the peeling of a sardine can). This pattern has been observed on some ships as a folding over of the shell plating beginning from the point of impact and running longitudinally. Under ideal circumstances, it would be desirable for these T-joints to remain intact increasing the

forces and the localized severity of the damage but reducing the torn length and thus spillage.

The proposed test of full-scale welds serves the following purposes:

1. Provides industry with a means of testing full-scale T-joint welds under web tension by bending a beam with a transversely welded T-joint at its center. The results give limit load per unit weld length (P_L), tearing work per unit weld length (R), and critical displacement for steady state weld cracking (u_{css}).

2. Test possible improvements in weld design.

A key design priority was to ensure that the test allow evaluation of full-scale welds in a laboratory sized environment with standard testing equipment (50 Ton load frame). Tearing resistance R is defined as the work per unit weld length necessary to induce fracture in a weld under web tension. It will be shown later that the transition from plate bending to weld tearing depends on the tearing work per unit length R. Present joint design procedures do not take R into account. R must be measured in full scale welds since the welding process does not scale. Tearing resistance R is a function of the limit load P_L and critical displacement for cracking u_c. This priority was defined to provide industry with an economically viable means of testing full scale T-joints.

3.2 Analysis of the Limit Loads

Limit load analysis is a critical component in the evaluation of T-joint performance (besides tearing work per unit length) because the limit load variation between the stiffener web and the weld can shift deformation from the weld to the stiffener (when weld limit load is greater than web limit load) avoiding peeling at the weld. Conventional analysis is based on equilibrium accross a cross-section and does not quantify accurately limit load. It is not a lower bound to the limit load because it fails to satisfy the equilibrium equations and the yield criterion everywhere and it is not an upper bound because it fails to provide a compatible displacement field (incompressible and compatible to the boundary conditions).

3.2.1 Assumptions

The discussion will focus primarily on leg length (d). It will furthermore focus on 45° angle welds. The driving assumption (confirmed by hardness tests, Middaugh (1994) is that the weld material (Fig.3.2) is relatively homogeneous. The steels used by the ship industry are usually ductile enough so that the accompanying plastic deformation is large compared to the elastic. We therefore consider the fracture mechanics of regions in which the elastic strains are negligible. Furthermore, we consider non-hardening plasticity as a useful, approximate limiting case, in which the changes in strength due to various amounts of deformation can be neglected.

3.2.2 Concept of the Limit Load and Exact Solutions

As shown schematically in Fig.3.3, the force deformation curve of a non-hardening plastic structure rises steeply in the elastic region and is nearly constant in the plastic region before falling off due to either thinning down, or cracking. The load for nearly constant force is called the limit load P_L. An exact solution for the limit load involves satisfying the following five conditions of mechanics (McClintock (1994)):

i) the partial differentiation equations for equilibrium with stress gradients,

ii) the definitions of components of strain in terms of displacement gradients,

iii) boundary conditions in terms of displacements or tractions (boundary forces per unit surface area).

iv) a yield locus which limits the magnitudes of the stress components,

v) linear functions relating only the increments of strain components to the currents stress components (not the total strain components to the current stress components, as in elasticity).

The exact solutions for plane strain with negligible elasticity and strain-hardening are best expressed in terms of possibly curved lines parallel to the two directions of maximum shear stress at a point. For tension on the web of a homogeneous 45° fillet-welded T-joint, these lines turn out to be just two sets of parallel straight lines meeting the surface at 45°, as shown in Fig.3.4a. Plane strain, incompressibility and Mohr's Circle mean that the normal components of strain along the slip lines are zero (the slip lines are inextensible), and the deformation along a slip line is pure shear.

3.2.3 Upper Bounds Concept

Fortunately, bounds to the limit load can be found by satisfying only certain of the five conditions for non-hardening homogeneous materials. If the bounds are close enough together for practical purposes, an exact solution need not be found. Roughly, lower bounds to the limit load are found from equilibrium, yield, and stress boundary conditions; upper bounds from the plastic work of incompressible displacement fields satisfying any displacement boundary conditions. Specifically, a lower bound to the limit load is given by any stress distribution which

a) satisfies any stress boundary condition,

b) everywhere satisfies the equilibrium equations for stress gradients, and

c) nowhere violates the yield criterion.

An upper bound to the limit load is given by a load for which a complete field of displacement increments $u_i(x_j)$ can be found such that it

a) satisfies any displacement boundary conditions,

b) gives no change in volume anywhere, and

c) gives an integral of the plastic work increment throughout the body that is the upper bound P_{ub} times the corresponding displacement increment in the direction of the load, u_p:

$$Pu_p \le P_{ub}u_p = W^p = \int_V Y\bar{\varepsilon}^p dV \qquad (3.1)$$

The deformation field that goes with the slip lines of Fig.3.4a is just a shear displacement discontinuity between the plate and the web, leading to the new web position and the slip line field of Fig.3.4b. A thorough discussion on crack initiation will not be presented here but is discussed in reference to this work by McClintock (1994) using the J integral technique where J can be interpreted as an energy release rate and is also related to crack tip opening displacement, CTOD).

3.2.4 Upper Bound for Weld Tension

Of specific interest to this project is the limit load of welded T-joints in tension (for homogeneous welds). As discussed in the introduction, for 45° welds, the limit load per unit length P_L is given in terms of the minimum leg length d and the shear strength of the weld k by

$$P_L = 2kd \tag{3.2}$$

For welds where the weld angles are other than 45°, P_L can be approximated by (Appendix D)

$$P_L = \frac{k}{\sin(\theta_{ab}-\theta_{bc})}\left(\frac{L_2\cos(\theta_{bc})}{\left[\left(\frac{L_2}{L_1}\right)\sin(\theta_{ab})+\cos(\theta_{ab})\right]}+\frac{L_1\cos(\theta_{ab})}{\left[\left(\frac{L_1}{L_2}\right)\cos(\theta_{bc})+\sin(\theta_{bc})\right]}\right). \tag{3.3}$$

Approximation using equation 3.2 turns out to be good to ±3%.

3.2.5 Upper Bound for Stiffener

When the limit load of the weld is greater than that of the web, deformation is shifted to the web inducing more work per unit length, a more desirable scenario when dealing with tearing. The limit load of the weld per unit length is to be compared to the upper bound for stiffener web tension, which is $P_{L,W}=2k_W t_W$ (k_W is web shear strength and t_W is web thickness). Consequently, to transfer

deformation from the weld to the web (as is desirable) when the shear strengths are comparable, requires a weld leg length d that is comparable to the web thickness (Nakamura (1994)). In general practice, this criterion is not observed (since tearing is not usually part of the design consideration) and weld tearing is a definite possibility.

3.2.6 Concept of Tearing Work

Consider the control volume of Fig.3.5, including the tearing zone and enough material either side such that the region is in steady state, with a critical bending moment M_C applied at the output resulting in a critical curvature κ_C there (The moment is opposed by shear forces on the ends of the web which perform no work and are not shown). Consider an element of motion δL of the material in the control volume. As it comes out, its slope changes by an angle $\delta\theta = \kappa_C \delta L$. The moment then does work $M_C \delta\theta = M_C \kappa_C \delta L$. By the principle of virtual work for bodies in equilibrium, this applied work will be the integral of the work per unit volume throughout the body. In steady state, that work will be just that on an element δL to take it from its initial unbent state to its final bent and separated state. If the plate is thick enough to not be pulled up locally near the weld, there will be little interaction between the work to bend the plate and that to tear the weld. The total work is then the sum of the works to bend the plate and to tear the weld:

Total work = Plate bending work + Weld tearing work,

$$M_c\kappa_c\delta L = \left(\int_0^{\kappa_c} M d\kappa\right)\delta L + R_c\delta L \therefore M_c\kappa_c = \int_0^{\kappa_c} M d\kappa + R_c \quad . \tag{3.4}$$

Integration by parts then gives the weld tearing work as the complementary plate bending work up to the critical moment as shown in Fig. 3.6:

$$R_c = M_c\kappa_c - \int_0^{\kappa_c} M d\kappa = \int_0^{M_c} \kappa dM \tag{3.5}$$

As shown in Fig.3.6, the complementary work of plate bending is limited by the limit moment of the base plate, M_{Lb}. If the weld tearing work is greater than that limit, denoted R_{Lb}, the weld will not tear and the whole structure will have to be deformed. For a typical application, with a ship plate having the following characteristics

$k_b = TS/\sqrt{3} = 327$ N/mm^2	shear strength of the base plate,
$E = 207\ 000$ N/mm^2	modulus of elasticity,
$\upsilon = 0.3$	Poisson's ratio,
$t_b = 20$ mm	thickness, and
$b_b = 2000$ mm	breadth of plate per stiffener.

and R_{Lb} given by

$$R_{Lb} = 2b_bt_bk_b^2(1-(\upsilon)^2)/E = 37{,}520 \text{ N mm/mm.} \tag{3.6}$$

Tearing work of the weld R_c, without cracking

In existing joint designs R_{Lb} often turns out to be more than R_c. If there were no fracture, the limit load of the weld shown in Fig.3.3 would fall off linearly to zero as the weld sheared off from the web. In such an ideal case, the critical tearing work would be the limit load times half the leg length; for a weld with the limit load per unit length $P_L = 2kd$ the tearing work per unit length would be

$$R_c \text{ ideal} = (2kd)(d/2). \tag{3.7}$$

Weld peeling off can occur far more easily with crack growth in the weld since the effective length of the weld is reduced as the crack progresses. The case is considered next.

Tearing work with cracking

Assume as in Fig.3.3 that the force displacement relation for a joint can be approximated by being constant at the limit load P_L until the a crack is initiated at the displacement u_i, after which it falls off linearly to zero at the displacement u_f. The fracture work per unit length (the "tearing resistance") R_c is then

$$R_c = P_L(u_i + u_f)/2 = P_L u_c, \tag{3.8}$$

where u_c is defined as an effective critical displacement.

Measurement of tearing work from other tests

Data is available for cracking, but without the constraint that is imposed by a symmetrical T-joint. Kardomateas and McClintock (1987) ran tests on six structural alloys with tensile to yield ratios of 1.2 to 1.5 and strain hardening exponents from 0.12 to 0.23. These experiments demonstrated that the critical displacement u_c might lie in the range of 0.4 to 1.1 mm for cross sections of similar size but varying materials (note that this range is partially due to the varying scaling effects of metallurgical structure and gap size of the various materials used). From (3.7) the tearing work will then be (for k = 467 N/mm^2 , for the E7016 electrode used in the TWB test) ranging from 2240 to 7850 N. From (3.8), the tearing work is a function of the limit load P_L , the initiation displacement u_i, and the growth displacement $u_f - u_i$. The limit load should increase linearly with size. The initiation displacement for a given metallurgical state and gap size should be independent of the leg length of the weld. The growth displacement should increase linearly with size, again for the same metallurgical state. Therefore since the initiation and growth displacements add to form the critical displacement u_c, and are of comparable magnitude, neither u_c nor $R_c = P_L u_c$ will follow any simple scaling law. Tests on full-scale welds are thus needed, hence the "TWB" test.

3.3 Determining Limit Load and Tearing Work from the "TWB" test

Prior to selection of the "TWB" specimen several other designs were considered. In some cases the specimen size required would have been too large to conveniently handle (specimen involving actual bending of the base plate, these were also stability limited) whereas in other cases the load required to initiate failure would have exceeded the capability of testing equipment available (limit load limited). A beam specimen was designed such as to allow convenient handling , stable tests, and a reasonable limit load. Stability and limit load considerations were such as to allow testing on a standard 50 ton load frame. The beam specimen, as shown in Fig. 3.7a, is transversely welded along the centerline giving a displacement gradient along the weld when the beam is subjected to a bending moment. Although the configuration used in Fig.3.7b was used for the experiment (transverse lap joints simulating the T-joint), we now recommend back to back T-welds with one pair larger to ensure yielding and cracking in the other.

3.3.1 Analysis of Experimental Calculations

The analysis for the limit load per unit weld length P_L in terms of the moment-bend angle (M-θ) data and the critical displacement is given in Appendix B and summarized here. The limit moment M_L of the uncracked weld is related to P_L by

$$M_L = P_L (L^2/4). \tag{3.9}$$

The next step is to relate the (M-θ) data from the test to a load displacement curve as the crack grows through the weld. Figs.3.8 and 3.9 illustrate the M-θ curves for the two principal categories of specimen tested (6mm and 9mm leg length). The displacement across the weld (u) is related to the bend angle of the beam (θ) and to the distance from the neutral axis (L/2) by simple geometry as follows:

$$\theta = u \Big/ \left(\frac{L}{2}\right). \tag{3.10a}$$

In principle, the displacement to initial growth of a through-crack could be obtained from the beginning of the drop in the moment-θ relation of the beam. However the displacement to initiate the growth of a through-crack will not be the same as that to propagate a through-crack past a given point along the weld because of metallurgical, geometrical, and weld bead effects. Instead, the quasi steady through-crack growth along the weld must be studied from the falling M-θ relation. It is shown in Appendix B that if the limit load per unit length of the weld is assumed to drop abruptly to zero at the displacement u_c, the bend angle is related to an initial end-effect (θ_0), the ratio of the cracked to uncracked moment M/M_L, and an effective critical angle $\theta_{c\ eff}$ by

$$\theta = \theta_0 + \theta_{c.eff} \Big/ \left(M/M_L\right)., \text{ where } \theta_{c.eff} = u_c \Big/ \left(\frac{L}{2}\right). \tag{3.10}$$

where u_C is related to R_C as per equation 3.8.

The value of ($\theta_{C\ eff}$) can be found graphically from the slope of the linear region in a plot of $1/(M/M_L)$ vs. θ as in Fig.3.8. From this u_C and R_C are then extracted. Note that although stability was not explicitly discussed, it was a key criterion in the design of the TWB specimen. Appendix A provides the detailed stability analysis.

3.3.2 Interpretation of Tests Results

General specifications for the specimen and test rig (illustrated in Fig.3.10) are given in Table 3.1. The seven specimen and three weld geometries tested are listed in Table 3.2. Note that the 9X9mm specimens had a shorter weld length L (to keep the test load within the loading capacity of the MTS410 load frame). It is desirable to maximize specimen weld length to minimize end effects.

Loading of the specimen was displacement driven at a crosshead displacement rate of $6.0x10^3$ (6000 seconds to achieve a full piston displacement of 0.5 inch). Data included load and crosshead displacement combined with readings of displacement accross the weld (taken at progressive loads as the experiment advanced). The maximum load sustained by individual specimen is denoted as P_{max} . The limit moment M_L was then evaluated by

$$M_L = (P_{max}/2)L_a, \tag{3.11}$$

where L_a is the moment arm. A data table with M, M_L, and Theta for each reading in the test was then compiled (Appendix B). The limit load $P_{L(test)}$ was then obtained for the test using M_L (from above) and L (the length of the weld) as follows:

$$P_{L(test)} = M_L \ (4/L^2) \tag{3.12}$$

A plot of M/M_L (recall equation 3.10) was then plotted as a function of θ for each set of data points. The reciprocal M_L/M, was then also plotted on the same graph (as shown in Fig.3.8). Recall that the weld displacements yielded θ (Fig.3.11). A rough curve fit was then applied to the data points and θ_{ceff} and θ_{co} extracted from the plot as shown in Fig.3.8. The critical displacement at steady state u_{css} was then obtained through its geometric relationship to $\theta_{c\ eff}$;

$$\theta_{c.eff}\left(\frac{L}{2}\right) = u_{css} \tag{3.13}$$

Recall, as above, that u_{css} is defined as the critical displacement to maintain steady state cracking as opposed to (for instance in fig.3.9) $u_{co} = (\theta_{co})(L/2)$ which is the critical displacement at start (on the tensile side of the specimen) to initiate cracking. u_{co} is subject to end effects specific to the configuration of the specimen and are thus not relevant to the steady state analysis.

The tearing work per unit length $R_{(test)}$ is then obtained by

$$R_{(test)} = P_{L(test)} u_{css} \tag{3.14}$$

where $u_{css} = u_i + \left(\frac{u_f - u_i}{2}\right)$,

and $u_f - u_i = \left(\frac{da}{du}\right) \times d$,

where $\frac{da}{du}$ is crack growth per unit displacement from Kardomateas (1987), and d is leg length.

The critical displacement u_C, limit load P_L, and tearing resistance R for the 6x6 mm, 9X6 mm, and 9x9 mm weld tests are displayed in Tables 3.3, 3.4, and 3.5 respectively. Ideal and test limit loads differ by ±3%. The critical displacements obtained (u_{CSS}) range from 0.44 to 0.78 mm and compare surprisingly well (in view of differences in material and boundary conditions) with results obtained by Kardomateas and McClintock (1987) predicting displacements ranging from 0.4 to 1.1 mm. Note that the 6X6 mm and 9X9 mm welds show average critical displacements of 0.72 and 0.78 mm respectively while the 6X9 mm weld indicates a much lower limit of 0.44 mm. Although only one specimen was tested with this weld configuration (30° weld angle), the result indicates a more brittle weld (which was confirmed by the appearance of the fracture). Similarly poor welds with angles lower than 45° have been reported from industry.

Tearing resistance for the symmetric welds (6X6 and 9X9 mm) showed a directly proportional increase with increased weld leg length ($R_{(test)}$=4187 N on average for 6mm leg length and 6476 N on average for the 9mm leg length). Note that test tearing resistance $R_{(test)}$ and ideal tearing resistance $R_{(ideal)}$ differ by a factor of approximately 10. This is a direct consequence of the idealization

used defining "ideal" critical displacement as the weld leg length d. Although demonstrating a limit load similar to that of the 6X6 mm weld, the 6X9 mm weld exhibited distinctly inferior tearing resistance (because of low critical displacement to fracture). Table 3.6 provides a summary of experimental results for the three weld configurations tested.

Critical displacement also scales with increased leg length but not proportionally. Average critical displacement for the 6 mm weld was 0.72mm while the average critical displacement for the 9mm weld was 0.78mm. The critical displacement noted for the asymmetric weld was 0.44mm.

3.4 Effects of Weld Penetration

The effects of weld penetration were not tested during the series of tests. In general, the limit load will rise (McClintock (94)), but at the expense of increased normal stress on the slip line at the end of the crack tip. This reduces the ductility of the weld. Furthermore, depending on the ratio of weld leg length d to web thickness t, and on hardness distribution in the weld region, a change-over from weld to web deformation will occur at some critical value of gap half-length a.

3.5 Conclusions

1. The tearing of T-joints in tension (peeling) is sometimes observed in grounding of ships.

2. Predicting peeling requires knowledge of tearing work per unit length R and limit load P_L. R is the product of the limit load per unit length (P_L) times the critical steady state displacement (u_{css}).

3. A new type of laboratory-scale test of full-scale welds is presented for finding P_L and u_c or R_c, for quality control, and for testing design changes. A bend test (TWB test) on a beam with a transversely welded T-joint has been used to find limit loads and critical tearing work per unit length, R_c, under web tension. With sectioning of partially cracked specimens, this test can provide the critical displacement for crack initiation and growth in the weld.

4. The utility of upper bound limit load analysis is confirmed by consistency of test data with theoretical predictions (±3% for limit load P_L). The slip line also confirms that weld angles of 45° give the most limit load per unit weld length. With typical weld dimensions, the peeling of the base plate from the web can occur.

5. Scaling laws vary. Limit load scales with weld leg length (d). Critical steady state displacement u_{css} (=$(u_f+u_i)/2$) is the sum of displacements for crack initiation (u_i) and growth (u_f-u_i). u_i probably depends only on metallurgical structure and gap size whereas (u_f-u_i) scales with leg length.

6. Peeling can be prevented if the welds are strong enough so that either

a) the base plate will go fully plastic before it can supply the critical tearing work per unit length to the weld, or
b) deformation due to web tension in the joint is shifted to the web, greatly increasing the tearing work per unit length.

7. For typical structures, strengthening the weld would first shift deformation to the web. Strengthening by increasing the size of the fillet weld seems to be less practical than slightly increasing the penetration (in spite of a small decrease in the weld tearing work per unit length).

Acknowledgments

The support of several organizations is deeply appreciated: the Joint MIT-Industry Consortium on Tanker Safety, The Office of Naval Research, the MIT Departments of Aerospace Engineering, Ocean Engineering, and Mechanical Engineering.

Special acknowledgment is also made to past and present team members, Professor T. Wierzbicki for his leadership and encouragement, Professor F. McClintock for his guidance, patience, and tireless hours of support, Professor K. Masubuchi and Mr. A. T. Supple for essential help and patience during the long hours of testing.

The following individuals also deserve special consideration in view of their key contributions to the project: A. Guerra, H. A.

McDonald, X.-D. Wang, R. A. Middaugh, S. Koga, M. D. Bracco, and P. E. Little.

Grateful thanks are also due to D. Sucharski and P. Lacey of ARCO marine, who arranged for the steel plate and its timely delivery

Specimen & Test Rig Specifications

1. Load Applying Beam (I-Beam)

- Depth 254 mm
- Flange 118 mm
- Section Area 4760 mm^2
- Weight 38 Kg/m
- Moment of Inertia $5.1x10^7$ mm^4
- Length 762 mm
- 20 mm thick inserts located 102 mm either side of centerline
- Material - Structural Steel

2. Load Bearing Beam (I-Beam)

- Same general specifications as Load Applying Beam
- Length 1143 mm
- 20 mm thick inserts located 324 mm either side of centerline

3. Specimen

- Base Plate, LR-EH36, YP 40.6 Kg/mm^2, TS 57.4 Kg/mm^2
- Thickness 20 mm
- Dimensions (see sketch)
- Weldment E7016 (Low Hydrogen) electrode

4. Loading Rollers (4)

- Diameter 38 mm
- Length 64 mm
- Hardened to Rockwell C 60

5. Loading Pads (8)

- A-2 Steel , Heat Treated to Rockwell C 60
- Dimensions, (64 mm x 64 mm x 25 mm)

TABLE 3.1 General Test Rig Specifications

Specimen	Size of Weld (mm)	Length of Weld (mm)
1	6x6	163
2	6x9	163
3	9x9	89
4	9x9	89
5	6x6	163
6	6x6	163
7	6x6	163
8	6x6	163

TABLE 3.2 Specimen Weld Characteristics

Critical Displacement (u_c), Limit Loads(P_L) , & Tearing Resistance (R) For Through Cracking of T-Joints (6 mm x 6 mm weld)

Test #	Limit Load (Test)	Limit Load (Ideal)	Critical Displ.			Tearing Resist. (Test)	Tearing Resist. (Ideal)
			At Start	Steady (Test)	State (Litrt.)		
	$P_{L(test)}$ (N/mm)	$P_{L(ideal)}$ (N/mm)	u_{co} (mm)	u_{css} (mm)	$u_{css(lit)}$ (mm)	$R_{(test)}$ (N.mm/mm)	$R_{(ideal)}$ (N.mm/mm)
1	5625	5598	1.3	0.70	0.4-1.1	3938	33590
2	5655	5598	0.8	0.80	0.4-1.1	4524	33590
4	6000	5598	0.8	0.70	0.4-1.1	4200	33590
6	5835	5598	1.1	0.70	0.4-1.1	4085	33590
	Avg 5779		Avg 1.0	Avg 0.72		Avg 4187	

Where: $P_{L(ideal)} = 2Kd$

$K = 0.75\ TS$

d = weld leg length (6mm)

$P_{L(test)} = M_L(4/L^2)$

M_L = limit moment (from test)

L = weld length

$R_{(ideal)} = P_{L(ideal)}\ (d)$

$R_{(test)} = P_{L(test)}\ (u_{css})$

TABLE 3.3 Experimental Results (6mm x 6mm welds)

Critical Displacement (u_c), Limit Loads(P_L) , & Tearing Resistance (R) For Through Cracking of T-Joints (6 mm x 9 mm weld)

Test #	Limit Load (Test)	Limit Load (Ideal)	Critical Displ.			Tearing Resist. (Test)	Tearing Resist. (Ideal)
			At Start	Steady State (Test)	(Litrt.)		
	$P_{L(test)}$ (N/mm)	$P_{L(ideal)}$ (N/mm)	u_{co} (mm)	u_{css} (mm)	$u_{css(lit)}$ (mm)	$R_{(test)}$ (N.mm) mm	$R_{(ideal)}$ (N.mm) mm
5	5640	5800	0.90	0.44	0.4-1.1	2482	34800

$$P_{L(test)} = M_L(4/L^2)$$

M_L = limit moment (from test)
L = weld length

$$R_{(ideal)} = P_{L(ideal)}\ (d)$$

$$R_{(test)} = P_{L(test)}\ (u_{css})$$

TABLE 3.4 Experimental Results (6mm x 9mm welds)

Critical Displacement (u_c), Limit Loads(P_L) , & Tearing Resistance (R) For Through Cracking of T-Joints (9 mm x 9 mm weld)

Test #	Limit Load (Test)	Limit Load (Ideal)	Critical Displ.			Tearing Resist. (Test)	Tearing Resist. (Ideal)
			At Start	Steady State (Test)	(Litrt.)		
	$P_{L(test)}$ (N/mm)	$P_{L(ideal)}$ (N/mm)	u_{co} (mm)	u_{css} (mm)	$u_{css(lit)}$ (mm)	$R_{(test)}$ (N.mm/mm)	$R_{(ideal)}$ (N.mm/mm)
9	8369	8397	1.98	0.85	0.4-1.1	7132	75573
10	8062	8397	2.49	0.72	0.4-1.1	5819	75573
	Avg 8216		Avg 2.23	Avg 0.78		Avg 6476	

Where: $P_{L(ideal)} = 2Kd$

$K = 0.75\ TS$

d = weld leg length (9mm)

$P_{L(test)} = M_L(4/L^2)$

M_L = limit moment (from test)

L = weld length

$R_{(ideal)} = P_{L(ideal)}\ (d)$

$R_{(test)} = P_{L(test)}\ (u_{css})$

TABLE 3.5 Experimental Results (9mm x 9mm welds)

Summary of Experimental Results

Weld Type (mm x mm)	Number of Specimen	Limit Load (test) $P_{L(test)}$ (N/mm)	Displacmt. (Stdy. State) u_{css} (mm)	Tearing Resistance (test) $R_{(test)}$ (N)
6 x 6	4	5779	0.72	4187
9 x 9	2	8216	0.78	6476
6 x 9	1	5640	0.44	2482

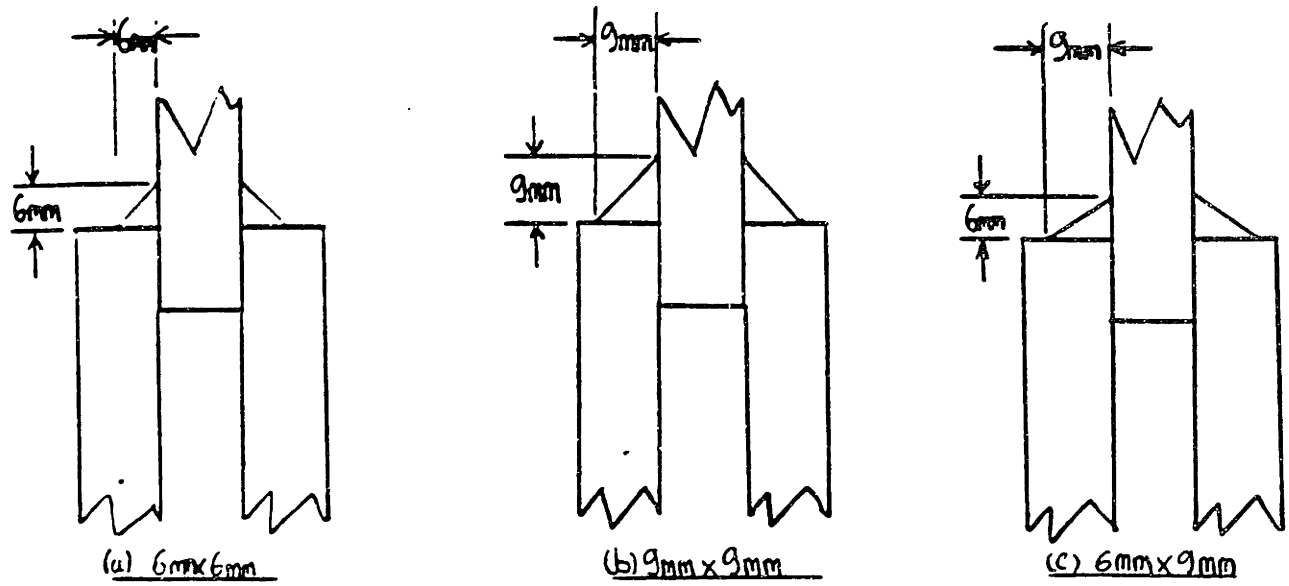

TABLE 3.6 Summary of Experimental Results

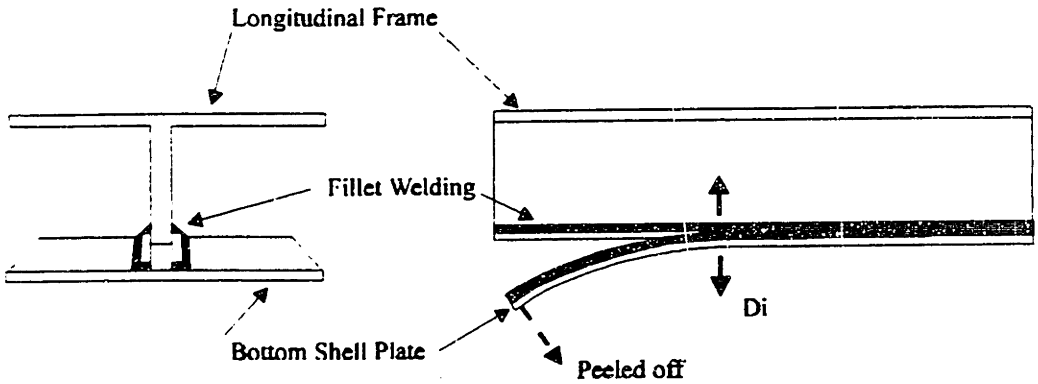

FIGURE 3.1 Peeling of Fillet Weld, (McDonald (1993))

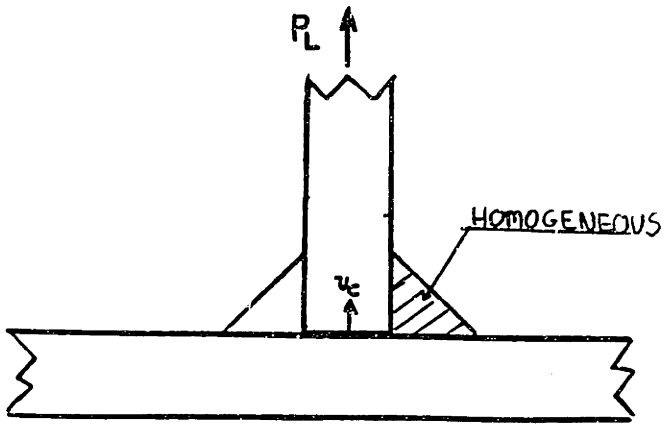

FIGURE 3.2 T-Joint

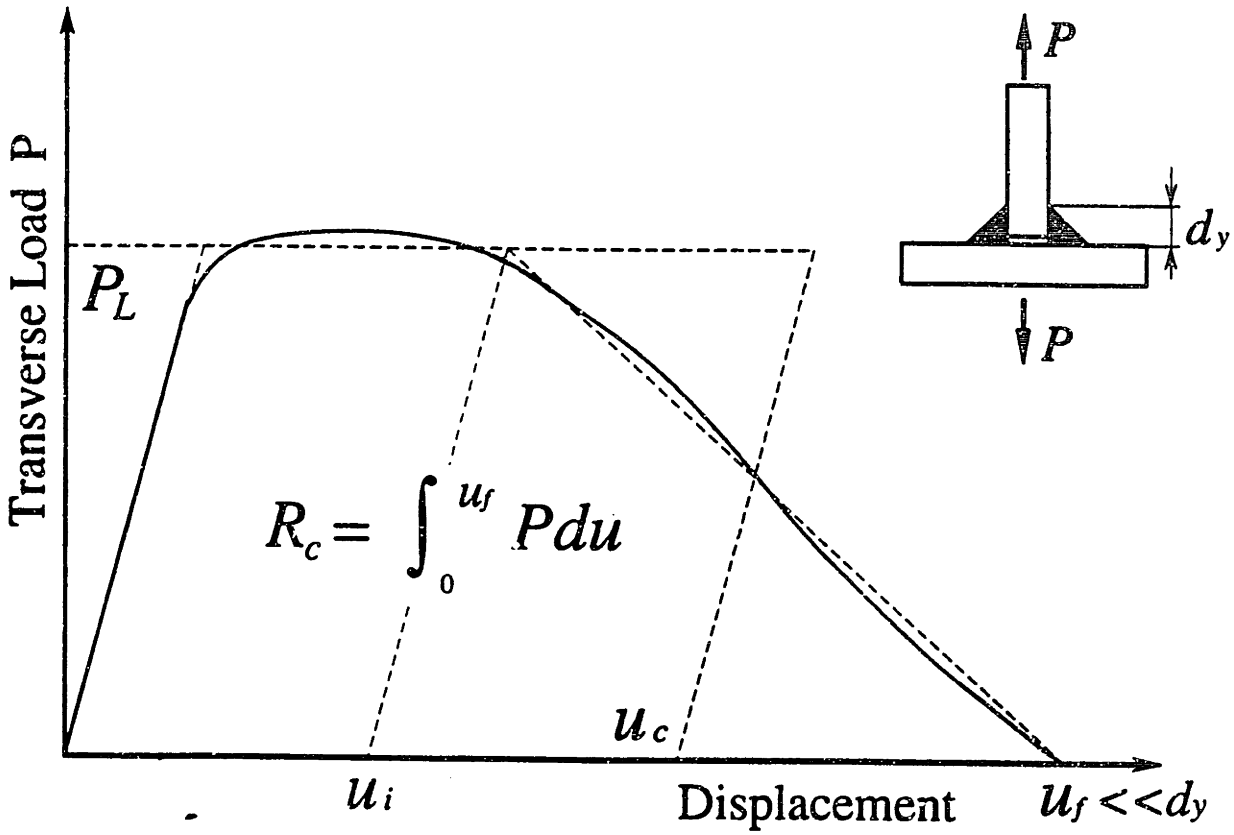

Force-displacement curve for web tension on a fillet-welded T-joint, showing the limit load per unit length, P_L, quasi-steady crack growth from u_i to u_f, the critical displacement $u_c \approx (u_i + u_f)/2$, and the critical tearing work per unit length R_c that more strictly defines the critical displacement: $u_c \equiv R_c / P_L$.

FIGURE 3.3 Force-Deformation Curve, (McClintock (1994))

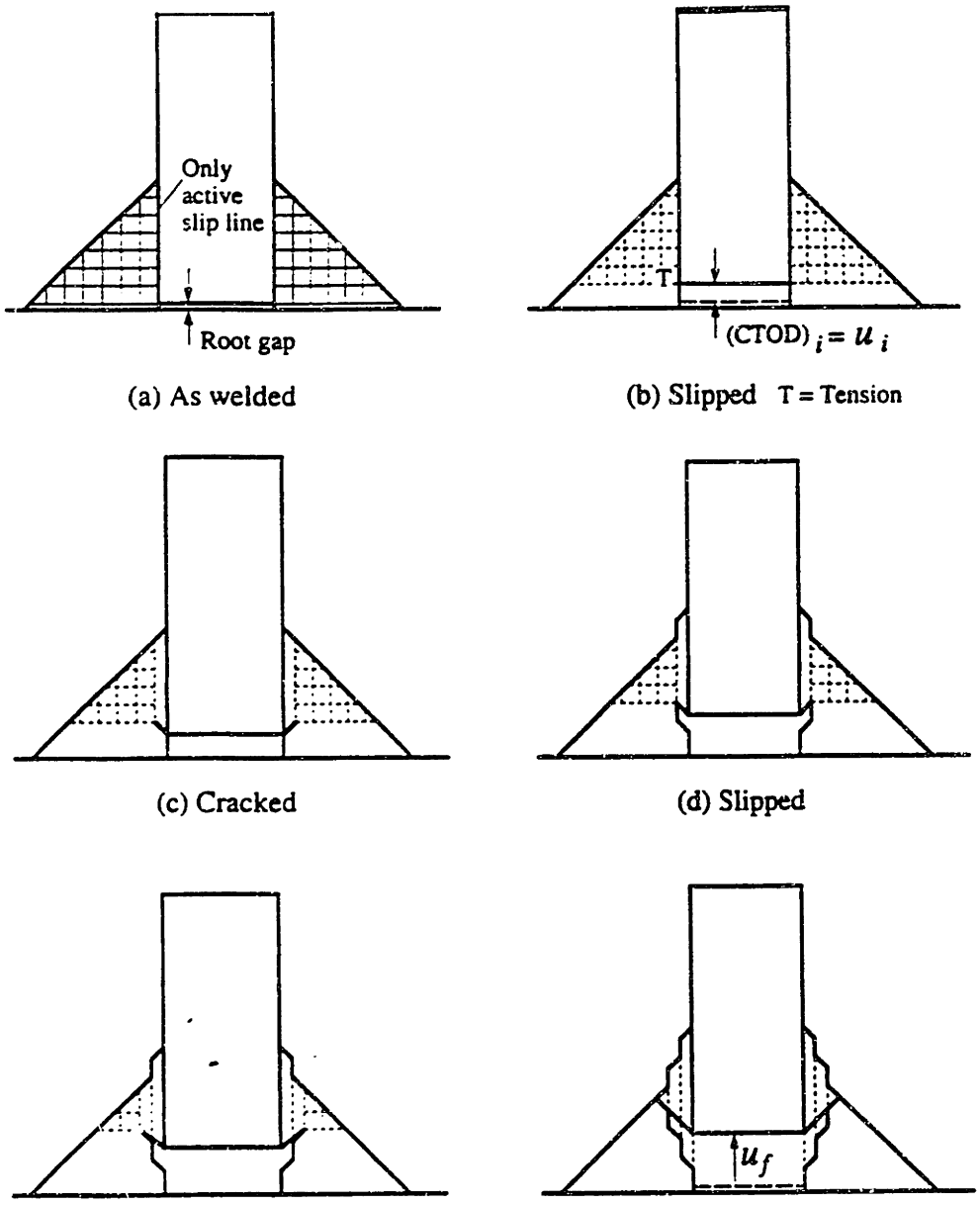

Slip line fields, crack tip opening displacement for initiation, $CTOD_i = u_i$, and alternating cracking and sliding off during crack growth to final separation at u_f.

FIGURE 3.4 Slip Line Fields, (McClintock (1994))

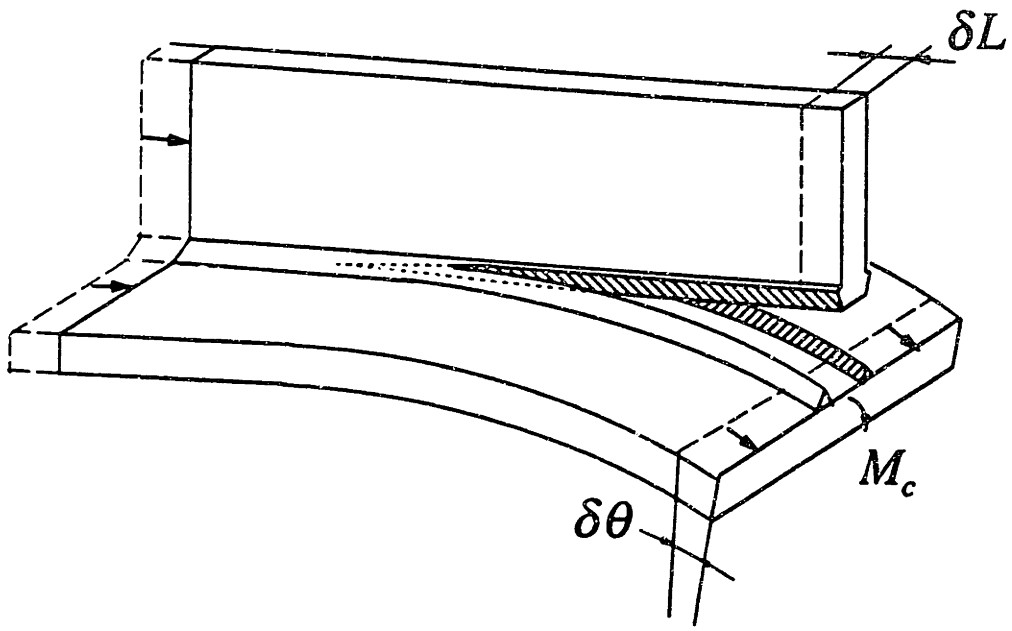

$$M_c(\delta\theta = \kappa_c \cdot \delta L = \delta L/\rho_c)$$

Total work = Plate bending work + Weld tearing work
(little interaction)

$$M_c \kappa_c \delta L = (\int_0^{\kappa_c} M d\kappa)\delta L + R_c \delta L$$

Control volume for the critical tensile tearing work per unit length R_c in a peeling test. Note that an oblique crack front leads to crack growth through the weld in locally plane strain conditions.

FIGURE 3.5 Control Volume for Tensile Tearing, (McClintock (1994))

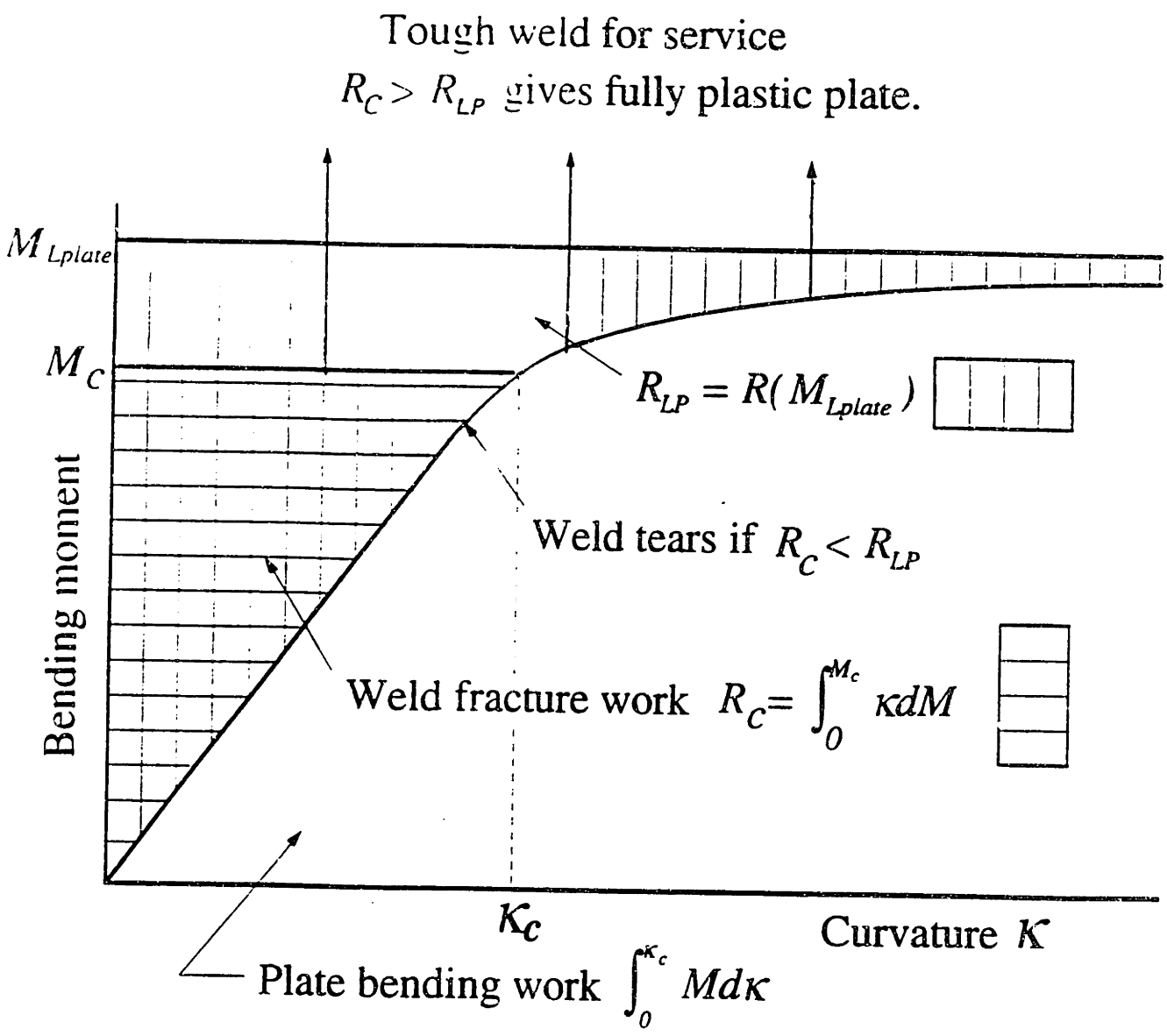

Finding the critical tearing work R_c needed to prevent a base plate from simply peeling off the stringers.

FIGURE 3.6 Moment Curvature Relation, (McClintock (1994))

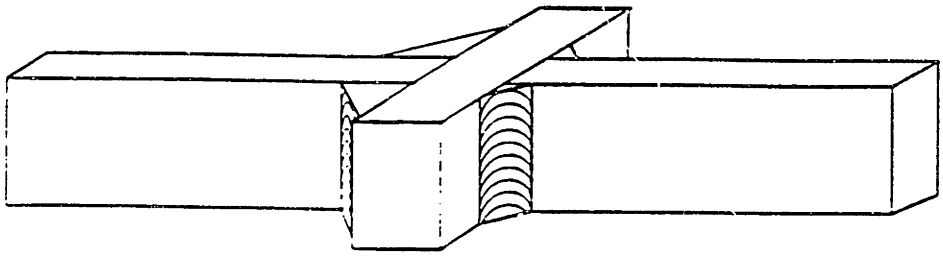

(a) Recommended

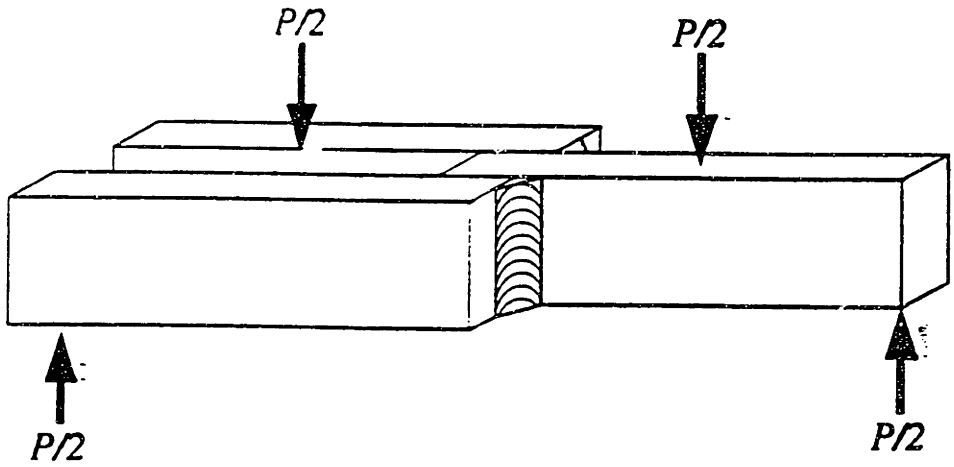

(b) As fabricated

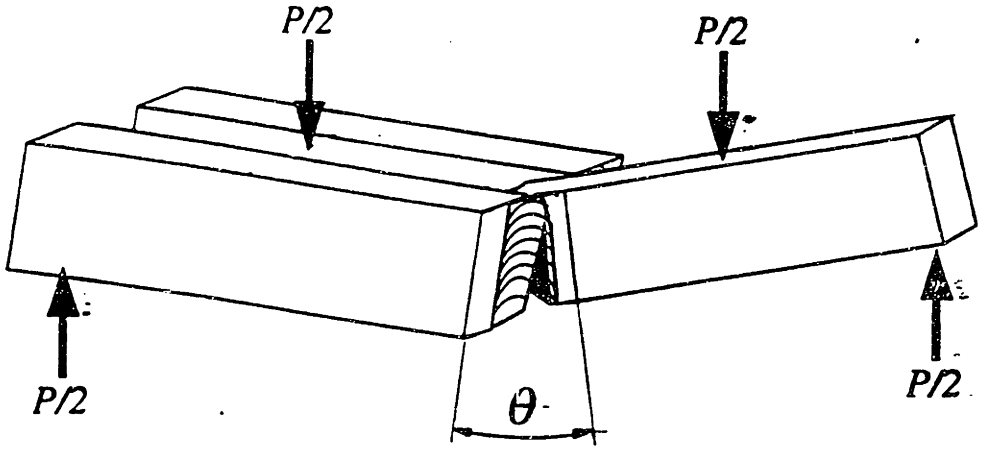

(c) Cracked

FIGURE 3.7 Beam "Bend" Test for the Critical Tearing Work per Unit Length in a T-joint

Non Dimensionalized Moment vs Bend Angle Plot Obtained From Experimental Data

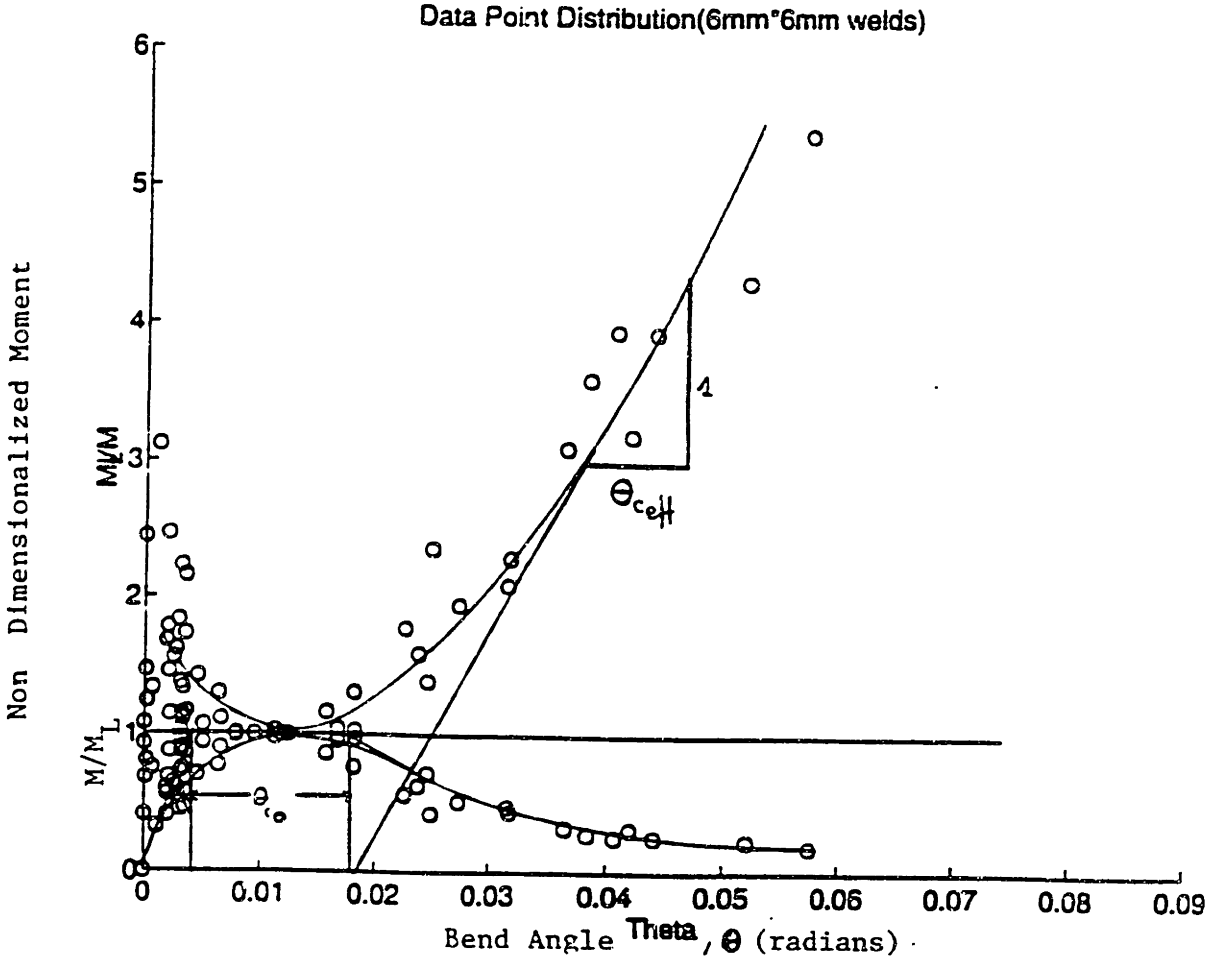

Where: M = moment at instantaneous time of data set recording
M_L= limit moment for experiment
Θ = bend angle (theta)

And: $u_{css} = \Theta_{Ceff}(L/2)$ $P_L=M_L(4/L^2)$ $R=P_L u_{css}$

FIGURE 3.8 M-θ Curve for 6mm x 6mm Weld

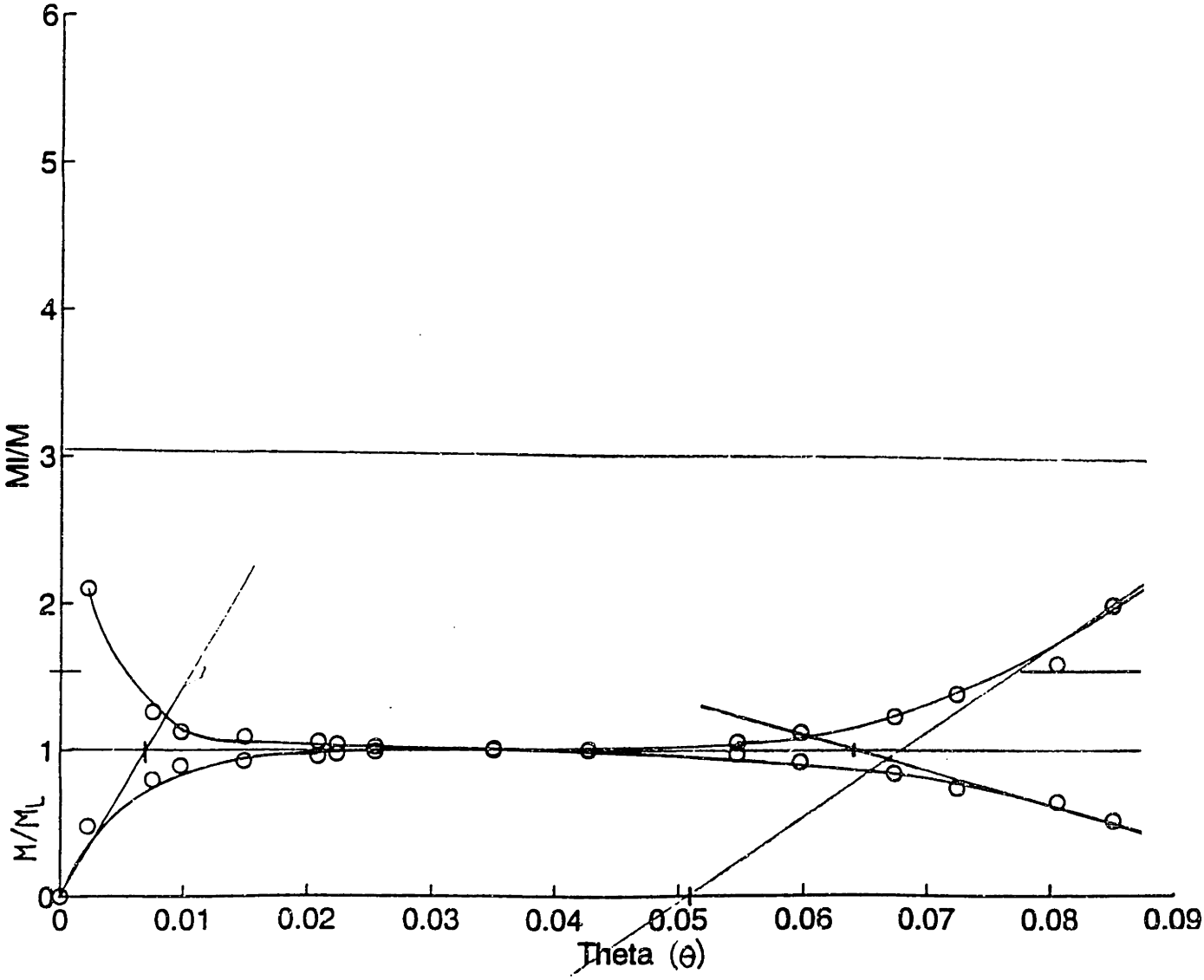

FIGURE 3.9 M-θ Curve for 9mm x 9mm Weld

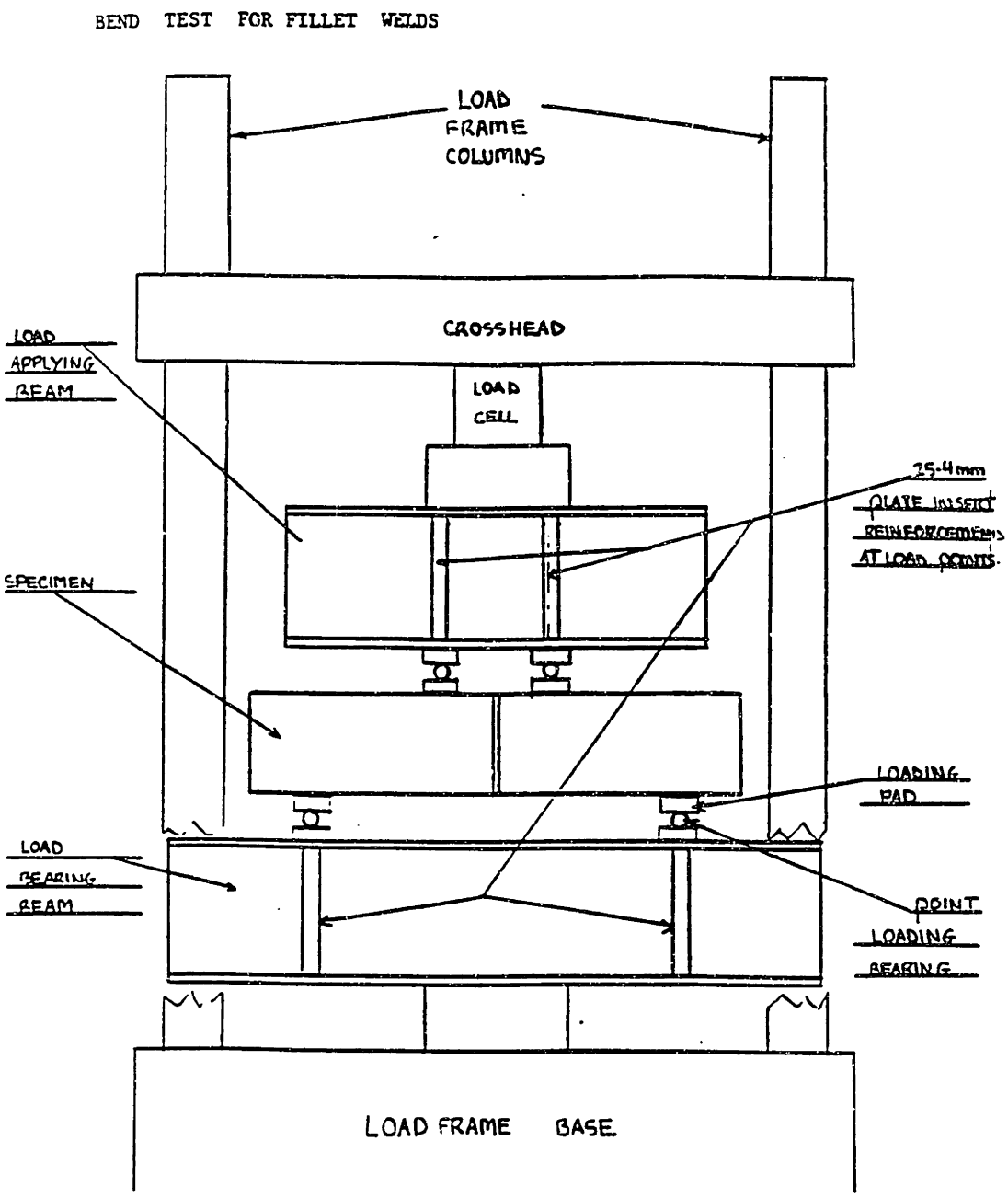

FIGURE 3.10 Specimen and Test Rig

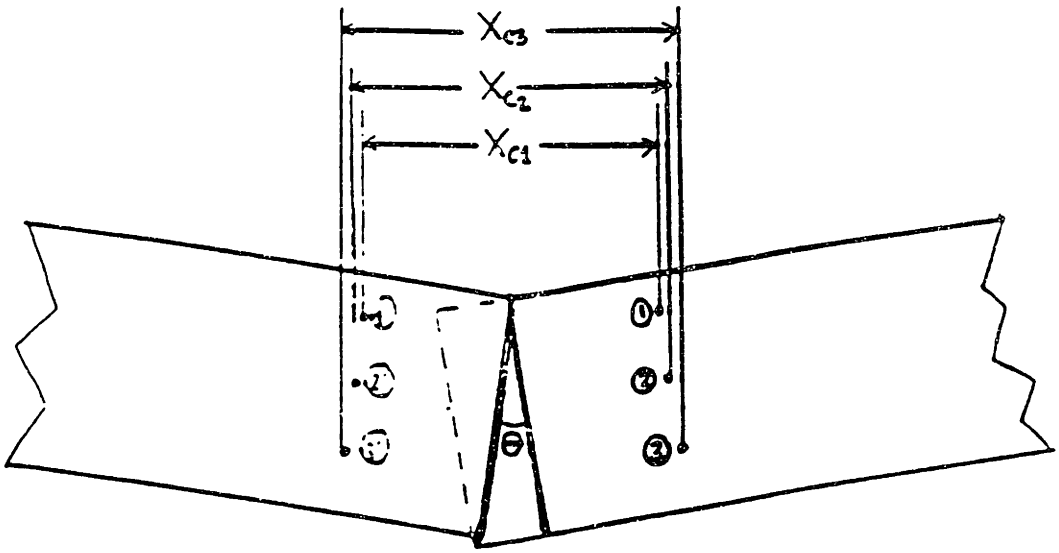

SCRIBE JOINT GEOMETRY: (LOADED SPECIMEN)

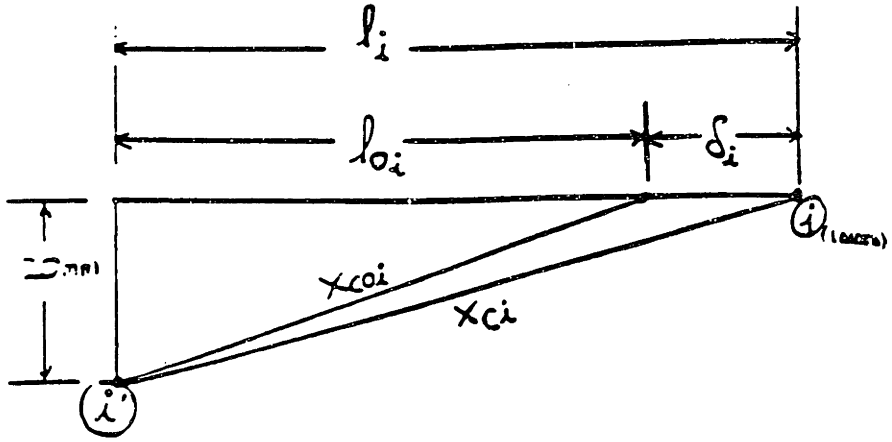

⊙ NOTE: $i = 1, 2, 3$

FOR A LOAD P:

$$\delta_i = l_i - l_{oi} = \left\{ \sqrt{X_{ci} - 20^2} - \sqrt{X_{co_i} - 20^2} \right\}$$

FOR A SMALL θ (SMALL ANGLE APPROXIMATION):

$$\theta = \theta_{12} = \frac{\delta_2 - \delta_1}{(z_1 - z_2)} = \theta_{23} = \frac{\delta_3 - \delta_2}{(z_2 - z_3)}$$

FIGURE 3.11 Specimen Geometric Relationships

CHAPTER 4

COST MODEL

A simple cost model was developed for the purposes of studying the cost implications of increasing weld leg length (for symmetric 45 degree welds). As experimentally demonstrated, tearing resistance **R** increases proportionally to the weld leg length **d**. Of particular interest to this study, is the cost differential resulting from an increase in leg length whereupon stiffener and plate failure would occur prior to joint (weld) failure.

For KA 36 steel (standard grade used for tanker construction in Japanese yards) the tensile strength upper limit S_l is of the order of 620 N/mm^2 (Masubuchi, Koga, McDonald, 1993). This indicates that for 15 mm KA 36 plate (as found in stiffeners) the limit load P_L is 9300 N/mm while for 20 mm plate (shell plating) the corresponding value is 12400 N/mm. These two limit loads can be achieved in weldments (E 7016 electrode, weldment shear strength **K**, 467 N/mm) with 10 and 13 mm leg lengths (using the ideal limit load approximation which provides results within 3% accuracy of those observed experimentally). From a crash worthiness point of view it is desirable for the welded T-joint to fail at the plate while maintaining its integrity at the weld such as to minimize the size of damage created by ship grounding. Present construction standards require 6 mm weld at these joints. It should further be noted that although the most common mode of failure observed at T-joints involves tripping of the stiffener and subsequent failure at the weldment side subject to tension, enough similarities exist between the two modes

(McClintock, 1994) to reinforce the idea that larger weld leg length would also reduce weldment failure occurrences during tripping. This particular mode of failure is currently under investigation and experimental data will soon be obtained in light of the above argument.

For the purposes of this analysis, a simple cost model was devised to obtain an estimate of the cost impact of weld leg length modification. The breakdown of costs as related to the overall ship costs is illustrated in Fig.4.1. In general, the model breaks down ship cost **C** into hull construction costs **HC** (including pipe fitting), total welding costs **WC** (as a subset of hull construction costs), and welding costs for the bottom hull structure **WCBHS** (welding costs for frames and stiffeners making up the hull or double hull). The relationship between these costs is described as follows:

$$HC = K_1 C \tag{4.1}$$

$$WC = K_2 HC = K_1 K_2 C \tag{4.2}$$

$$WCBHS = K_3 WC = K_1 K_2 K_3 C \tag{4.3}$$

The values for the cost fractions K_1, K_2 and K_3 were obtained from a generalized welding cost study performed by Kawasaki Heavy Industries for ships of various sizes and uses (Masubuchi, Koga, McDonald, 1993). It should thus be noted that since these values are not limited to a particular class of tankers and instead represent an average for all classes, they may not be taken as exact. Furthermore,

the cost fractions include labor, materials, and all associated production costs. The baseline value taken for the total cost fraction of welding the bottom hull structure was 1.5% (or $K_1K_2K_3$ = 0.015). A sensitivity analysis was carried out by changing the latter to an upper limit of 3% (0.03) or effectively doubling the costs of welding for the bottom hull structure (recall only the bottom hull structure is subjected to peeling during grounding).

In general, four categories of welding are in use for ship construction in Japan :

1. GMAW - CO_2(flux cored wire (FC))

2. GMAW - CO_2(solid wire (SW))

3. SMAW - (Single Pass)

4. SMAW - (Multi Pass)

It should further be noted that the principal process used for the majority of welding (specially in the bottom hull structure) is the GMAW - CO_2 process (Fig.4.2). Fig 4.3, Fig 4.4, and Fig 4.5 illustrate the full process of ship hull construction with an emphasis towards the welding processes (Koga, 1994). Much of the stiffener/shell plate (T-joint) welding performed for longitudinal stiffeners is performed by GMAW automatic carriage (Fig.4.6). Modern stiffener/shell plate T-Joints are designed such as to convey shear stress along the longitudinal axis (length) of the weld (Fig.4.7) and not for any other

purposes (such as tensile tearing (Fig.4.8a), web folding or "tripping" (Fig.4.8b), and web bending (Fig.4.8c)). As a consequence of present design philosophy, the welding processes employed for the joining of longitudinal stiffeners to shell are one-pass. Using a one pass weld is justified by two key reasons:

1. Required fillet weld leg lengths are smaller than 10 mm, and
2. One-pass welding is less time consuming and more economical.

The present technological limit for one-pass processes used in most ship building is 12-13 mm for the leg length. Keeping in mind the longitudinal strengthening characteristics for most V.L.C.C. newbuildings (single bottom and double bottom) illustrated in Figs.4.9 through 4.12 (Masubuchi, Koga, McDonald, 1993), longitudinal welding characteristics can be broken down into the two categories presented in Table 4.1.

Keeping our analysis limited to the economically realistic one-pass welding procedures, relative costs for the four categories previously listed are presented in Fig. 4.13. Note that SMAW (single and multi pass) is only illustrated for comparative purposes. The key variable affecting cost is welding operation time and its subsequent impact on construction expenses related to welding (i.e. labor costs, material costs, power costs etc...).

The welding cost model "Weldcostmdl" was developed on spreadsheet. Data input and model parameters are controlled by three modules. The first module is the "Control Module" and contains

a listing of ship purchasing costs for tankers (ranging from 30 000 dwt to 250 000 dwt). The baseline costs for the "Single Skin" cost control column were obtained from "Shipping Statistics and Economics" , No. 270 (Drewry, April 1993). The "Double Skin" costs are re-calculated by the spreadsheet based on a typical cost differential fraction (15% higher new building costs for double skinned ships). The cost differential fraction can also be changed from the " Control Module".

Welding process and cost characteristics are stored in the "Welding Characteristics Module" which is a tabulated and discretized version of the plots in Fig.4.13. Note that the discretized values of "Increasing Rate of Total Ship Cost" are applied in the form of factor K_4 where:

$$C_{new} = C\ (1+K_4) \qquad (4.4)$$

The model cost breakdown characteristics (K_1,K_2,K_3) are controlled from the "Production Cost Breakdown Module" . The latter uses the following values:

$K_1 = 0.30$ (30%)

$K_2 = 0.25$ (25%)

$K_3 = 0.20$ (20% & up to 40% for sensitivity anal.)

"Weldcostmdl" converts the parameters contained within the three previously described modules into costs as a function of welding process and leg length.

Limiting the analysis to the GMAW-CO_2 processes (the principal bottom hull welding processes in use to day in modern shipbuilding) , "Weldcostmdl" yields the results shown in Table 4.2 for a 250 000 dwt tanker.

Note that the 15% cost differential is carried throughout the calculations due to the linearity of the assumptions and relations in the cost breakdown (K_1,K_2,K_3,&K_4). In view of the technological limitations of present processes (single pass - 12mm for flux cored vs 10mm for solid wire), modifying the weld leg length entails the following cost differences for initial ship construction (Providing only the Bottom hull structure weld leg lengths are increased for improved Tearing Resistance - only the shell plating welded to longitudinals would require the larger welds in reality):

1. **Single Skin;** modifying the bottom hull structure alone from 6mm to 12mm weld leg lengths using Flux Cored wire (e.g. longitudinal stiffening) would cost 30 000$ (from Table 4.2; |[WCBHS, CO_2(FC) 6mm Weld,K_3=0.2]-[WCBHS, $C0_2$(FC)12mm Weld,K_3=0.2]| = |1.37 Million- 1.40 Million| = 0.03 Million = 30 000 $).

2. **Double skin;** modifying the bottom hull structure from 6mm to 12 mm leg length 40 000$. Essentially, most of the cost would be associated with extra electrode material (wire) and

increased welding time. |[WCBHS, CO_2(FC) 6mm Weld,K_3=0.2]-[WCBHS, $C0_2$(FC)12mm Weld,K_3=0.2]| = |1.57 Million- 1.61 Million| = 0.04 Million = 40 000 $).

further point of interest focuses on the issue of weld penetration. The Tearing Resistance tests carried out as part of this project (Chapter 3) were performed with low penetration welds. (12-25% of the web thickness per side). Industry knowledge confirms that increased penetration can substantially increase weld strength by shifting. It should be noted that increasing K_3 as done in the two last rows of Table 4.2 results in increased cost differentials. Doubling K_3 would double the differentials for (1) and (2) above to 60 000$ and 80 000 $ respectively. The baseline K_3 value of 0.2 used was obtained (Koga, 94) through a survey of welding practices in a Japanese shipyard and represents an average of welding practice for various ship types, and was used as a lower limit. . K_3 of 0.4 was used as an upper limit (doubling the costs). The doubling effect is associated to the linear model assumptions. It should be noted that the above value should only be taken as an indicators of the general magnitude of cost increase associated with weld modification, in other words the general welding costs increase for a 250 000 dwt tanker if strengthening for the bottom hull is achieved through an increase in weld leg length from 6mm to 12mm using the CO_2 Flux Cored Process. Similarly, costs for different displacement tankers can be extracted from the welding cost model (Weldcostmdl) in Appendix C using the procedure illustrated from Table 4.2. As it can be seen, modification of the weld leg length in the bottom hull structure

entails relatively small increased costs even for a VLCC. Consequently, a detailed discussion is not put forth for smaller vessels. Should further research confirm the beneficial aspects of increased leg length with respect to other failure modes (as well as tearing resistance), the associated costs could be justified.

In conclusion, strengthening the welds along the longitudinal axis of a vessel's hull could provide improved resistance and minimize the length of damage during a grounding. An increased expense of 80 000 $ for a 250 000 dwt Double Skin V.L.C.C. has been estimated using Weldcostmdl.

Characteristic	Stiffener Thickness (mm)	Weld Leg Length (mm)
Major Stiffeners	20	9
Minor Stiffeners	15	6

Note: 1. Major stiffeners consist of longitudinal bulkhead plates, and longitudinal girder plates.

2. Minor stiffeners consist of longitudinal built-up frames.

TABLE 4.1 Ship Stiffener Characteristics

Parameters (250 000 dwt)	Single Skin (Cost)	Double Skin (Cost)	Difference (Δ Cost)
Total Ship Cost 6mm weld	91	104.65	13.65
Total Ship Cost 12mm weld,CO_2(FC)	93.29	107.29	14.00
Total Ship Cost 10mm Weld,CO_2(SW)	92.72	106.63	13.91
WCBHS, CO_2(FC) 6mm Weld,K_3=0.2	1.37	1.57	0.20
WCBHS, CO_2(SW) 6mm Weld,K_3=0.2	1.37	1.57	0.20
WCBHS, $C0_2$(FC) 12mm Weld,K_3=0.2	1.40	1.61	0.21
WCBHS, CO_2(SW) 10mm Weld,K_3=0.2	1.39	1.60	0.21
WCBHS, CO_2(FC) 12mm Weld,K_3=0.4	2.8	3.20	0.40
WCBHS, CO_2(SW) 10mm weld,K_3=0.4	2.78	3.20	0.44

Note: FC = Flux Cored Wire

SW= Solid Wire

WCBHS= Welding Costs Bottom Hull Structure

TABLE 4.2 Costs Associated with Weld Leg Length ($ Million)

Rate of Bottom Hull Structure Welding Cost in the Total Cost of Ship

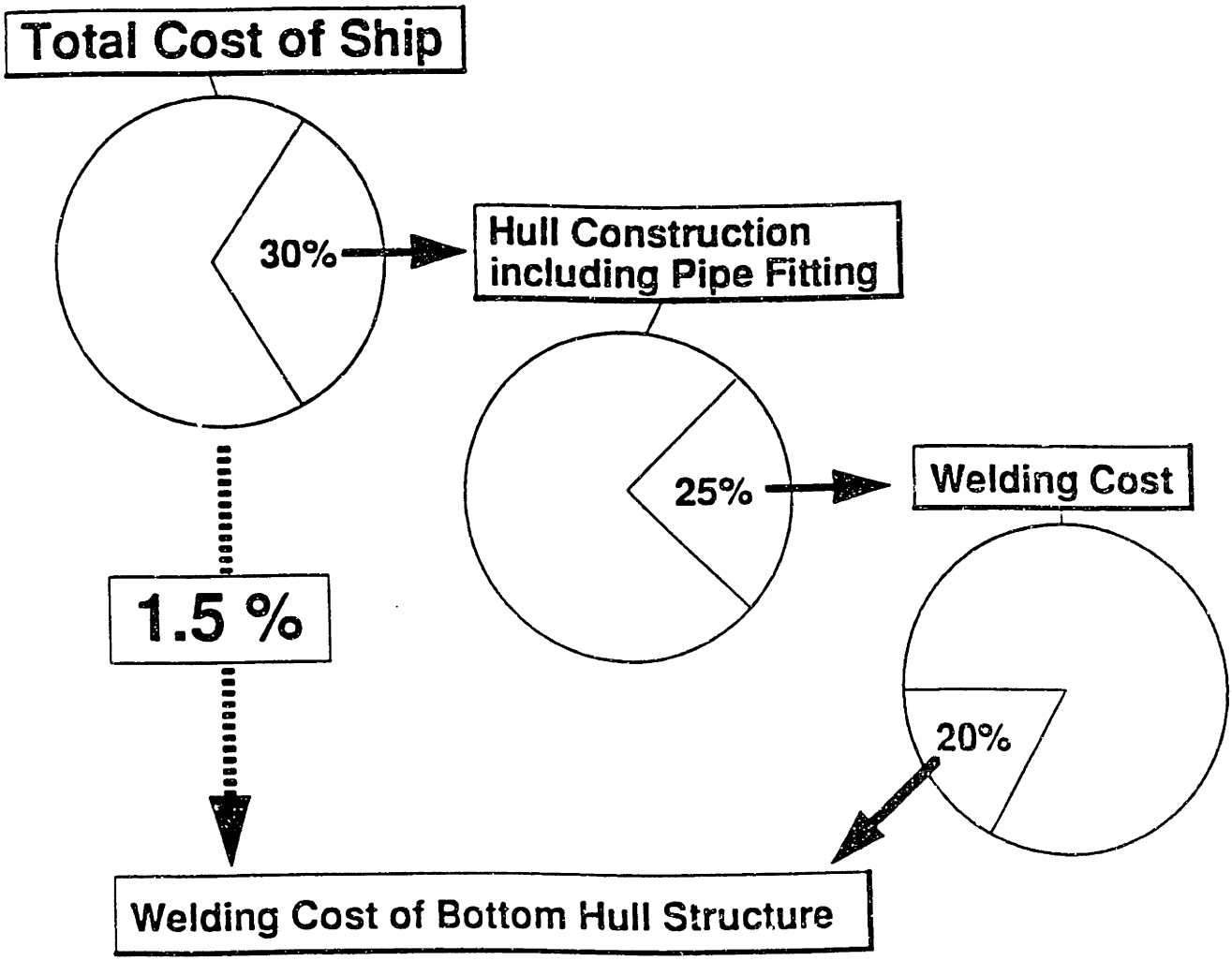

FIGURE 4.1 Cost Breakdown as Function of Total Ship Cost, Koga (1994)

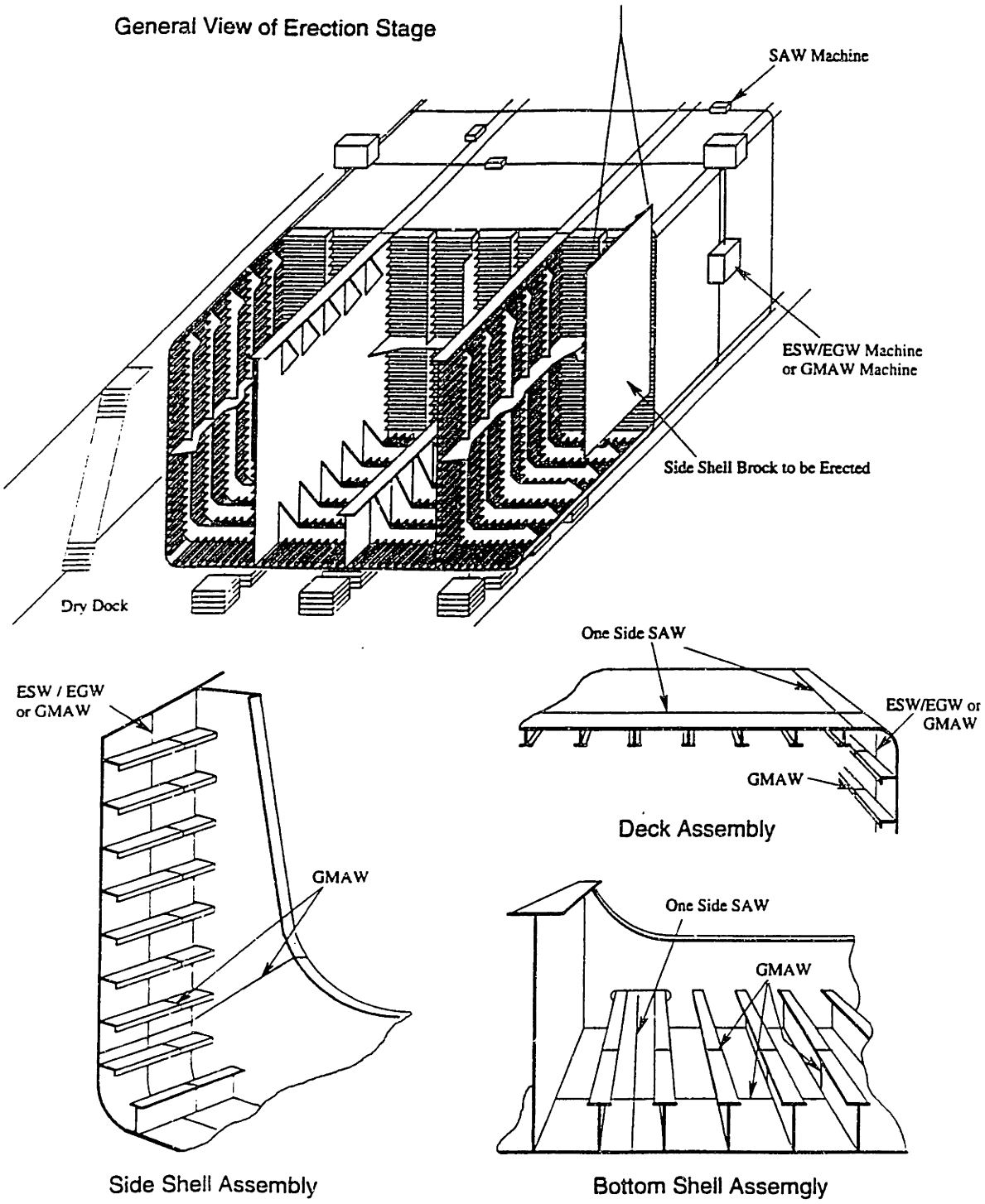

Welding Processes used for Erection Joints of Ship Hull

FIGURE 4.2 GMAW-CO_2 Process, Koga (1994)

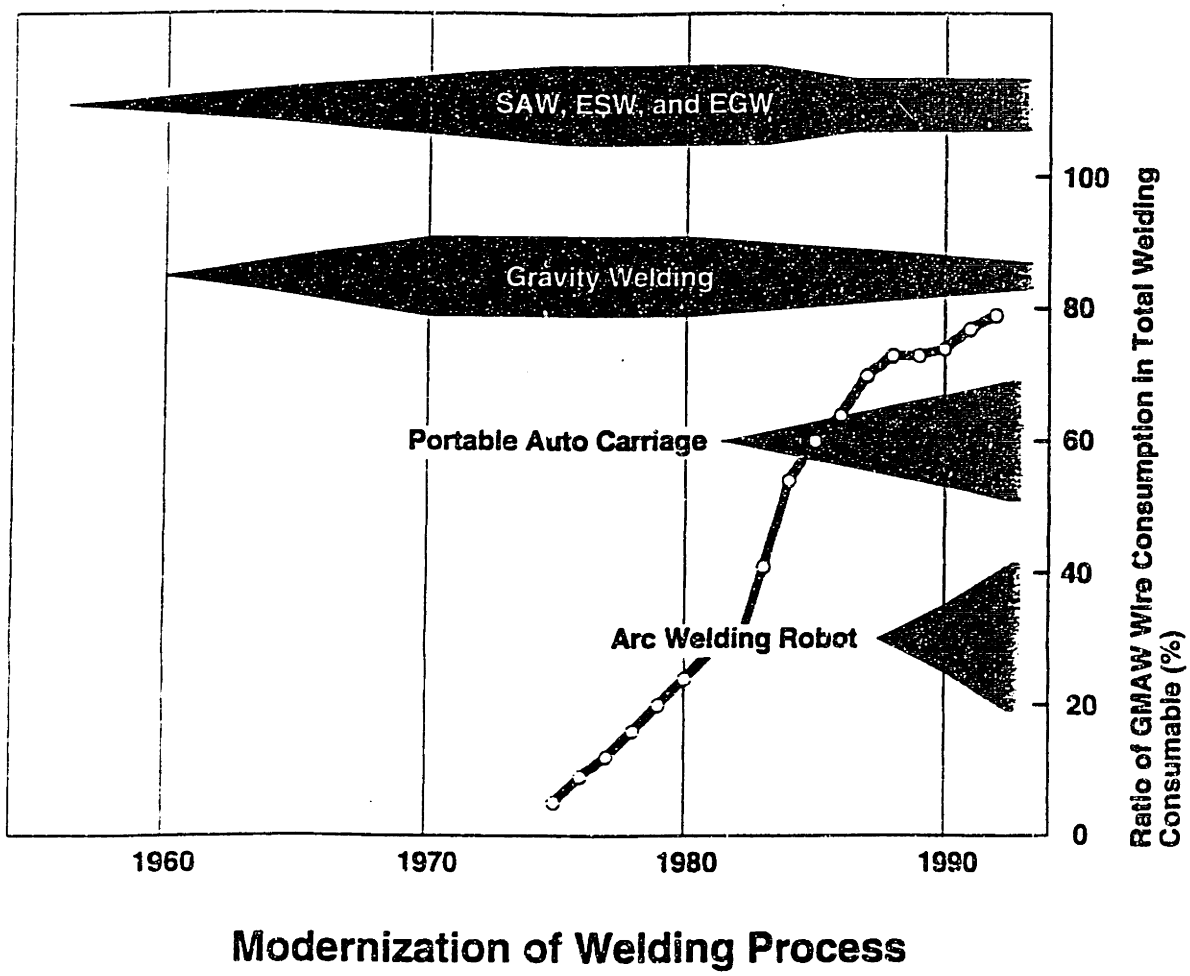

FIGURE 4.3 Welding Processes Used For Erection Joints of Ship Hull, Koga (1994)

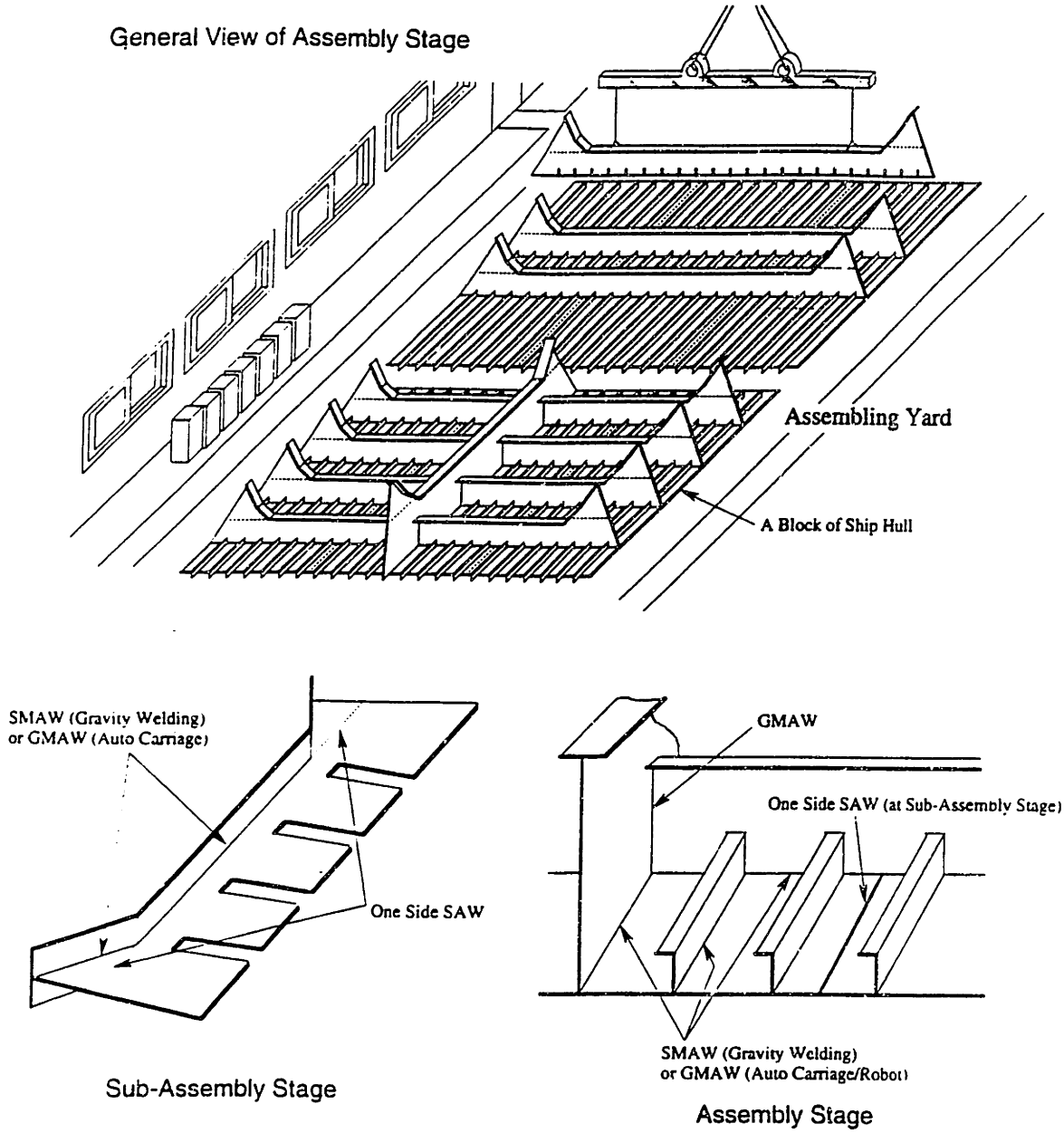

FIGURE 4.4 Ship Assembly Stages, Koga (1994)

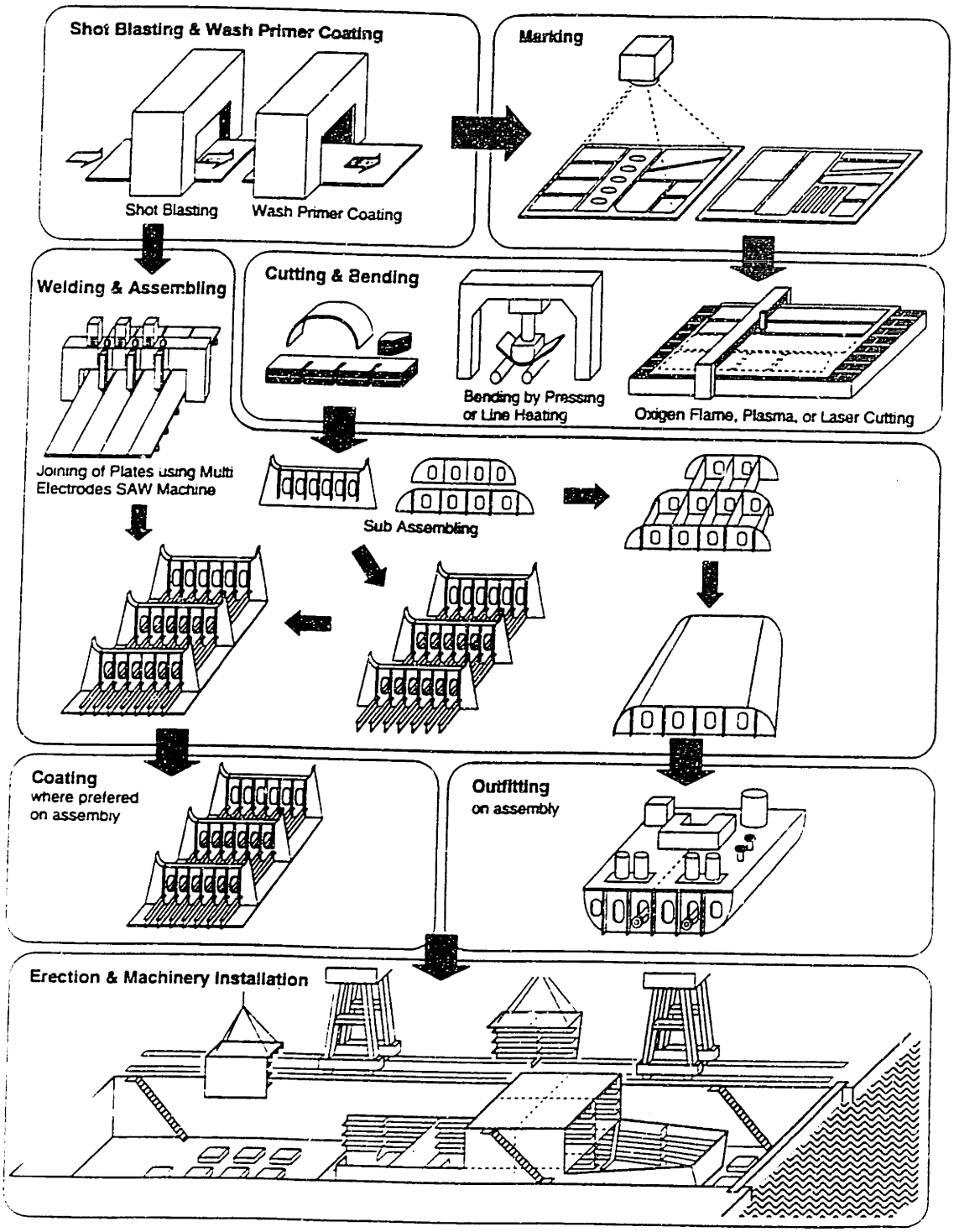

Schematic Drawing of Ship Hull Construction

FIGURE 4.5 Schematic Drawing of Ship Hull Construction, Koga (1994)

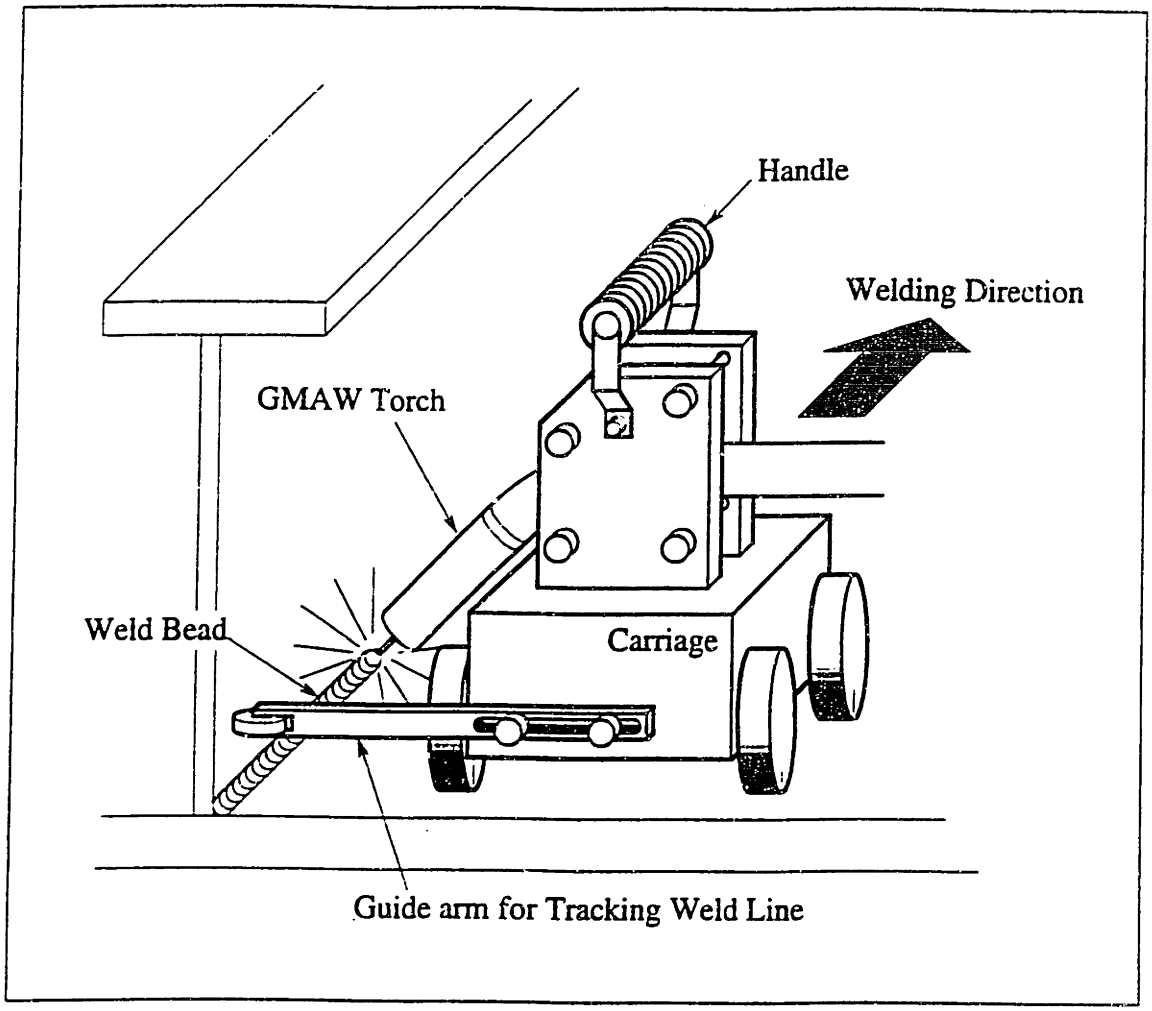

Automatic carriage for GMAW process

FIGURE 4.6 GMAW Automatic Carriage, Koga (1994)

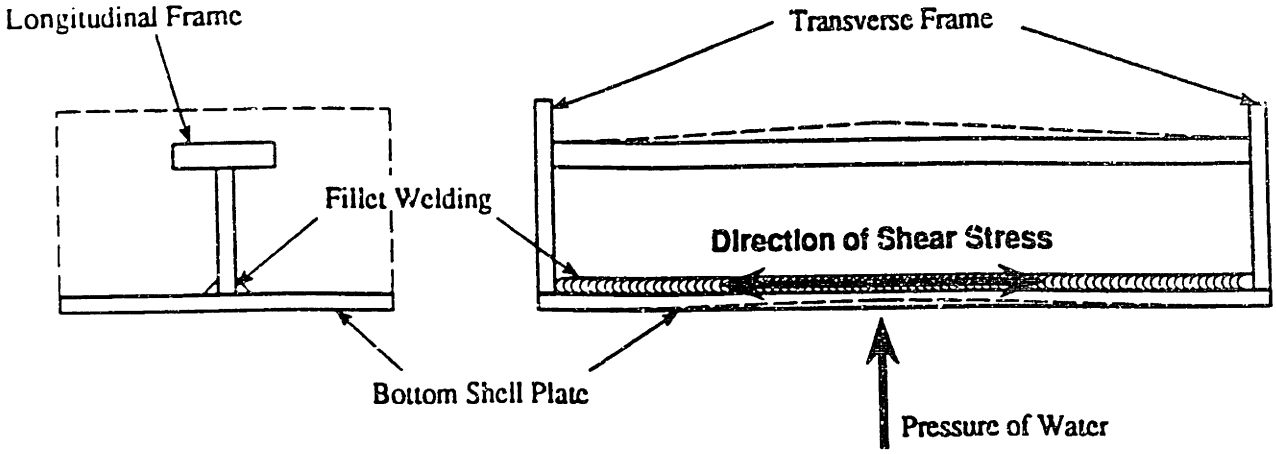

Figure 7 Schematic Drawing of Stress at Weld Joint for Present Design of Fillet Welds

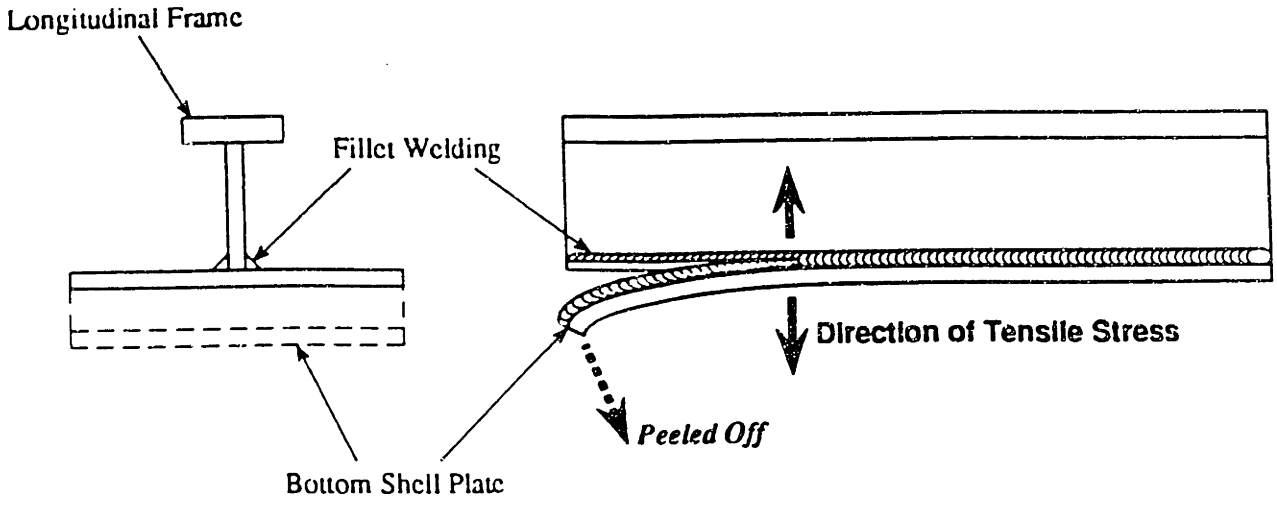

FIGURE 4.7 Shear Stress Distribution Along a T-joint (Masubuchi, McDonald, Wang, (1993))

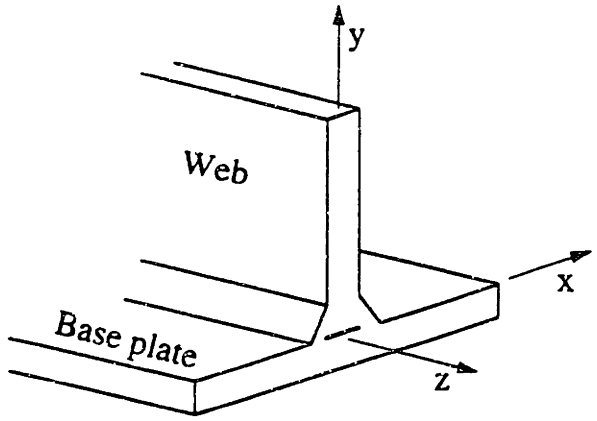

Coordinate axes for a T-joint

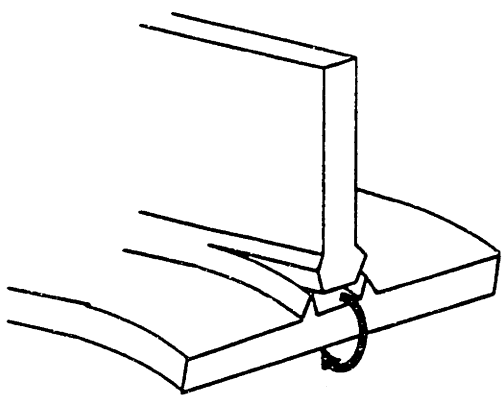

(a) Tearing

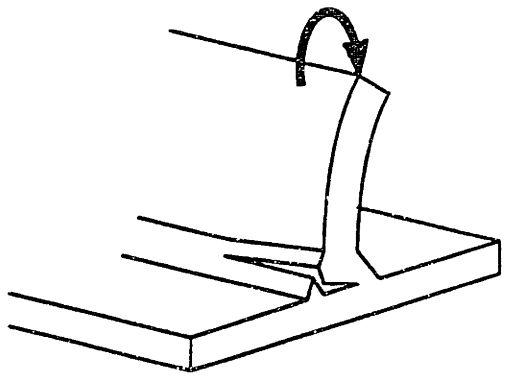

(b) Web folding

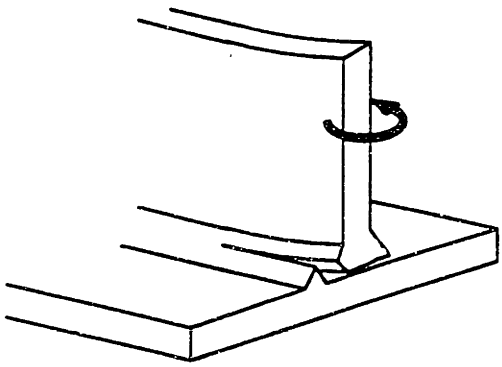

(c) Web bending

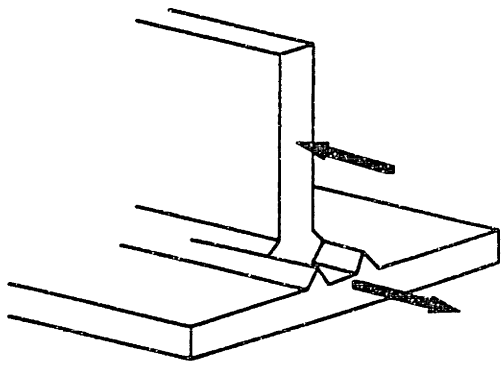

(d) Longitudinal shearing

FIGURE 4.8 T-joint Failure Modes

Midship Section of Single Bottom VLCC

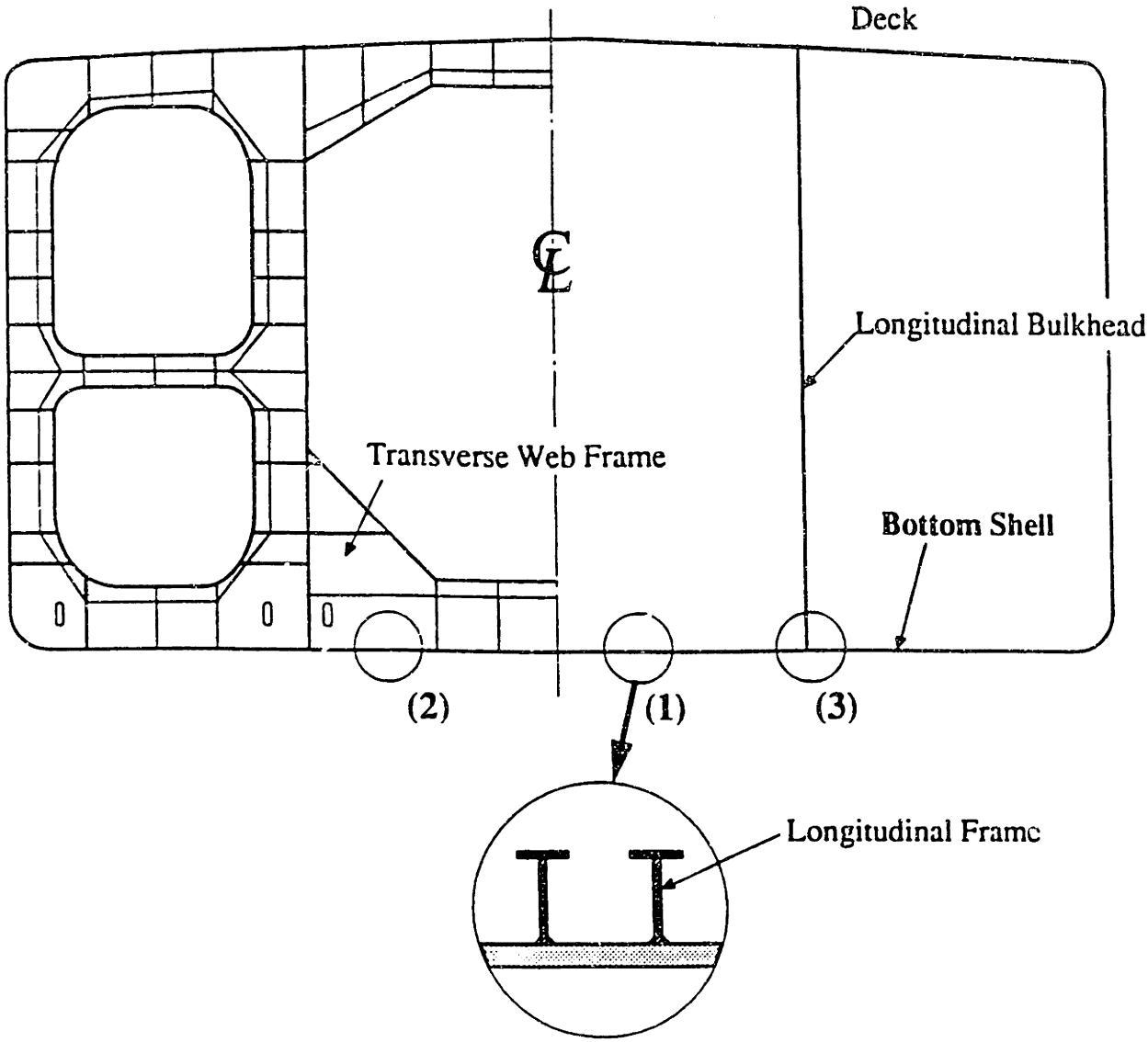

Components fillet welded to the Bottom Shell Plating

(1) Longitudinal Frame

(2) Transverse Web Frame

(3) Longitudinal Bulkhead

(4) Transverse Bulkhead
(not drawn in the figure)

FIGURE 4.9 V.L.C.C. Single Hull Midship Section, (Masubuchi, McDonald, Wang, (1993))

Midship Section of Double Bottom VLCC

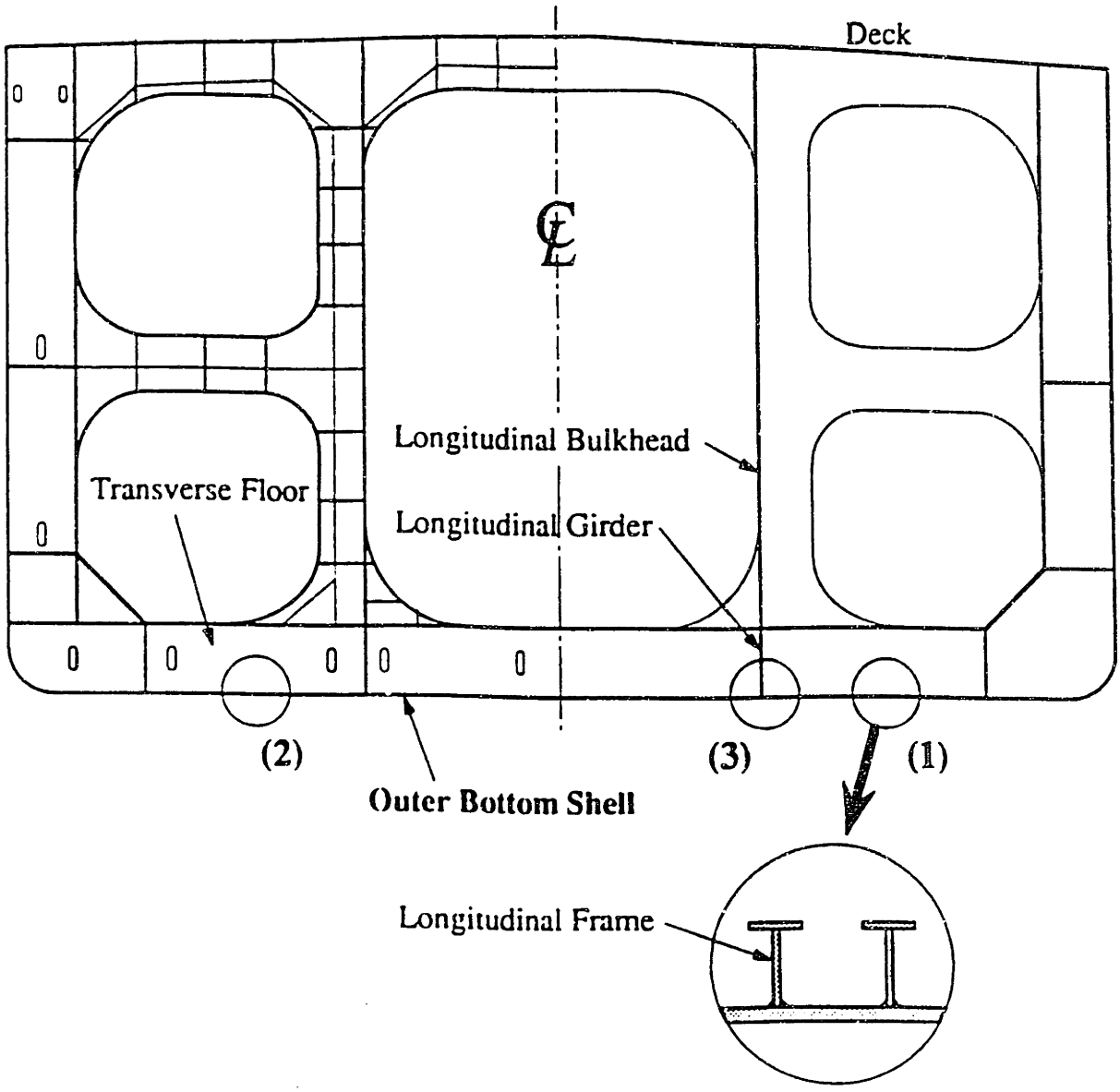

Components fillet welded to the Outer Bottom Shell Plating

(1) Longitudinal Frame

(2) Transverse Floor

(3) Longitudinal Girder

(4) Transverse Bulkhead
(not drawn in the figure)

FIGURE 4.10 V.L.C.C. Double Hull Midship Section, (Masubuchi, McDonald, Wang (1993))

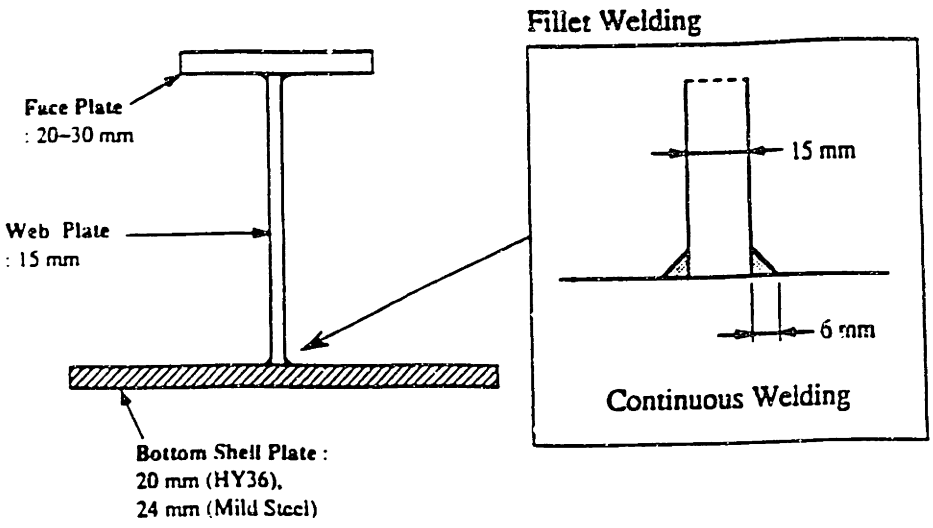

(1) Longitudinal Built-Up Frame

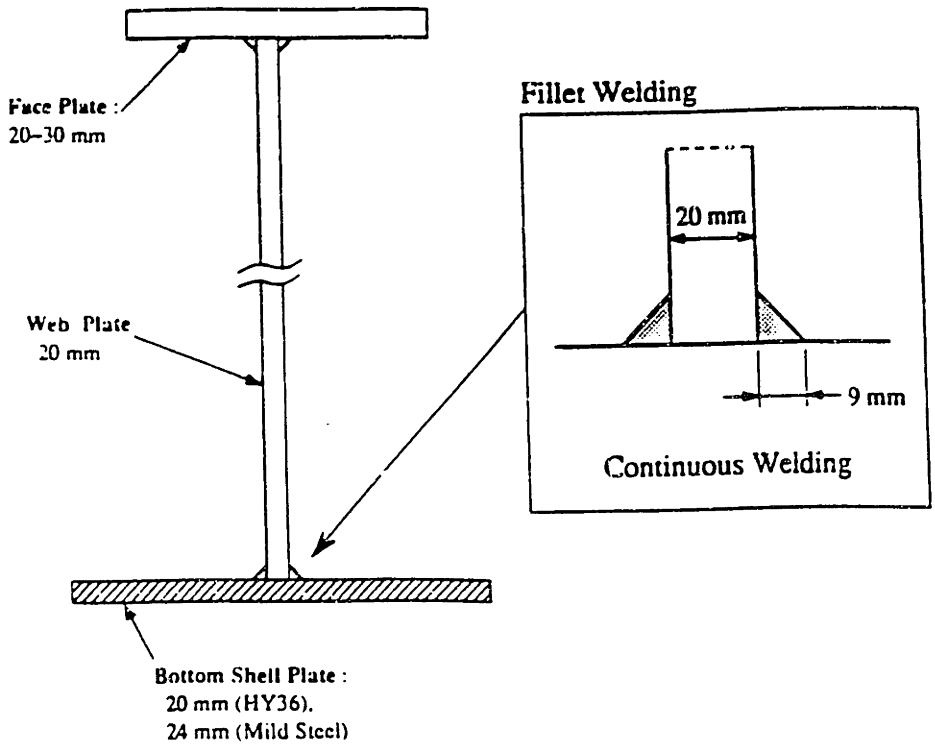

(2) Transverse Web Plate

FIGURE 4.11a Details of Welding Designs for Single Hull Structures, (Masubuchi, McDonald, Wang (1993))

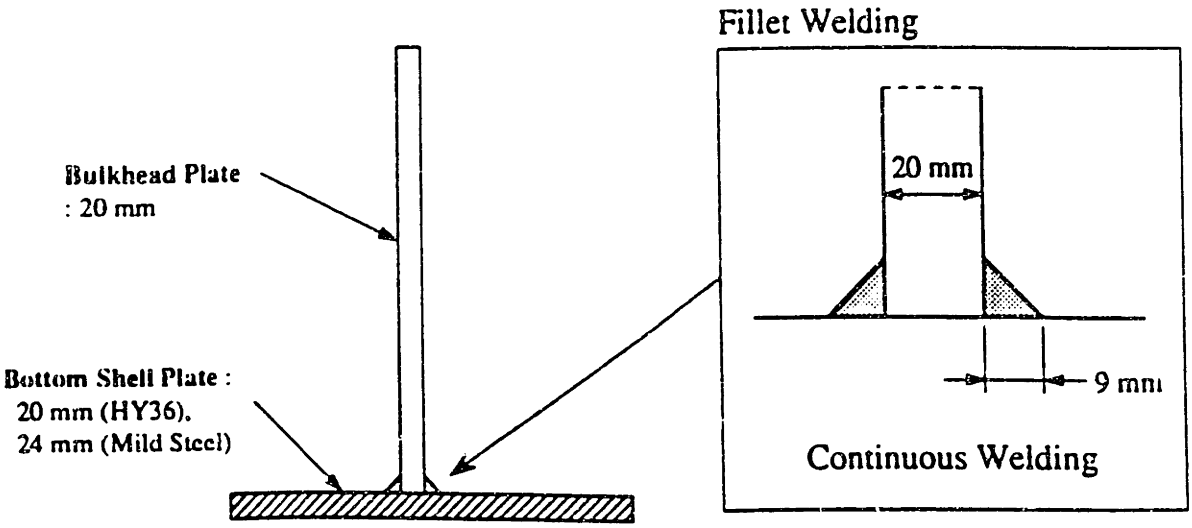

(3) Longitudinal Bulkhead Plate

Note : Transverse Bulkhead Plates are also welded in the same way to the Bottom Shell Plate

FIGURE 4.11b Details of Welding Designs for Single Hull Structures

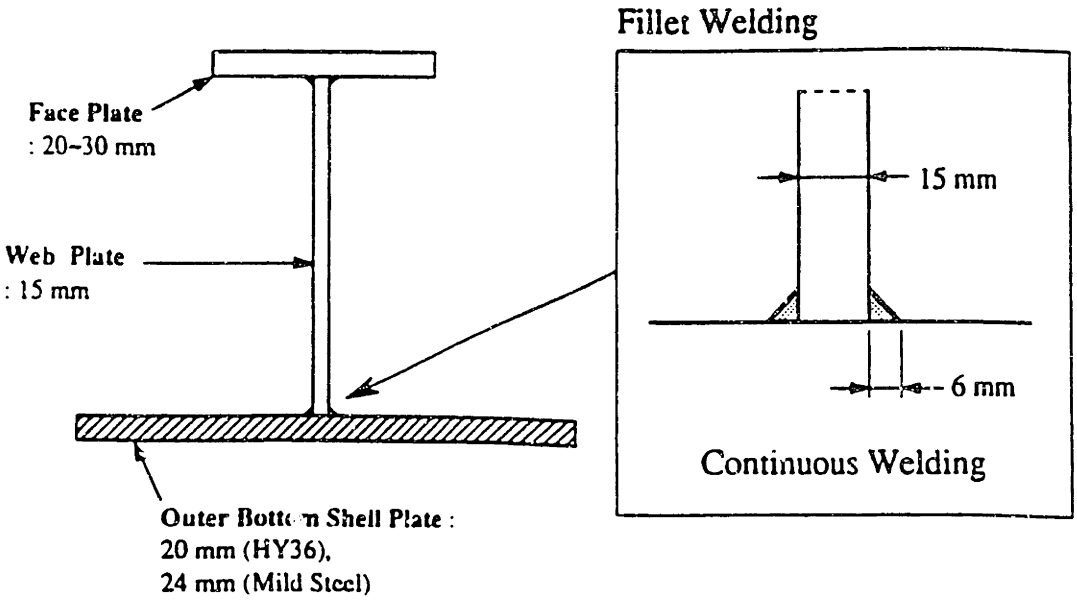

(1) Longitudinal Built-Up Frame

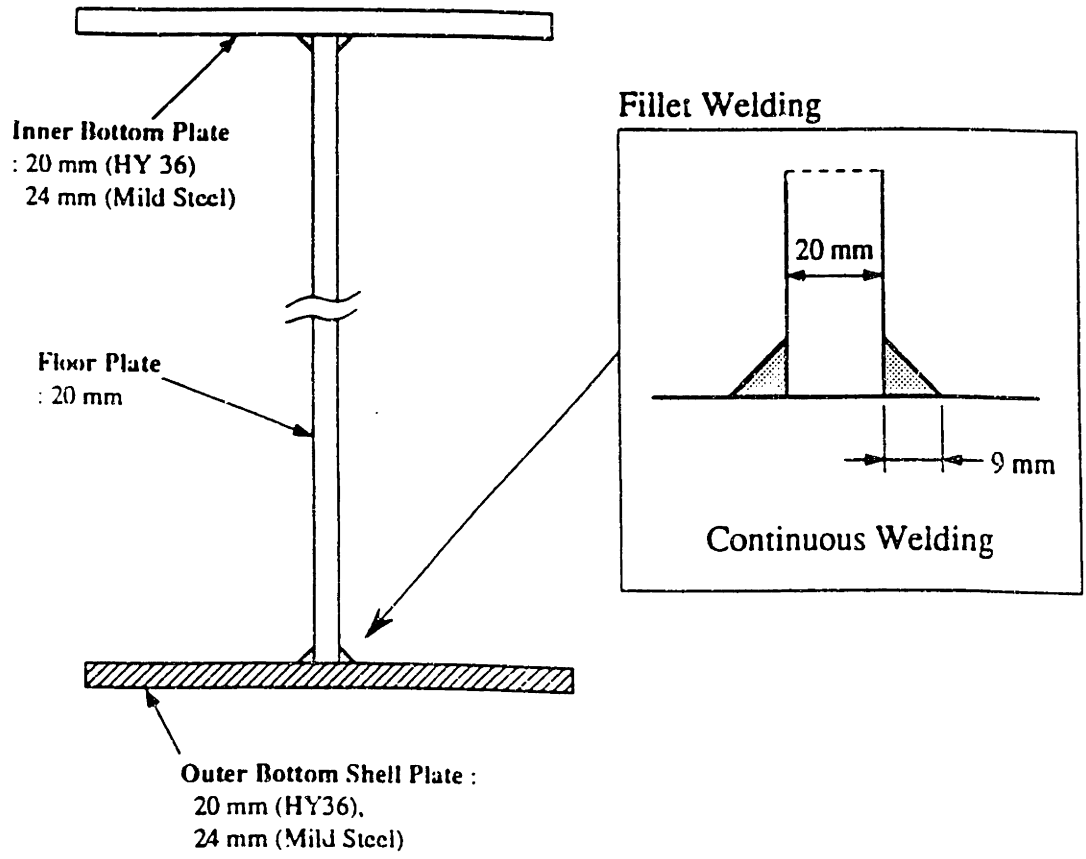

(2) Transverse Floor Plate

FIGURE 4.12a Details of Welding Designs for Double Hull Structures

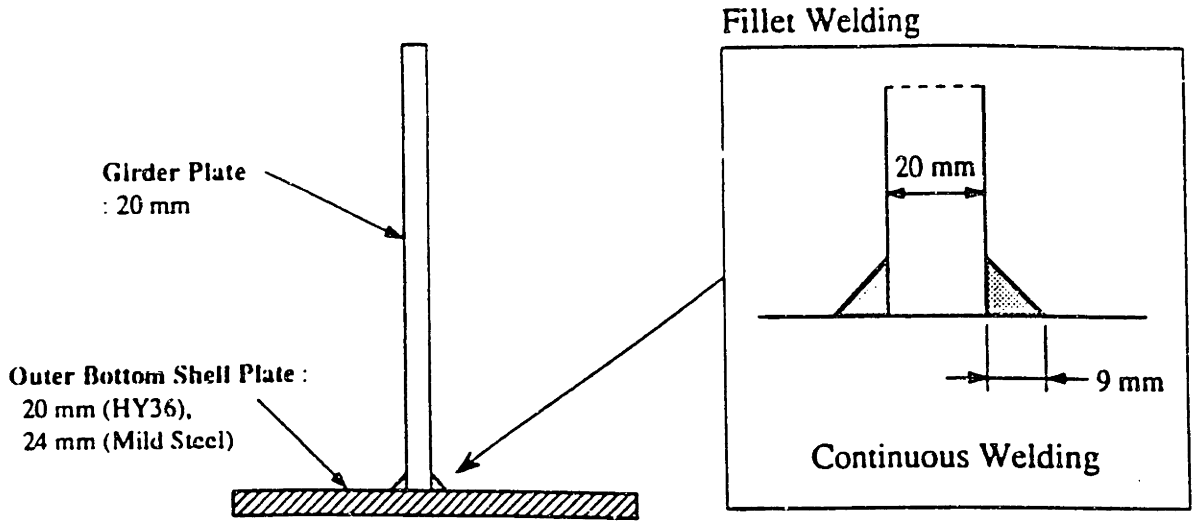

(3) Longitudinal Girder Plate

Note : Transverse Bulkhead Plates are also welded in the same way to the Bottom Shell Plate

FIGURE 4.12b Details of Welding Designs for Double Hull Structures

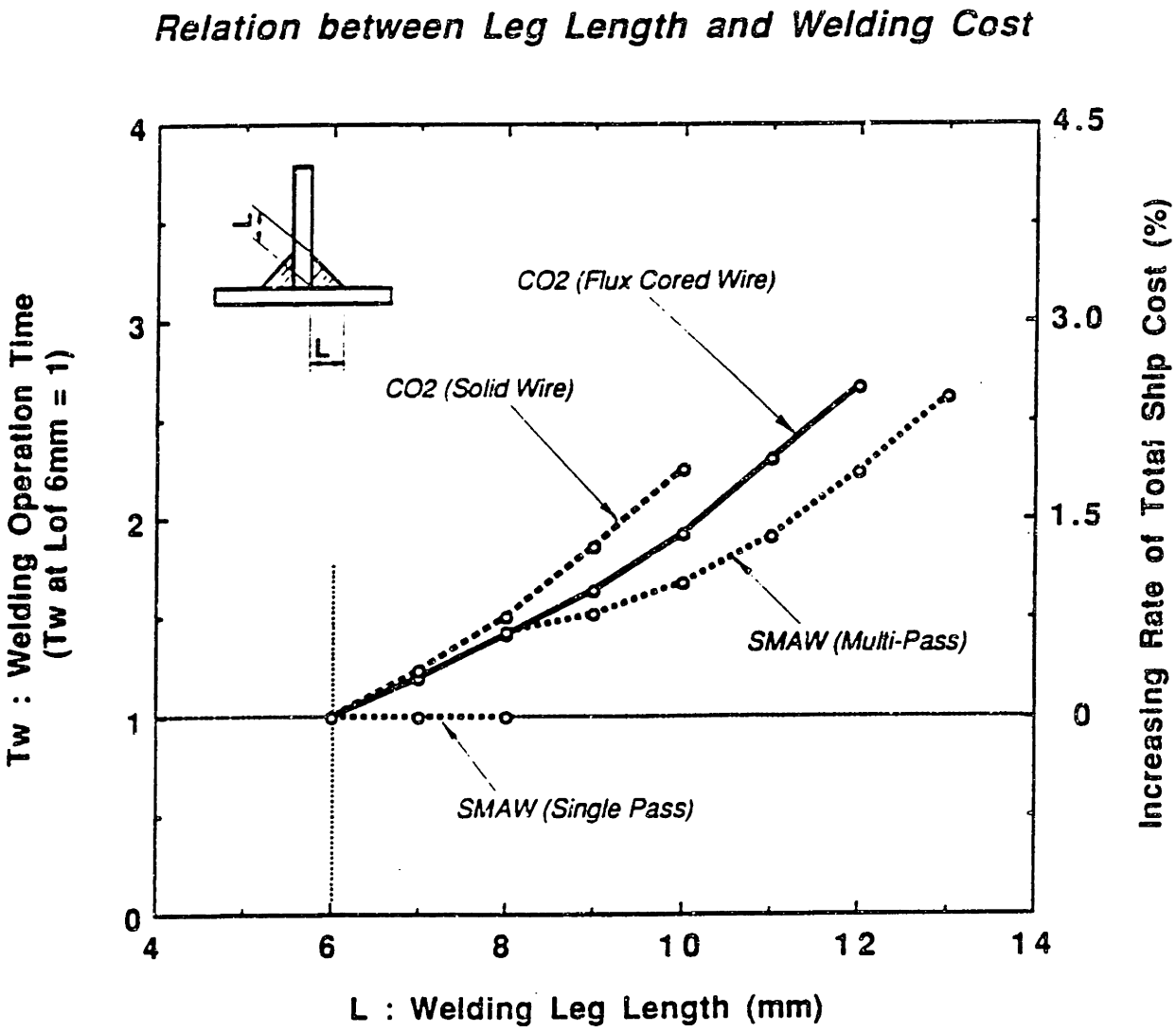

FIGURE 4.13 Relation Between Leg Length and Welding Cost

CHAPTER 5

CONCLUSIONS

1. The tearing of T-joints in tension (peeling) is sometimes observed in grounding of ships.

2. Predicting peeling requires knowledge of tearing work per unit length R and limit load P_L. R is the product of the limit load per unit length (P_L) times the critical steady state displacement (u_{CSS}).

3. A new type of laboratory-scale test of full-scale welds is presented for finding P_L and u_C or R_C, for quality control, and for testing design changes. A bend test (TWB test) on a beam with a transversely welded T-joint has been used to find limit loads and critical tearing work per unit length, R_C, under web tension. With sectioning of partially cracked specimens, this test can provide the critical displacement for crack initiation and growth in the weld.

4. The utility of upper bound limit load analysis is confirmed by consistency of test data with theoretical predictions (±3% for limit load P_L). The slip line also confirms that weld angles of 45° give the most limit load per unit weld length. With typical weld dimensions, the peeling of the base plate from the web can occur.

5. Scaling laws vary. Limit load scales with weld leg length (d). Critical steady state displacement u_{CSS} (=$(u_f+u_i)/2$) is the sum of displacements for crack initiation (u_i) and growth (u_f-u_i). u_i probably

depends only on metallurgical structure and gap size whereas (u_f-u_i) scales with leg length.

6. Peeling can be prevented if the welds are strong enough so that either

a) the base plate will go fully plastic before it can supply the critical tearing work per unit length to the weld, or

b) deformation due to web tension in the joint is shifted to the web, greatly increasing the tearing work per unit length.

7. For typical structures, strengthening the weld would first shift deformation to the web. Strengthening by increasing the size of the fillet weld seems to be less practical than slightly increasing the penetration (in spite of a small decrease in the weld tearing work per unit length).

8. The welding cost model developed for the purposes of analyzing the cost effects of increasing weld leg length along the bottom hull structure (longitudinal at shell plating) provided a first estimate of the magnitude of extra production expense associated with the strengthening of the hull for tearing resistance. Predicted production cost increases (using Weldcostmdl) approximate an upper limit at 80 000 $ for a 250 000 dwt Double Skin (hull) VLCC using the Flux Cored CO_2 process (equivalent upper limit for a similar Single Skin vessel is 60 000 $).

References

Atkins, A.G. & Mai, Y.W., (1985) "Elastic and Plastic Fracture", Ellis Horwood, West Sussex, England.

Avallone, E. A. and Baumeister III, T. "Mark's Handbook, 9th edition", McGraw-Hill.

Dowling, N. "Mechanical Behavior of Materials", Prentice Hall, p 410.

Drewry consultants, " Shipping Statistics and Economics", No 240, April 1993.

Guerra, A., and McClintock, F.A. (1994) " Upper Bounds to the Tensile Limit Loads of Cracked Welded T-joints, Report No. 28, Joint M.I.T.-Industry Project on Tanker Safety , M.I.T. Dept. of Ocean Eng.

Kardomateas, G.A. and McClintock, F.A. (1989) "Tests and Interpretation of Mixed Mode I and II, Fully Plastic Fracture from Simulated Weld Defects", Int. J. of Fracture v35.

Koga, S. (1994),"Slides on Ship Construction and Welding Processes in Japan", not published.

Masubuchi, K., Koga, S., and McDonald, H.A. (1993) " Present Status of V.L.C.C. Welding Procedures in Japan", Welding Systems Laboratory, M.I.T.

McClintock, F.A.,& Argon, A.S., eds., (1966) " Mechanical Behavior of Materials" Addison Wesley, Reading MA. Reprinted 1993 by Tech Books, Fairfield, VA.

McClintock, F.A. (1994) "Fully Plastic Fracture Mechanics for Welded T-joints", Joint MIT-Industry Consortium on Tanker Safety, Report #26.

McClintock, F.A., Masubuchi, K., andWang, X., (1993) "The peeling resistance of a T-joint with light fillet welds", A Brief Report for The International J ournal of Fracture.

McDonald, H.A., (1993) "Required Strength and Tear Resistance for Fillet Welds in Ships Exposed to Grounding or Collision Loads", M.S. Thesis, M.I.T. Dept. of Ocean Eng., May 1993.

Middaugh, G., (1994) "Hardness Tests Performed on E7016 Electrode Fillet Welds". No paper published, for test results see F.A. McClintock, M.I.T. Dept. of Mechanical Eng.

Nakamura, Y., (1994) "Quality Control System & Examples of Weldment Damage", in 'Special Report, Fourth Steering Committee Meeting, January 26&27 1994', Joint M.I.T.-Industry Project on Tanker Safety, M.I.T. Dept. of Ocean Eng.

National Research Council, "Tanker Spills, Prevention by Design", National Academy Press, 1991.

Shanley, F. R. (1946), " The Column Paradox", J. Aero Science 13, 768. see also "Inelastic Column Theory", J. Aero Science 14, 261-268.

Singer & Pytel , "Strength of Materials", 3rd Edition, Harper & Row Editors.

Yang, W.C, Roark, R.J., (1975) "Formulas for Stress and Strain", 4th Edition, New York.

APPENDIX A

"TWB" DETAIL DESIGN

APPENDIX A

"DESIGN OF THE TRANSVERSELY WELDED BEAM SPECIMEN"

A.1. INTRODUCTION

The transversely welded beam specimen illustrated in Fig.A1.1 simulates a standard T-joint. A pair of matching fillet welds join a stiffener (web) to the shell (base) plating. The loading applied to the specimen (Exhibit 1) induces a moment which at its maximum is defined as M_L, the limit moment, and occurs just prior to the onset of plastic deformation. ;

$$M_L = (P_{max}\ L / 2)(K_2 L - K_1 L) \qquad (A1.1)$$

M_L is the "uncracked limit moment" and occurs prior to or just after weld cracking. M_L is the highest moment the weld will carry. M_L and the limit load P_L are related as follows (Exhibit 1):

$$P_L = M_L\ (4 / L^2) \qquad (A1.2)$$

The above is based on a step-wise idealization of P_L along the weld length. McClintock, Masubuchi and Wang (1983) provide the following idealization based on slip line fields and crack growth estimates for a pair of fillet welds.:

$$P_{Lideal} = 2kd \qquad (A1.3)$$

where k is the material shear strength (approximated as 0.75X(Tensile Strength)) and d is the weld leg length of a 45^0 (Fig. A1.2). Using the above estimation of P_{Lideal} as the starting point for the specimen design we find that a 45^0 weld with a 6mm leg length will require an absolute load P_{max} ranging from 260 to 370 kN to initiate failure in a weld of length 162 mm. (Exhibit 2). Similarly, for a 9 mm 45^0 weld P_{max} ranges from 390 kN to 550 kN (Exhibit 3). In view of the fact that the maximum loads permissible on the available load frame (MTS 410 , 4 column) are of magnitude 446 kN , a shorter weldment length L' was selected so as to remain within the limits of the load frame.

Consequently, to accommodate load frame limitations while still allowing adequate weldment length so as to enable for eventual sectioning of the specimen and analysis of the crack tip zone, a weldment length of 89 mm length for a 9 mm weld leg length was selected. Furthermore, specimen lengths K_2L and K_1L were set at 324 mm and 102 mm to allow failure in the specimen as a consequence of P_{max} (Exhibits 2 and 3).

Having thus determined the basic dimensions of the " beam test " specimen, further analysis was carried out to confirm the specimen's suitability with respect to:

1. design of the surrounding test rig,

2. deflections, compliances and stability of the overall test rig,

3. bearing stresses,

4. local yielding,

5. edge effects ,

6. minimization of test rig size and weight.

A1.1.1 Design of the Test Rig

A test rig providing the specimen with the appropriate loading conditions for the four point bending nature of the test was designed to interface between the load frame and the specimen. (Fig. A1.3). The test rig components are as follows (Exhibit 4):

1. load applying beam,
2. load bearing beam,
3. specimen,
4. point loading bearings (4),
5. loading pads (8).

Figs. A1.4 and A1.5 provide additional specifications for the dimensions of the specimen and the associated weldments. It should be noted that both the load applying and load bearing beams are of standard cross section.

The specimen is cut from 20 mm thick LR-EH36 plating commonly used for shell plating and structural steel stiffeners in the

Korean shipbuilding industry. Additional material specifications for the plating are given in Exhibit 5.

Both the point loading bearings and the loading pads were procured with hardnesses of 60 HR_C to avoid local yielding at the points of contact based on the estimate of Exhibit 9 which predicts contact stresses on the order of 2310 N/mm^2 brought about by an expected 88 kN load on each bearing. Loading pads were used to distribute the loads along a larger area on the specimen , load applying beam and load bearing beam to avoid local yielding at the affected areas. Local yielding was undesirable for the following two reasons:

1. local yielding would reduce the point loading effect desired,
2. local yielding could adversely affect unloading compliance and loading stability characteristics of the test.

A1.1.2 Compliance and Stability Analysis of the Test Rig

For clarification purposes, the compliance C of the test rig can essentially be equated to the inverse of the stiffness K:

$$C = 1 / K \qquad \text{(A1.4)}$$

System stability is dependent on the compliances of the system components. In a test rig as set up for this experiment, compliance is

defined as (dv/dP) where dv is the incremental displacement generated along the loading axis and dP is the corresponding incremental change in loading. System stability can best be described with a circuit diagram analogy. Consider the circuit diagram of the load frame as shown in Fig.A1.6. A tensile force in the testing section of the machine (between the load cell and load frame base as shown in Fig. A1.3) will be defined as positive P_t . Equilibrium dictates that there be a corresponding reaction load of opposite sign in the load frame columns $P_r = -P_t$. For elastic elements, the deflection v is defined as the compliance times the load:

$$v = P\,C \tag{A1.5}$$

Compatibility requires that the total extension in the test section of the circuit including that due to the control setting extension v_c (setting for load cell actuator) and the equivalent negative extension due to bending at the weld v_w, should equal that in the load frame, piston and cylinder :

$$\delta(\Sigma\, C_t P_t + v_c + v_w) = \delta(\Sigma\, C_r P_r) \tag{A1.6}$$

Noting that $P_r = -P_t$ (equilibrium) and that the overall deflection of all spring elements is denoted by v_s , we rewrite A1.6 as follows:

$$\delta((\Sigma\, C_t + \Sigma\, C_r)\, P_t + v_c + v_w) = \delta(v_s + v_c + v_w) = 0 \tag{A1.7}$$

$$\text{or } v_c = -(v_w + v_s)$$

The corresponding graphical representation is illustrated in Fig.A1.7. It should be noted that in the limiting case of very stiff springs, v_w would follow the control command v_c and the test would be stable. For softer springs, a point is reached where crack growth at the weld will occur with no input from the control command. Any softer springs will lead to instability. This is best illustrated by following the straight line on the P_w - v_w curve (Fig A1.7) corresponding to a constant control setting. In this situation, the testing machine applies more force to the specimen weld than needed to continue stable growth , and the system becomes unstable. This unstable scenario can be visualized in Fig. A1.8 (typical load displacement diagram from testing machine). On a load displacement diagram as typically encountered during similar tests, instability can be observed by a sharp drop in the test loading (as observed on the machine display) which can often be followed by catastrophic failure of the specimen. To avoid such a situation, the testing machine is set to a displacement controlled (versus load controlled) loading mode acting through a ramp function setting.

During the design of the specimen, special attention was thus devoted to the avoidance of instability. The stability analysis was based on a specimen with a standard 6 mm leg 45° weld. The unknown terms in equation A1.7 for the purposes of the analysis were ΣC_t and v_w, with C_r (compliance of the load frame)being

obtained from the load frame manual and from load displacement unloading curves (Fig A1.9). Considering the system at equilibrium (setting $v_c = 0$) and rewriting v_w as $v_w = C_w P_t$,we can rewrite A1.7 as:

$$(\Sigma\ C_t + C_r + C_w)P_t = 0 \qquad \text{(A1.9)}$$

or for stability

$$C_w \leq \Sigma\ C_t + C_r$$

where C_r is obtained from the test machine manual and

$$\Sigma\ C_t = C_{\text{Load Applying Beam}} + C_{\text{Load Bearing Beam}} + C_{\text{Specimen.}} \qquad \text{(A1.10)}$$

It should also be noted that the compliances of the point loading bearings and loading pads were assumed to be negligible .

A1.1.2.1 Evaluation of Total Compliance $\Sigma\ C_t$

The following analysis is based on the previously selected I-beams (Exhibit 4). Although for the preliminary analysis, larger I-beams were chosen, re-design of the test rig to reduce the overall weight resulted in the selection of the 254 mm depth ($I = 5.1 \times 10^7$ mm^4) beam. The iterations will not be presented here since they do not contribute to the analysis, suffice it to say all calculations performed and illustrated here are based on the 254 mm depth.

Annex 1A provides the sample calculation performed for obtaining ΣC_t. Σ C_t was evaluated to be 2.7 x 10^{-6}mm/n.

A1.1.2.2 Evaluation of Load Drop per Unit Deflection of Test Machine due to Weld, C_w

The fully plastic limit moment of a pair of fillet welds with shear strength k (equivalent to 0.75 x Tensile Strength of weld material - E 7016 electrode)., leg length d (45°), and weld length L, after crack growth from one end by a distance a, is given by:

$$M = 2kd(L-a)^2/4. \qquad \text{(A1.11)}$$

Given a bend test with the geometry as depicted in Fig.A1.10a and using a small angle approximation , the following relation is obtained:

$$\theta = 2v / [(K_2 - K_1)L] . \qquad \text{(A1.12)}$$

From equation A1.11, the uncracked limit moment M_L(at a = 0) is:

$$M_L = kdL^2 / 2 . \qquad \text{(A1.13)}$$

The moment as resulting at the weld (Fig.A1.10b) is consequently as follows:

@ weld (point A in Fig. A1.10b)

$$M = P\ (L/2)(K_2 - K_1) \qquad \text{(A1.14 a)}$$

$$M_L = P_L\ (L/2)(K_2 - K_1) \text{ where } P_L = P_{max} \qquad \text{(A1.14 b)}$$

From McClintock's relation of crack length to bend angle (Appendix E, equation A.11), we obtain the following:

$$M = M_L\ (\theta_c / \theta)\ . \qquad \text{for } \theta \geq \theta_c \qquad \text{(A1.15)}$$

and where (θ_c) is the critical bend angle at crack initiation and is given by:

$$(\theta_c) = u_c / (L/2)\ . \qquad \text{(A1.16)}$$

Combining A1.14, A1.15, and A1.16, we are able to convert the moment-bend angle relation (Fig. A1.11) to a load deflection relation as follows:

$$P = [\ P_L u_c(K_2 - K_1)] / v\ , \qquad \text{(A1.17)}$$

thus giving the following relationship

$$dP / dv = -\ [\ P_L u_c(K_2 - K_1)] / v^2. \qquad \text{(A1.18)}$$

Since we are concerned with the test stability limit state , we want the value of dP/dv at the steepest slope (Fig. A1.11) ,

essentially at $(\theta / \theta_c) = 1$. At this point, the following is true (combining equations A1.12 and A1.16):

$$v = u_c (K_2 - K_1). \qquad \text{(A1.19)}$$

Inserting A1.19 into A1.18, we obtain

$$(dP / dv)_{weld} = - P_L / [u_c (K_2 - K_1)] . \qquad \text{(A1.20)}$$

From A1.19 and A1.20 , at the limit state (a=0) we obtain

$$P_L = kdL / (K_2 - K_1) . \qquad \text{(A1.21)}$$

A1.21 can be rewritten to obtain the load drop per unit deflection of testing machine due to the weld C_W as follows;

$$C_W = (dv / dP)_{weld} = [-u_c (K_2 - K_1)^2] / kdL. \qquad \text{(A1.22)}$$

A1. 22 can be rewritten as follows (assuming as an initial guess that $u_c = d/2$):

$$(dv/dP)_{weld} = - (K_2 - K_1)^2 / 2kL \qquad \text{(A1.23)}$$

Estimation of weld compliance using equation A1.23 (Exhibit 6) $(dv/dP)_{weld}$ ranging from 1.11 - 1.58 x 10^{-5} mm/N (based on a range for k of 70 000 psi to 100 000 psi for E 7016 electrode).

A1.1.2.3 Load Frame Compliance C_r

The load frame compliance for the MTS 410 is obtained from the user's manual and is given as 9.5 x 10^{-7} mm/N. This value is not exact in that load frame compliance is slightly non-linear and is a function of cross-head and load cell piston position. During the actual experimental phase, load frame and specimen compliance can be obtained by loading and unloading the specimen and analyzing the curve slope.

A1.1.2.4 Conclusions On Test Stability

Adding C_t and C_r results in a compliance of the order of 3.70 x 10^{-6} mm/N. Comparatively, the weld compliance C_w ranges from 1.11-1.58 x 10^{-6} mm/N. These initial estimates indicate a test bordering on instability, however taking into account the conservative assumptions formulated for the weld (u_c = d / 2 whereas a more accurate assumption would be d/6 or smaller) compliance analysis and for the test rig compliances, it was rightfully assumed that the tests would remain stable.

The degree of instability was sacrificed to obtain better weight savings in order to allow easier handling of the test rig and specimen. It should also be noted that other modes of deflection were analyzed as possible complimentary causes of increased compliance (shear deflection, Exhibit 7), these were however found to be of lower order than the primary deflection mode analyzed in this study.

A1.1.3 Design Requirements For Bearing Stresses and Deflection

During the design of the Point Loading Bearings and Loading Pads, a key area of concern was the maintenance of bearing stresses to within tolerable limits. It was clearly identified early in the process that both the Point Loading Bearings and the Loading Pads would require to meet a hardness threshold of 60 HR_C (Exhibit 8) to sustain without deformation the loads applied (of magnitude 176 000 N - 80 000 psi based on the limit load analysis). Consequently, a bearing stress analysis was carried out to ensure that adequate provisions were made. The 64 mm length of the bearings (and width of the loading pads) was derived from the bearing analysis (in order to provide a linear distributed load of acceptable magnitude on the bearing). Exhibit 8 provides the sample calculations of this analysis.

The next step in the analysis of the reaction mechanisms between the bearing and support plate is the analysis of the relative deflections between the two bodies. This issue was of special concern in the region where both extremities of the Loading Pads overhang the single thickness portion of the beam specimen (Fig. A1.12). The Loading Pad is subjected to a deflection (δ_1), and the bearing to a deflection (δ_2). The concern here is to maintain (δ_2) > (δ_1) so as to maintain the approximately linear load distribution on the bearing thus avoiding point loading (which would result in local yielding and deformation). The calculations for (δ_1) and (δ_2) are shown in Exhibit 9 and indicate a favorable pattern of deflection where (δ_2) > (δ_1). Furthermore, these calculations were performed

using conservative values for Poisson's ratio (ν) and the Elastic Modulus (E) thus yielding greater deflections than expected for material of the specified hardness (HR_C 60).

A1.1.4 Estimates of Local Yielding Between Pads and Bearings

Local yielding was an other issue of interest since excessive yielding in any one area can modify the deflection patterns of the test rig. The primary area of concern was the loading line between the bearing and the pad since the stresses carried through from the pads to the specimen and Load Bearings/Applying Beams are distributed there. The local load per unit area was of concern due to the dissimilarity in material yield stresses. The primary aim of the analysis was to ensure that the linear distributed loading would not cause yielding at the line of contact (Exhibit 10). Having confirmed that the magnitude of local yielding would be negligible (2.54×10^{-6} mm), the analysis was concluded.

A1.1.5 Edge Effects

To avoid potential edge effects between the welds and the edge of the single thickness plate (simulating a stiffener), a distance of two plate thicknesses (40 mm) was left between the weld extremity of the plate. This excess was also meant to allow for a smooth hinging action between the double and single thickness halves of the beam specimen.

A1.1.6 Minimization of Test Rig Weight

Overall test rig size and weight were a concern for the following reasons:

1. lack of availability of load frames of greater capacity (than 50 Tons),
2. safety and ease of handling.

The overall test rig weight amounted to approximately 105 kg. Individual component weights are as follows:

1. Load Applying Beam - 29 kg,
2. Load Bearing Beam - 43 kg, and
3. Specimen - 32 kg.

These dimensions and weights were established based on previously discussed constraints associated with stability, compliance, bearing stresses, and localized yielding.

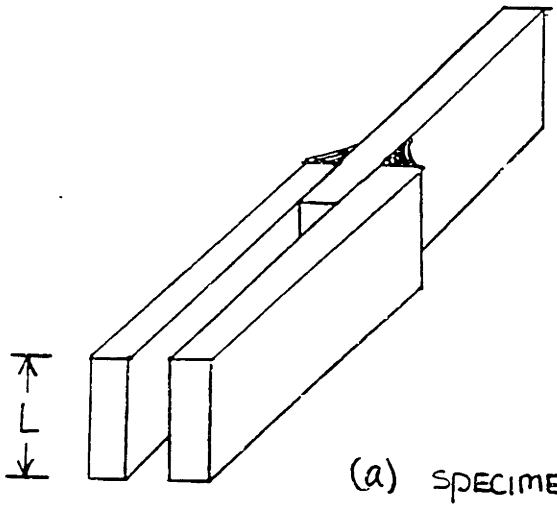

(a) SPECIMEN GEOMETRY

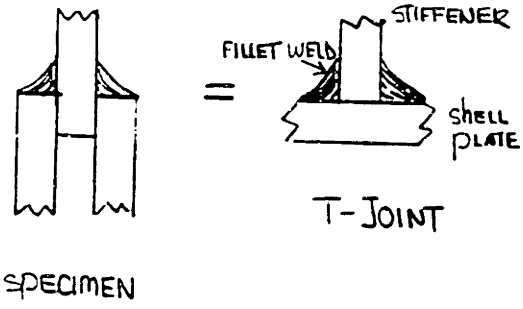

(b) SPECIMEN SIMULATION OF T-JOINT

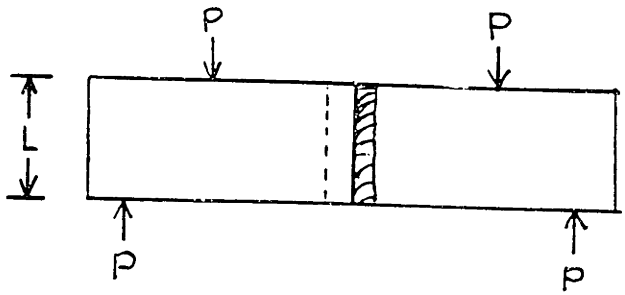

(c) LOADING ON TEST

FIGURE A1.1

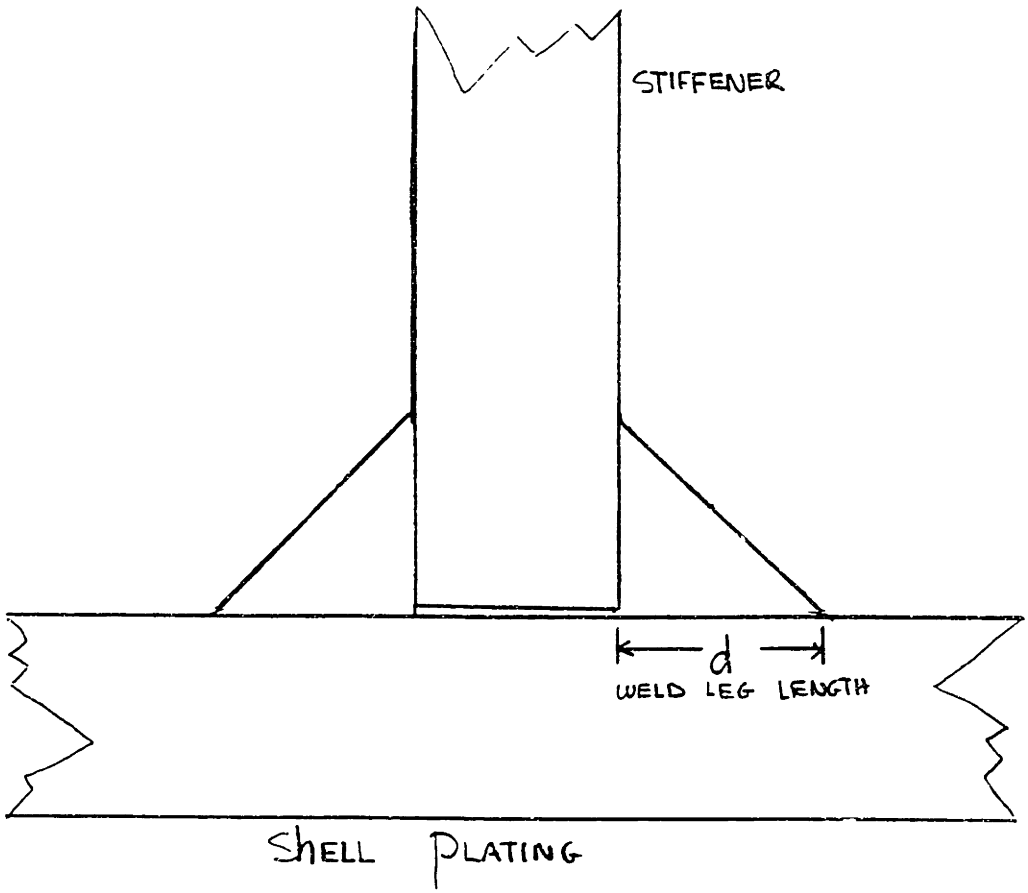

FIGURE A1.2

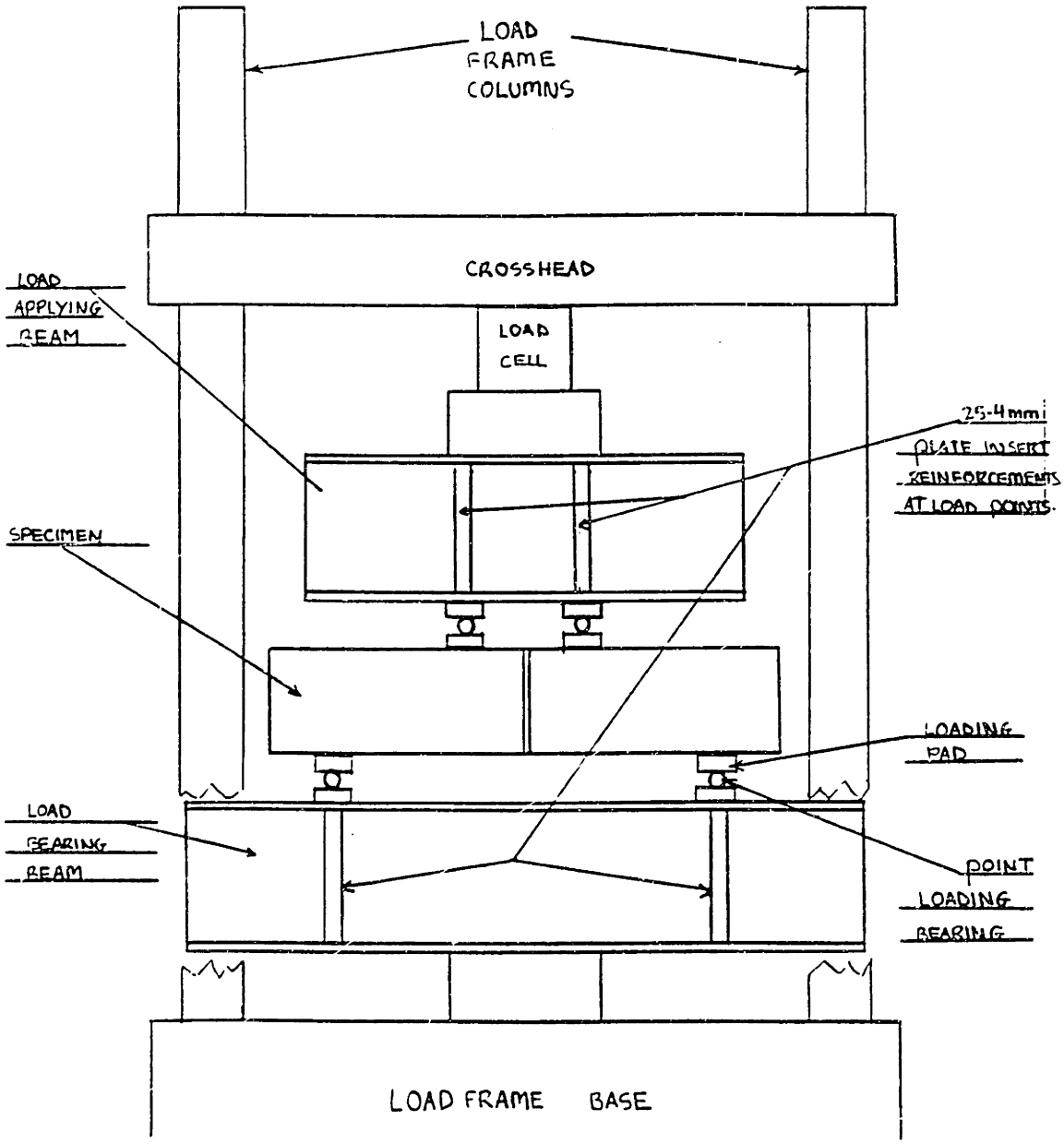
LOAD
FRAME
COLUMNS
CROSSHEAD
LOAD
APPLYING
BEAM
LOAD
CELL
25·4mm
PLATE INSERT
REINFORCEMENTS
AT LOAD POINTS
SPECIMEN
LOADING
PAD
LOAD
BEARING
BEAM
POINT
LOADING
BEARING
LOAD FRAME BASE

FIGURE A1.3

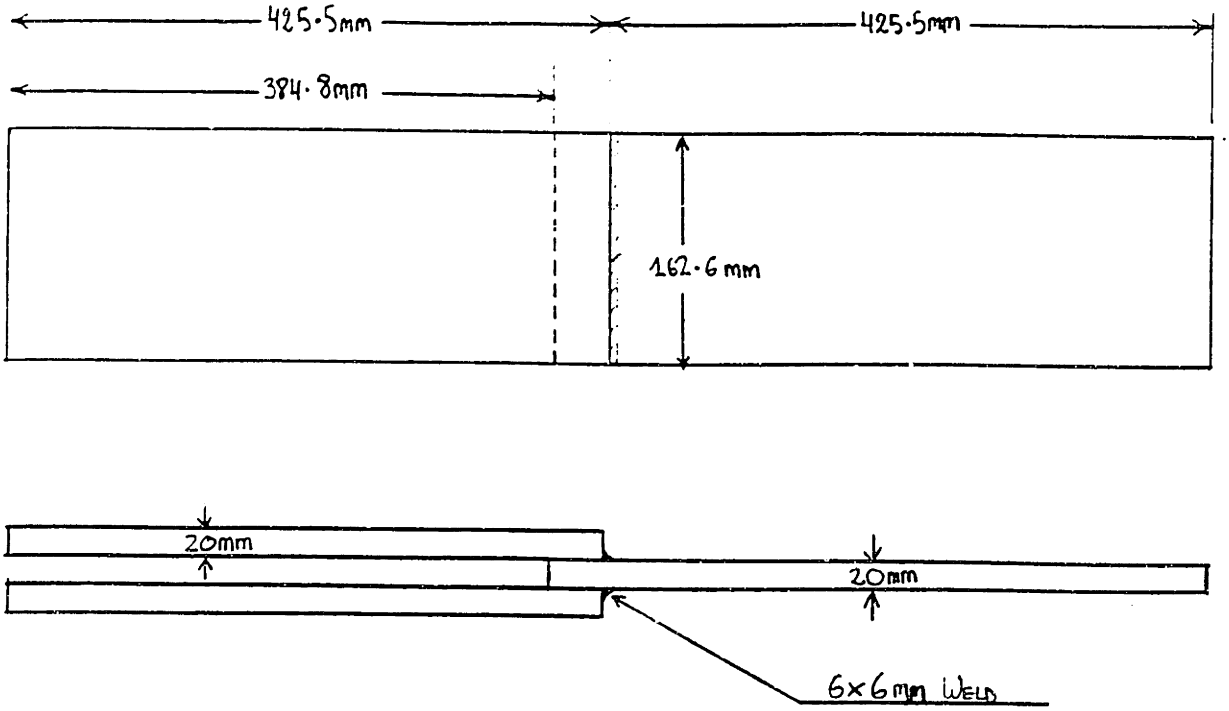

NOTE: TOLERANCES ON ALL DIMENSIONS: ± 0.4 mm ($\pm \frac{1}{64}$")

① For 9mm x 9mm WELDMENT this DIMENSION IS 88.9 mm

FIGURE A1.4

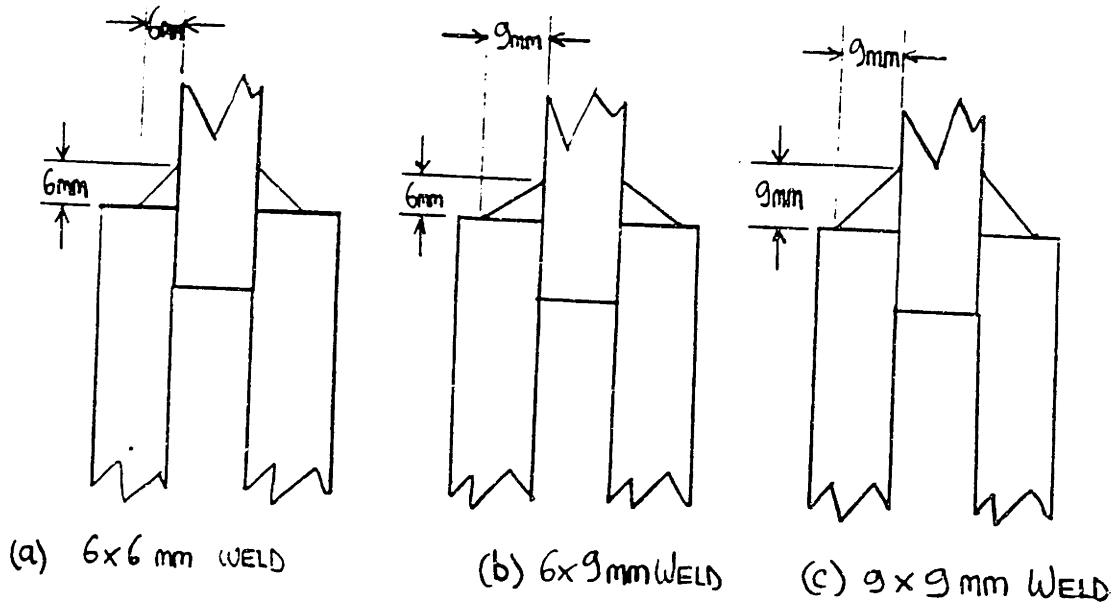

FIGURE A1.5

INTENTIONALLY LEFT BLANK.

FIGURE A1.6

INTENTIONALLY LEFT BLANK.

FIGURE A1.7

INSTABILITY OF SPECIMEN

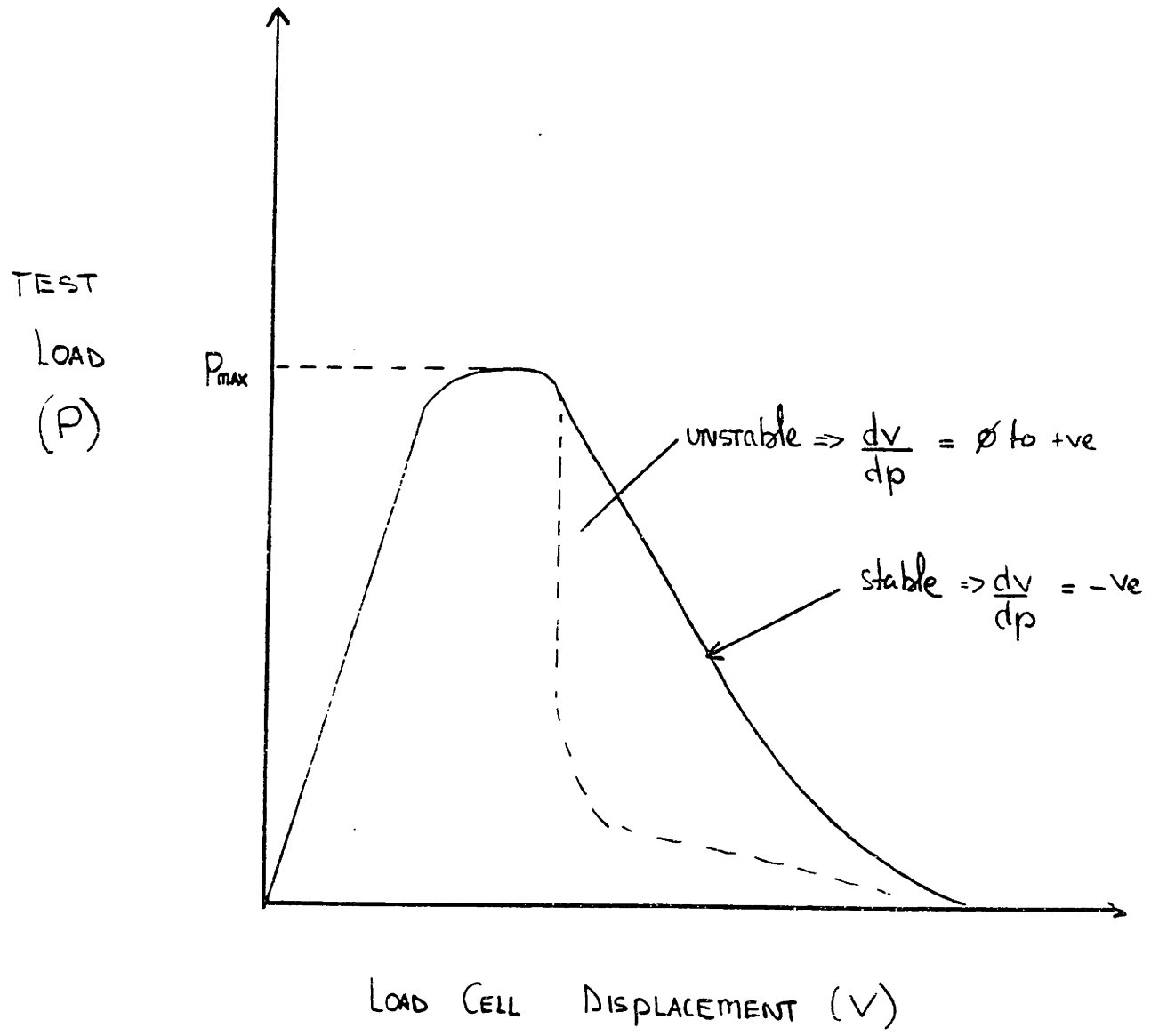

Note: IN UNSTABLE SCENARIO CRACK GROWTH IS UNCONTROLLED

FIGURE A1.8

·INTENTIONALLY LEFT BLANK·

FIGURE A1.9

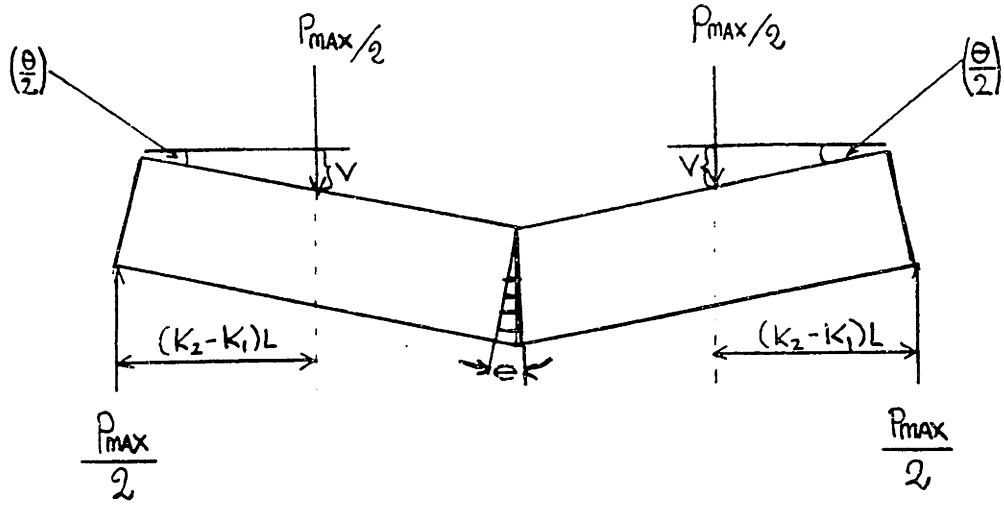

(a). OVERALL GEOMETRY

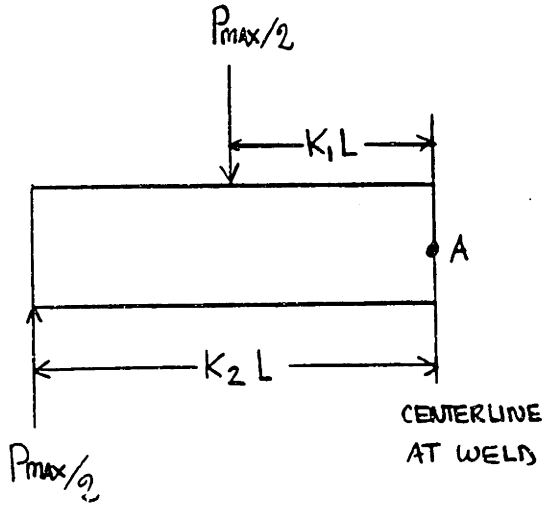

(b). HALF SECTION

FIGURE A1.10

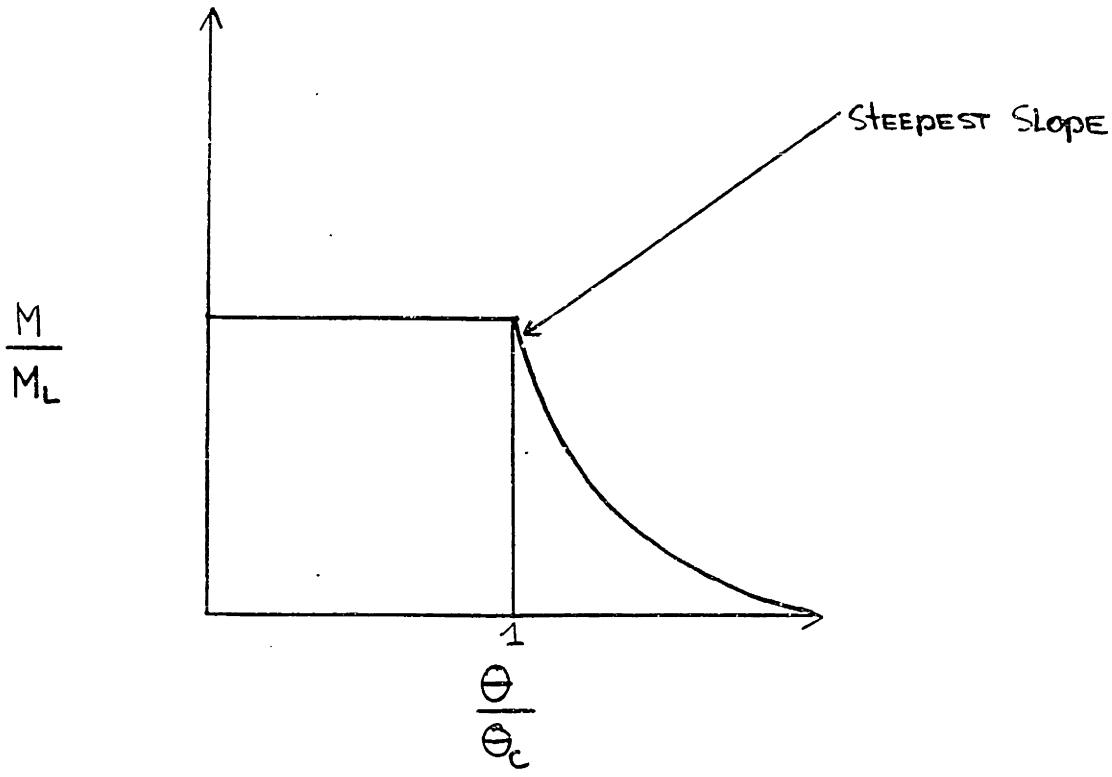

FIGURE A1.11

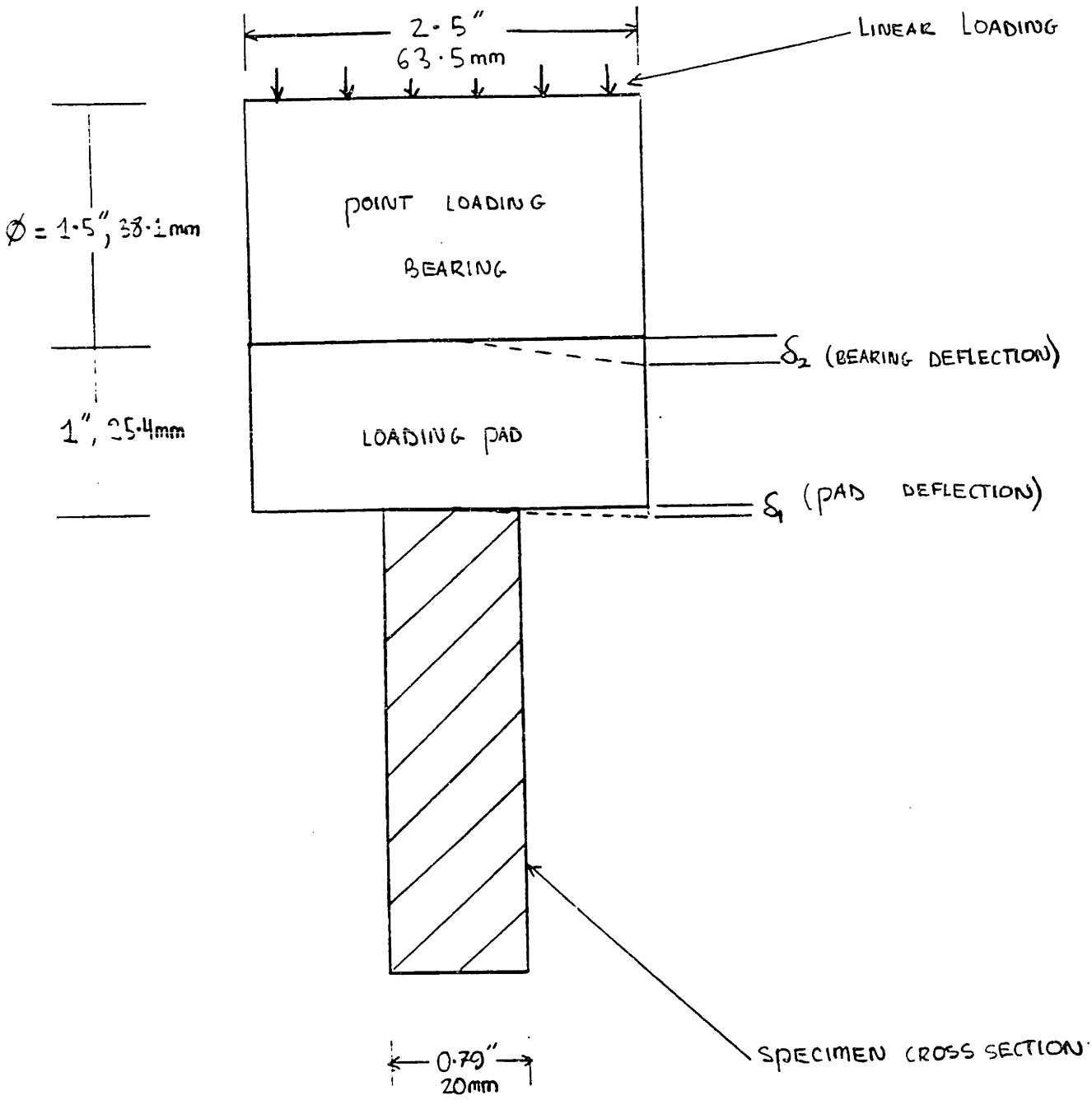
2·5"
63·5mm
LINEAR LOADING
Ø = 1·5", 38·1mm
POINT LOADING
BEARING
δ2 (BEARING DEFLECTION)
1", 25·4mm
LOADING PAD
δ1 (PAD DEFLECTION)
0·79"
20mm
SPECIMEN CROSS SECTION

FIGURE A1.12

EXHIBIT 1: LOADING OF "BEND TEST" SPECIMEN (IDEALIZATION)

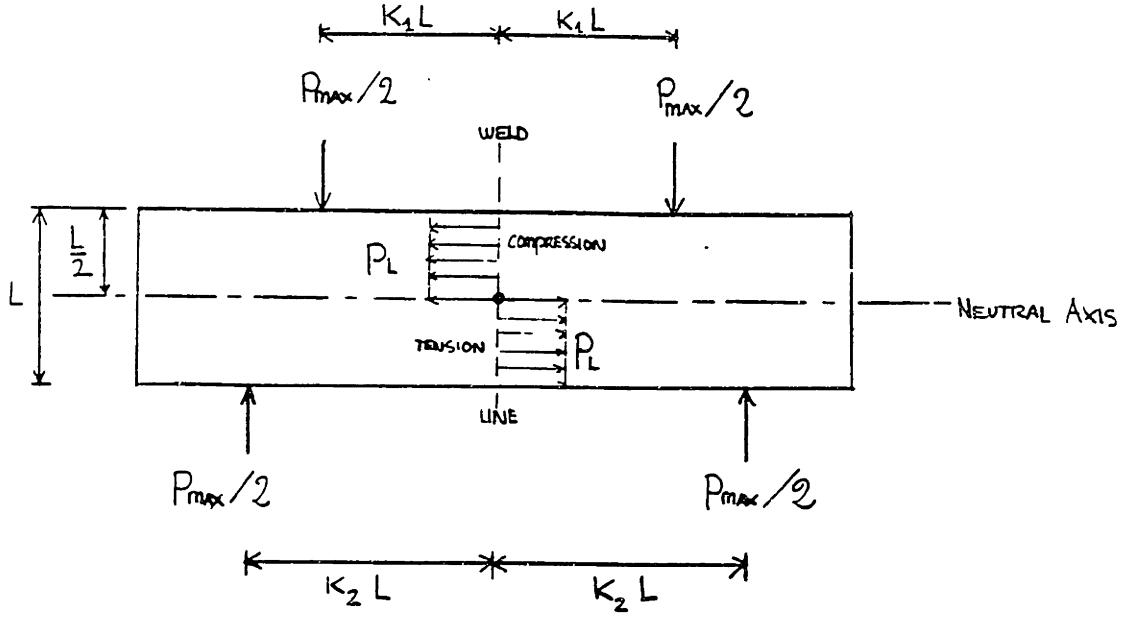

P_{MAX} = MAXIMUM COMPRESSIVE LOAD APPLIED BY TESTING MACHINE

L = WELDMENT LENGTH

P_L = LOAD / UNIT LENGTH (TRAPEZOIDAL LOADING IDEALIZATION) APPLIED TO WELDMENT

K_1 = SCALING CONSTANT

K_2 = SCALING CONSTANT

EXHIBIT 1

Exhibit 2: Estimated range of limit loads for a 6mm Leg length symmetric pair of fillet welds (E7016 electrodes)

Given: Tensile strength for E7016 Electrode Ranges from 70 000 to 100 000 $\frac{lb}{in^2}$ (483.8 to 691.1 $\frac{N}{mm^2}$)

a] $P_{L\,IDEAL\,(MIN)} = 2\,K_{MIN}\,d$ (A3).

$= 2\,(0.75)\left(483.8\ \frac{N}{mm^2}\right) 6mm$

$= 4354.2\ N/mm$

b] $P_{L\,IDEAL\,(MAX)} = 2\,K_{MAX}\,d$

$= 2(0.75)\left(691.1\ \frac{N}{mm^2}\right) 6mm$

$= 6219.9\ N/mm$

From A2 & A1, assuming a weld length L = 162 mm, K_2 = 324mm, K_1 = 102mm.

$$P_L\left(\frac{L^2}{4}\right) = M_L = \frac{P_{MAX}\,L}{2}\cdot(K_2 - K_1)$$

such that.

$$P_{MAX} = \frac{P_L\left(\frac{L}{2}\right)^2 \times (2)}{L\,(K_2 - K_1)}$$

For: $P_{L\,IDEAL\,(MIN)}$, $P_{MAX\,(MIN)} \cong 257\,369\ N$ (57 718 lb)

$P_{L\,IDEAL\,(MAX)}$, $P_{MAX\,(MAX)} \cong 367\,647\ N$ (82 449 lb)

EXHIBIT 2

Exhibit 3: Estimated range of Limit Loads for a 9mm leg Length symmetric pair of fillet welds (E 7018).

Given: Same as exhibit-2

a] $p_{L_{IDEAL(MIN)}} = 6531.3$ N/mm

b] $p_{L_{IDEAL(MAX)}} = 9329.9$ N/mm

For; $L = 162$ mm, $K_2L = 324$ mm, $K_1L = 102$ mm

$P_{MAX_{(MIN)}} \cong 386\,053$ N (86 578 lb)

$P_{MAX_{(MAX)}} \cong 551\,472$ N (123 676 lb)

For; $L' = 89$ mm, $K_2'L' = 324$ mm, $K_1'L_1' = 102$ mm

$P_{MAX_{(MIN)}} \cong 116\,519$ N (26 131 lb)

$P_{MAX(MAX)} \cong 166\,446$ N (37 328 lb)

EXHIBIT 3

EXHIBIT 4: SPECIMEN & TEST RIG SPECIFICATIONS

1. LOAD APPLYING BEAM (I-BEAM)

- DEPTH: 254 mm (10")
- FLANGE: 118.4 mm (4.66")
- SECTION AREA: 4761.3 mm^2 (7.38 m^2)
- WEIGHT: 37.0 $\frac{kg}{m}$ (25.4 $\frac{lb}{ft}$)
- MOMENT OF INERTIA: $5.09 \times 10^7 mm^4$ ($122.4 m^4$)
- LENGTH: 762 mm (30")

- I-BEAM REINFORCED AT 101.6 mm EITHER SIDE OF MIDLENGTH POINT WITH 25.4 mm (1") THICK PLATE (SEE FIGURE 3)
- MATERIAL: STRUCTURAL STEEL

2. LOAD BEARING BEAM (I-BEAM)

- SAME BEAM SPECIFICATIONS AS LOAD APPLYING BEAM WITH EXCEPTION OF LENGTH & LOCATION OF REINFORCING INSERTS

- LENGTH: 1143 mm (45")
- REINFORCEMENT INSERTS CENTERED AT 324 mm EACH SIDE OF MIDLENGTH POINT (SEE FIGURE 3)

3. SPECIMEN

- BASE PLATE, LR-EH36, YP 40.6 $\frac{KG}{mm^2}$, TS 57.4 $\frac{KG}{mm^2}$
- (FOR MORE INFORMATION SEE Exhibit 5)
- THICKNESS OF PLATE: 20 mm
- SPECIMEN DIMENSIONS: SEE FIGURE 4.
- WELDING ELECTRODE: E 7016

4. POINT LOADING BEARINGS

- 38.1 mm DIAMETER ($1\frac{1}{2}$")
- LENGTH: 63.5 mm (2.5")
- HARDENED TO ROCKWELL C 60

5. LOADING PADS

- A-2 STEEL HEAT TREATED TO ROCKWELL C 60
- DIMENSIONS: 63.5 mm x 63.5 mm x 25.4 mm ($2\frac{1}{2}$" x $2\frac{1}{2}$" x 1")

EXHIBIT 5

122

계약번호 CONTRACT : SPPA12AB

주문번호 ORDER NO : STOCK

품명 COMMODITY : PLATE

제품규격 SPECIFICATION : LR-EH36

품질검사증명서 MILL TEST CERTIFICATE

포항종합제철 POHANG IRON & STEEL CO. (POHANG WORKS)

수요가 CUSTOMER : H.M.D LTD.CO.

공급자 SUPPLIER : H.M.D LTD.CO.

증명서번호 CERTIFICATE NO : 92-PP-0504-03

발행일자 DATE OF ISSUE : MAY. 04. 1992

G:GOOD

제품치수 DIMENSIONS	수량 Quantity	중량 WEIGHT (KG)	제강번호 CHARGE NO	제품번호 PRODUCT NO	인장시험 TENSILE TEST 방향	시험편	항복강도 YP KG/MM²	인장강도 TS KG/MM²	연신율 EL %	충격시험 IMPACT (V) NOTCH 방향	시험편	흡수에너지 ENERGY -40°C KG-M	전단면적 SA %	열처리 HEAT TREATMENT	C 3	Si 2	Mn 2	P 3	S	SAL 3	Cu 2	Nb 3	V 3	Ni 2	Mo 2	Cr 2
1X2400X12000	1	4,746	Y800505	9493402	T	C A	40.6	57.4	23	T	L	A3 7.9		N	170	38	140	16	7	45	30	3	52	20	TR	2
** $PECIMEN NO : TENSION ==>		5949361		IMPACT ==>			5949341																			
*** SUB TOTAL (020)***		1		4,746 (KG)																						
** HEAT TREATMENT **																										
NORMALIZING ===> 890 DEG C X 37MIN																										
*** GRADE TOTAL ***		1		4,746 (KG)																						
*** GRAND TOTAL ***		1		4,746 (KG)																						

=== LAST ITEM ===

ORIGINAL

NOTE: POSITION T:TOP, M:MIDDLE, B:BUTTOM DIRECTION L:LONGITUDINAL, C:CROSSWISE, Z:THICKNESS GL (GAUGE LENGTH) RECTANGULAR (A:200mm, B:C:100mm, D:60mm, E:5.65√A) ROUND (F:50mm, G:70mm, H:5.65√A) IMPACT SUB-SIZE 1:2.5mm, 2:3.3mm, 3:5.0mm, 4:7.5mm SA SHEAR AREA UST ULTRASONIC TEST HEAT TREATMENT N:NORMALIZED, Q:QUENCHED, T:TEMPERED, PILAC:POSCO IN LINE ACCELERATED COOLING, DQ:DIRECT QD CR:CONTROLLED ROLLED DIVISION C:CHECK ANALYSIS, L:LADLE ANALYSIS SAL Sol-Al TAL Total-Al

(CALCULATION of ESTIMATED VALUE FOR $\mathbb{C}_\omega$)

given: $(K_2 - K_1) = 1.366$

$k = 0.75\,TS$

TS range for E7016 = 70 000 psi to 100 000 psi

$L = 6.4''$

$$\mathbb{C}_\omega = \frac{dV}{dp} = \frac{-(K_2 - K_1)^2}{2\,k\,L}$$

$$\mathbb{C}_{\omega_{mm}} = 2.78 \times 10^{-6} \frac{m}{lb} = 1.58 \times 10^{-5} \frac{mm}{N}$$

$$\mathbb{C}_{\omega_{MAX}} = 1.94 \times 10^{-6} \frac{m}{lb} = 1.11 \times 10^{-5} \frac{mm}{N}$$

EXHIBIT 6

(DEFLECTION ASSOCIATED TO SHEAR DEFORMATION)

GIVEN: LOAD BEARING BEAM

HALF LENGTH : $K_2 L = 12.75'' \cong 324\,mm$

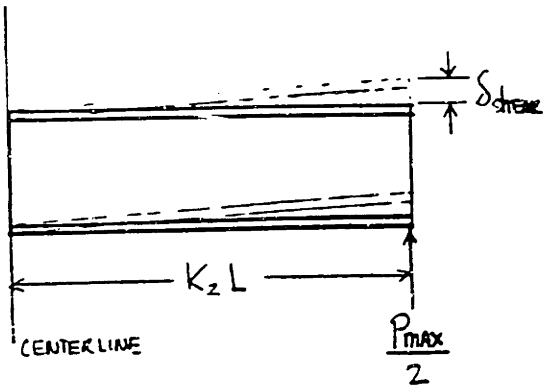

$$\delta_{SHEAR} = K_2 L\, \gamma$$

where: $\gamma = \frac{\tau}{G} = \frac{[(P_{MAX}/2)/(\text{X-SECTION AREA})]}{G}$

and : $G = \frac{E}{2(1+\nu)}$

FOR : $E = 30\times10^6 psi = 2.14\times10^5\ N/mm^2$

$\nu = 0.3$

$G = 11.54\times10^6 psi = 7.98\times10^4\ N/mm^2$

$A_{xSECTION} = 7.38\ m^2 = 4761\ mm^2$

$P_{MAX} = 80\,000\,lb = 176\,000\ N$

$$\tau = \frac{(P_{MAX}/2)}{A_{x\,SECTION}} = 5420\ \frac{lb}{in^2} = 37.5\ \frac{N}{mm^2}$$

$$\gamma = \frac{\tau}{G} = 4.70\times10^{-4}$$

$$\delta_{shear} = \gamma \cdot K_2 L = 5.99\times10^{-3}\ inches = 1.52\times10^{-1}\ mm$$

$$C_{shear} = \frac{\delta_{shear}}{P_{MAX}} = 7.49\times10^{-8}\ \frac{IN}{lb} = 4.27\times10^{-7}\ \frac{mm}{N}$$

(Bearing Stress Analysis for point Loading Bearings)

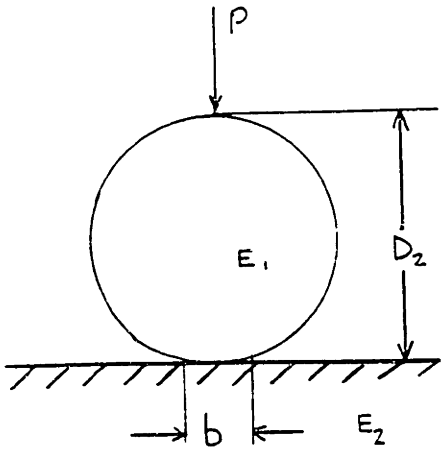

ASSUMPTIONS:

- CYLINDER of LENGTH L Large as compared with D; p = load per linear in = $\frac{P}{L}$
- $E_1 = E_2$, $\nu_1 = \nu_2 \simeq 0.3$

FORMULAS: (10)

$$b = 2.15\sqrt{\frac{p K_D}{E}}$$

Maximum Compressive Stress σ_c:

$$\text{MAX } \sigma_c = 0.591\sqrt{\frac{p E}{K_D}}$$

=> FOR a CYLINDER ON A FLAT PLATE: $K_D = D_2$

=> GIVEN:

$K_D = D_2 = 1.5'' = 38.1$ mm
$L = 2.5'' = 63.5$ mm
$E \cong 30 \times 10^6$ PSI $= 2.14 \times 10^5$ N/mm²
LOAD (PER BEARING) = 40 000 lb = 88 000 N = P

$$p = \frac{P}{L} = 16\,000 \text{ lb/m} = 2310 \text{ N/mm}$$

$$\text{MAX } \sigma_c = 334.32 \times 10^3 \text{ PSI} = 2.31 \times 10^3 \text{ N/mm}^2.$$

1. NOTE: that FOR MATERIAL at R_c 60, $\sigma_{yield} \simeq 340 \times 10^3$ PSI (2.35×10^3 N/m

∴ WE ARE IN AN ACCEPTABLE RANGE

2. NOTE- $\sigma_c = 2.31 \times 10^3$ N/mm² IS AN EXTREME UPPER boundary in View of the fact that E for the R_c 60 material is lower than 30×10^6 psi

EXHIBIT 8

(Relative Deflections between point loading Bearing & Bearing Pad

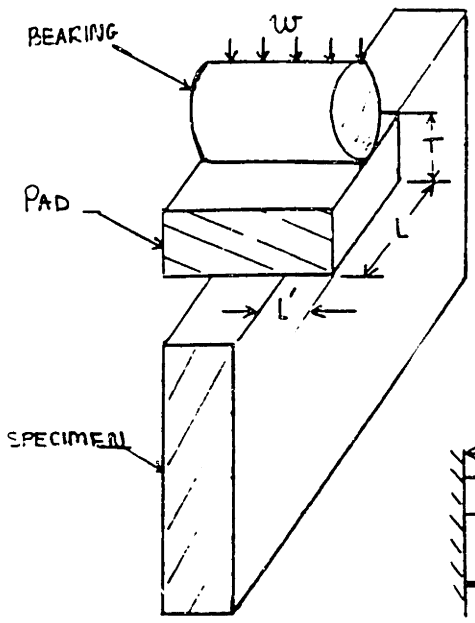

GIVEN: LENGTH of CYLINDER L = 2.5" = 64mm

ξ = FACTOR of SAFETY = 2

Distributed Load $w = \frac{P_{max}}{L} = 32000 \frac{lb}{in} = 5717 \frac{N}{mm}$

a] PAD DEFLECTION δ_1 (11):

$E = 30 \times 10^6$ PSI $= 2.14 \times 10^5 N/mm^2$

W = PAD WIDTH = 2.5" = 64mm

L' = " LENGTH = 2.5" = 64mm

T = Thickness

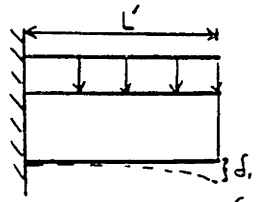

$$\delta_1 = \frac{w (L')^4}{8EI}$$

*Note E is not f(σ_{max})

NOTE. $L' \simeq 0.85" = 21.6$ mm = OVERHANG

$$I = \frac{LT^3}{12}$$

MAXIMUM ALLOWABLE $\delta_1 = 1 \times 10^{-3}" = 2.54 \times 10^{-2}$ mm

$$\therefore \quad T = \left\{ \frac{3}{2} \frac{w (L')^4}{E L \delta_1} \right\}^{1/3} = 0.69" = 17.6\text{mm} \text{ Minimum}$$

b] BEARING DEFLECTION δ_2 (12):

From Reference (12), For deflection between bodies of Two Spheres R_1 & R_2

$$\delta_2 = \mathcal{U}_2 - \mathcal{U}_1 = \sqrt[3]{\frac{9}{16} P^2 \frac{(R_1 + R_2)}{R_1 R_2} \left(\frac{(1-\nu_1^2)}{E_1} + \frac{(1-\nu_2^2)}{E_2} \right)}$$

Taking: $\nu_1 = \nu_2 = 0.3$ & $R_2 \to \infty$ (flat plate) $E_1 = E_2 = E$

$R_1 = \phi$ of bearing $= 0.75" = 19$mm, $P = w L' = 27200 lb$ (121284N)

$$\delta_2 = \sqrt{\frac{9}{16} \frac{P^2}{R_1} \left(\frac{2 (1-\nu^2)}{E} \right)^2} = 1.27 \times 10^{-2} \text{ inches}$$

$\therefore$ Since $\delta_2 > \delta_1$ bearing & pad remain in contact

Note: In Test δ_2 & δ_1 are smaller because ν is smaller in Harder Material

EXHIBIT 9

(LOCAL YIELDING / INDENTATION

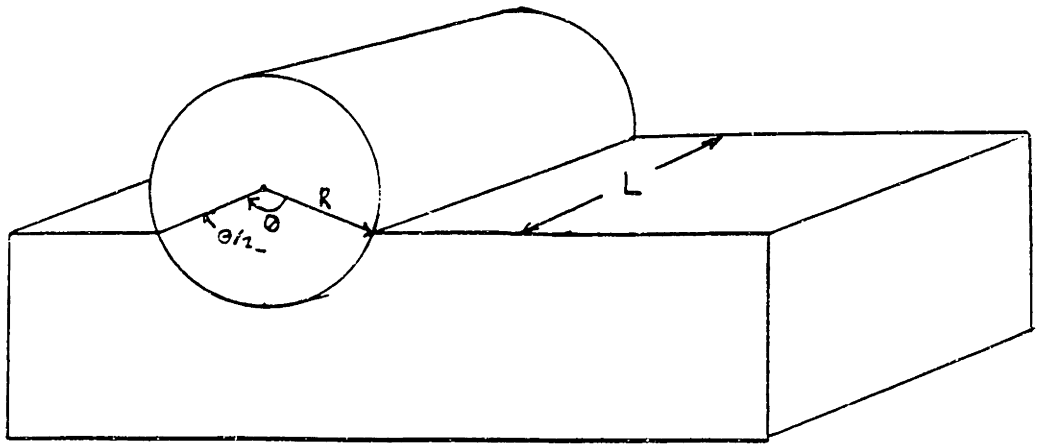

GIVEN $\frac{P_{max}}{2} = 40\,000 \text{ psi} = 88\,000 \text{ N}$

$\sigma_{y_{RC60}} \cong 340 \times 10^3 \text{ psi} = 2.35 \times 10^3 \frac{N}{mm^2}$

$R = 0.75'' = 19 \text{ mm}$

$L = 2.5'' = 64 \text{ mm}$

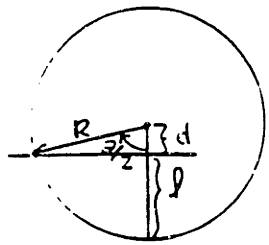

$$\theta = \left[\left(\frac{P_{max}}{\sigma_{y_{RC60}}}\right) \Big/ (2R \cdot L)\right] \; ; \; \frac{\theta}{2} = 3.137 \times 10^{-2} \text{ rad}$$

$$d = R\cos\left(\frac{\theta}{2}\right)$$

$$l = R - d = \underline{O(10^{-7}) \therefore \text{negligible.}}$$

EXHIBIT 10

Relation of Crack Length to bend Angle ④

→ For a crack length equal to a, the neutral axis measured from the Tensile side of the bend specimen is at $(L-a)/2$ and the displacement increment at y is: (y along axis of weld)

$$du = \left[y - \frac{(L-a)}{2} \right] d\theta \qquad (1)$$

→ the crack growth will be the displacement increment at the tip from (1) divided by the current slope at the crack tip of the plot of displacement vs y: $(du/dy)_{tip}$:

$$da = \frac{(L-a)\, d\theta}{\left[2 (du/dy)_{tip} \right]} \qquad (2)$$

→ The increment in slope du/dy at the crack tip are found by differentiating (1):

$$d\left(\frac{du}{dy}\right) = d\theta \qquad (3)$$

→ From which the slope of the displacement-y curve (for $\theta \ll 1$) is just θ. Introducing this into (2) gives the differential equation for crack growth:

$$\frac{da}{(L-a)} = \frac{1}{2} \frac{d\theta}{\theta} \qquad (4)$$

→ Integration gives

$$\left[L/(L-a) \right]^2 = \theta/\theta_c \quad \text{or} \quad a/L = 1 - \sqrt{(\theta_c/\theta)} \quad \text{for } \theta \geq \theta_c^{\circledast} \ (5$$

⊛ θ_c is the critical bend angle at crack initiation: $\theta_c = \mu_c / (\frac{L}{2}$

→ Equation (5) shows the crack length constant at $a/L = 0$ until $\theta = \theta_c$, after which it increases, with an initial slope of

$d(a/L)/d(\theta/\theta_c) = 1/2$ asymptotically to 1 as $\theta \to \infty$

The M − θ relation: use (5) to eliminate (a/L) in $M = 2kd(L-a)^2/4$

When this is normalized in terms of the uncracked limit moment $M_L = k d L^2/2$

the result is: $M/M_L = \theta_c/\theta$ for $\theta \geq \theta_c$

EXHIBIT 5B

ANNEX 1A

PART A: (EVALUATION OF ΣC_f)

1. DEFLECTION OF LOAD APPLYING BEAM & COMPLIANCE (C_{LAB})

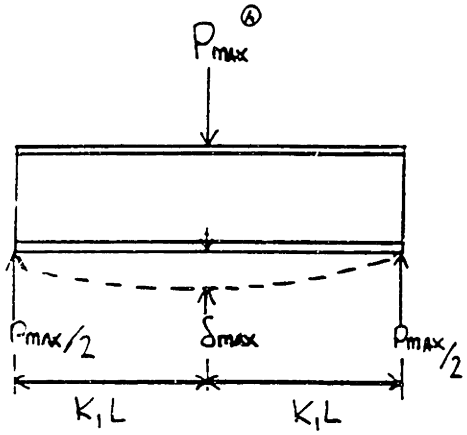

δ_{max} @ Midpoint ⑦: (CRANDALL p 531)

$$\delta_{MAX} = \frac{P_{max}(K_1L)\left[(2K_1L)^2-(K_1L)^2\right]^{3/2}}{9\sqrt{3}\,(2K_1L)\,EI}$$

GIVEN (for STEEL):

$E = 30\times10^6$ psi $(2.07\times10^5 \frac{N}{mm^2})$

$I = 122.4\ m^4$ $(5.09\times10^2\ mm^4)$

AND:

P_{max} ⑧ $= 80\,000$ lb $(368\,000$ N$)$

$K_1L = 4'' = 102$ mm

$\delta_{max} = 2.32\times10^{-4}$ inch $= 5.9\times10^{-3}$ mm

$$C_{LAB} = \frac{\delta_{max}}{P_{max}} = 2.9\times10^{-9}\ \frac{m}{lb} = 1.65\times10^{-8}\ \frac{mm}{N}$$

2. DEFLECTION OF LOAD BEARING BEAM & COMPLIANCE (C_{LBB})

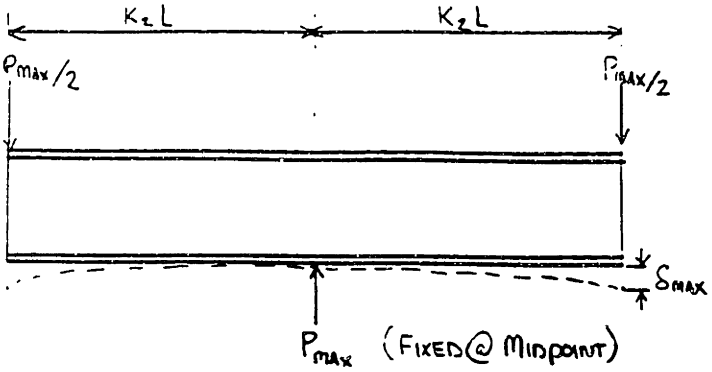

δ_{max} @ EDGES: (CRANDAL p531) ⑦

$$\delta_{max} = \frac{P_{max}(K_2L)[(2K_2L)^2-(K_2L)^2]}{9\sqrt{3}(2K_2L)EI}$$

given: E = same as (1)
I = same as (1)
P_{max} = same as (1)

$K_2L = 12.75\ m = 324\ mm$

$\delta_{max} = 7.53 \times 10^{-3}\ mch = 1.91 \times 10^{-1}\ mm$

$$C_{L_{BB}} = \frac{\delta_{max}}{P_{max}} = 9.41 \times 10^{-8}\ \frac{m}{lb} = 5.36 \times 10^{-7}\ \frac{mm}{N}$$

3. DEFLECTION OF SPECIMEN BEAM & COMPLIANCE ($C_{SPECIMEN}$)

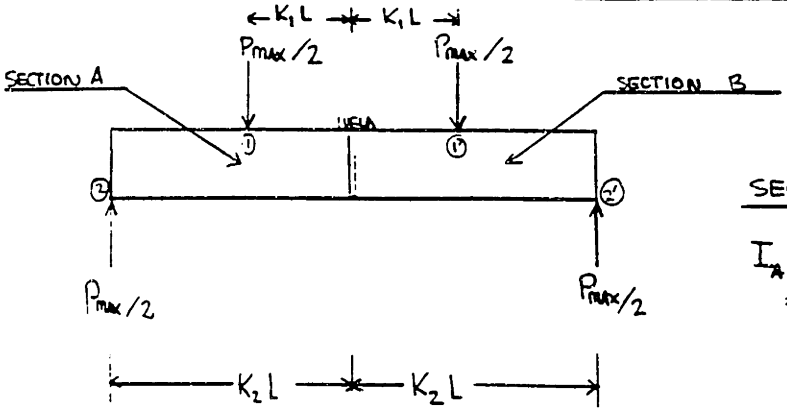

SECTION A

$I_A = 34.52\ m^4$
$= 1.44 \times 10^7\ mm^4$

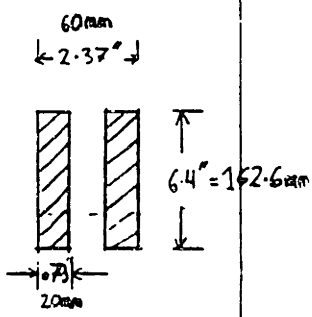

SECTION B

$I_B = 17.26\ m^4$
$= 7.18 \times 10^6\ mm^4$

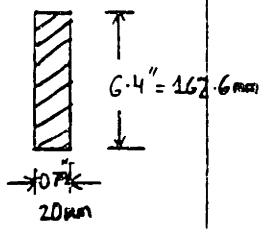

PART A] CONTINUED

MODELLING THE SPECIMEN AS A CANTILEVERED BEAM (SECTIONED @ MIDPOINT)

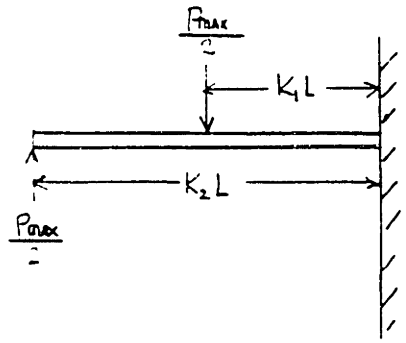

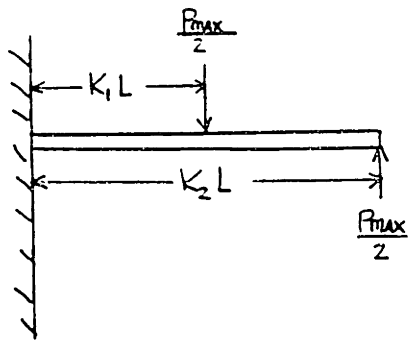

SUPERIMPOSING THE DEFLECTIONS

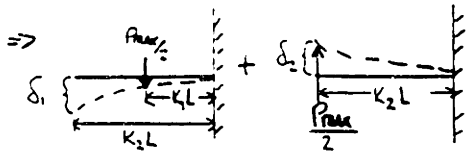

SUPERIMPOSING THE DEFLECTIONS

SYMMETRIC MODEL

$\Rightarrow$ SAME ANALYSIS

ASIDE (CRANDALL) GENERIC FORMULA

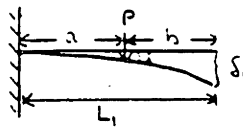

A] $\delta = \frac{P}{6EI}\left(x-a\right)^3 - x^3 + 3x^2a)$

B] $\delta_{MAX} = \frac{Pa^2(3L_1 - a)}{6EI}$

FOR δ_1:

$a = K_1L$

$P = P_{MAX}/2$

$$\delta_1(x) = \frac{\left(\frac{P_{MAX}}{2}\right)\left[\langle x-K_1L\rangle^3 - x^3 + 3x^2(K_1L)\right]}{6EI_A}$$

$$\delta_1(x) = \frac{\left(\frac{P_{MAX}}{2}\right)\left[\langle x-K_1L\rangle^3 - x^3 + 3x^2(K_1L)\right]}{6EI_B}$$

FOR δ_2:

$a = K_2L$

$P = P_{MAX}/2$

$$\delta_2(x) = \frac{\left(\frac{P_{MAX}}{2}\right)\left[\langle x-K_2L\rangle^3 - x^3 - 3x^2(K_2L)\right]}{6EI_A}$$

$$\delta_2(x) = \frac{\left(\frac{P_{MAX}}{2}\right)\left[\langle x-K_2L\rangle^3 - x^3 - 3x^2(K_2L)\right]}{6EI_B}$$

δ_{TOTAL}

$$\delta_{TOTAL}(x) = \delta_2(x) - \delta_1(x)$$

$$\delta_{TOTAL}(x) = \delta_2(x) - \delta_1(x)$$

AT LOADING POINT K_1L FROM MIDPOINT ①

$$\delta_{TOTAL\,①} = \frac{P_{MAX}}{4EI_A}(K_1)^2L^3[K_2-K_1]$$

@ $x = K_1L$

$$\delta_{TOTAL\,①'} = \frac{P_{MAX}}{4EI_B}(K_1)^2L^3[K_2-K_1]$$

But Note that $I_{FB} = \frac{I_A}{2}$

$\therefore \delta_{TOTAL\,①'} = 2\,\delta_{TOTAL\,①}$

AT LOADING POINT K_2L FROM MIDPOINT ②

$$\delta_{TOTAL\,②} = \frac{\left(\frac{P_{MAX}}{2}\right)}{6EI_A}\left[3(K_2L)^3-(K_2L-K_1L)^3-3(K_2L)^2(K_1L)\right]$$

@ $x = K_2L$

$$\delta_{TOTAL\,②'} = \frac{\left(\frac{P_{MAX}}{2}\right)}{6EI_B}\left[3(K_2L)^3-(K_2L-K_1L)^3-3(K_2L)^2(K_1L)\right]$$

@ $x = K_2L$

But Since $I_{FB} = I_A/2$

$\therefore \delta_{TOTAL\,②'} = 2\,\delta_{TOTAL\,②}$

GIVEN: $L = 6.4'' = 162.6$ mm

$K_1 = 0.625$ "

$K_2 = 1.992$ "

$E \simeq 30\times10^6 \frac{lb}{in^2} \simeq 2.07\times10^5 \frac{N}{mm^2}$ "

$I_A = 34.52\,in^4 = 1.44\times10^7\,mm^4$ $I_{FB} = 2I_A$

$P_{MAX} = 80\,000\,lb$ (368 000 N) "

We obtain the following deflections [relative to weld [$x=\phi, y=\phi$]]

⇒ at ①, $\delta_{TOTAL\,①} = 2.70\times10^{-3}'' = 6.87\times10^{-2}$ mm

⇒ at ①', $\delta_{TOTAL\,①'} = 5.40\times10^{-3}'' = 1.37\times10^{-1}$ mm

⇒ at ②, $\delta_{TOTAL\,②} = 2.32\times10^{-2}'' = 5.88\times10^{-1}$ mm

⇒ at ②', $\delta_{TOTAL\,②'} = 4.64\times10^{-2}'' = 1.18\times10^{0}$ mm

FINDING EFFECTIVE DEFLECTION OF ENTIRE SPECIMEN @ MID POINT (WELD LINE)

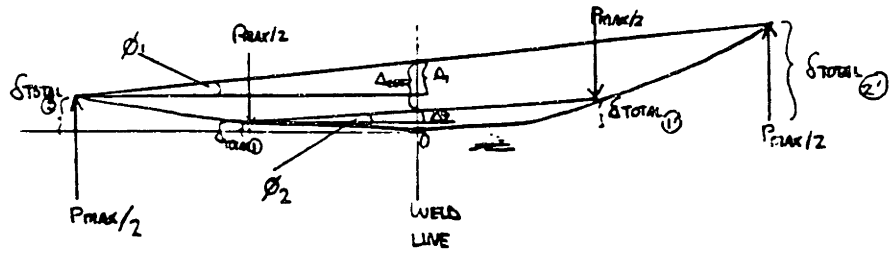

ANNEX to APPENDIX A

USING TRIGONOMETRIC RELATIONS:

$$\tan \phi_1 = \frac{\delta_{TOTAL_{(2)}} - \delta_{TOTAL_{(1)}}}{2(K_2 L)} = \frac{\Delta_1}{K_2 L}$$

$$\tan \phi_2 = \frac{\delta_{TOTAL_{(1)}} - \delta_{TOTAL_{(1)}}}{2(K_1 L)} = \frac{\Delta_2}{K_1 L}$$

giving : $\tan \phi_1 = 9.10 \times 10^{-4}$

$\tan \phi_2 = 3.38 \times 10^{-4}$

$\Delta_1 = 1.16 \times 10^{-2}$ " $= 2.95 \times 10^{-1}$ mm

$\Delta_2 = 1.35 \times 10^{-3}$ " $= 3.43 \times 10^{-2}$ mm

Now : $\Delta_{eff} = \left[\left(\delta_{TOTAL_{(2)}} + \Delta_1 \right) - \left(\delta_{TOTAL_{(1)}} + \Delta_2 \right) \right]$

$\Delta_{eff} = 3.08 \times 10^{-2}$ " $= 7.81 \times 10^{-1}$ mm $= \delta_{MAX}$

Therefore $C_{SPECIMEN} = \frac{\delta_{MAX}}{P_{MAX}} = 3.85 \times 10^{-7} \frac{in}{lb} = 2.12 \times 10^{-6} \frac{mm}{N}$

4. OVERALL COMPLIANCE of TEST RIG (ΣC_t)

$$\Sigma C_t = C_{LAB} + C_{LBB} + C_{SPEC}$$

$$= 1.65 \times 10^{-8} \frac{mm}{N} + 5.36 \times 10^{-7} \frac{mm}{N} + 2.12 \times 10^{-6} \frac{mm}{N}$$

$$= 2.90 \times 10^{-9} \frac{m}{lb} + 9.41 \times 10^{-8} \frac{m}{lb} + 3.85 \times 10^{-7} \frac{m}{lb}$$

$$\therefore \Sigma C_t = 4.82 \times 10^{-7} \frac{m}{lb} = 2.67 \times 10^{-6} \frac{mm}{N}$$

APPENDIX B

PROCESSED EXPERIMENTAL DATA

	B	C	D	E	F	G
		Data Analysis For Test #				
	P(load)-Volts	X1 (mm)	X2 (mm)	X3 (mm)	U1 (mm)	U2 (mm)
6	0	79.68	80.01	80.15	0	0
7	3	80.18	80.04	80.13	=(SQRT(C7*C7-400)-SQRT(P6*P6-400))	=(SQRT(D7*D7-400)-SQRT(Q6*Q6-400))
8	4	79.45	80.18	80.3	=(SQRT(C8*C8-400)-SQRT(P7*P7-400))	=(SQRT(D8*D8-400)-SQRT(Q7*Q7-400))
9	4.52	79.52	80.35	80.34	=(SQRT(C9*C9-400)-SQRT(P8*P8-400))	=(SQRT(D9*D9-400)-SQRT(Q8*Q8-400))
10	5	79.72	80.14	80.21	=(SQRT(C10*C10-400)-SQRT(P9*P9-400))	=(SQRT(D10*D10-400)-SQRT(Q9*Q9-400))
11	5.49	79.47	80.22	80.04	=(SQRT(C11*C11-400)-SQRT(P10*P10-400))	=(SQRT(D11*D11-400)-SQRT(Q10*Q10-400))
12	5.91	79.71	79.98	80.22	=(SQRT(C12*C12-400)-SQRT(P11*P11-400))	=(SQRT(D12*D12-400)-SQRT(Q11*Q11-400))
13	6.4	79.36	80.08	80.24	=(SQRT(C13*C13-400)-SQRT(P12*P12-400))	=(SQRT(D13*D13-400)-SQRT(Q12*Q12-400))
14	6.6	79.58	80.52	80.47	=(SQRT(C14*C14-400)-SQRT(P13*P13-400))	=(SQRT(D14*D14-400)-SQRT(Q13*Q13-400))
15	6.8	80	80.2	80.16	=(SQRT(C15*C15-400)-SQRT(P14*P14-400))	=(SQRT(D15*D15-400)-SQRT(Q14*Q14-400))
16	7.1	79.41	80	80.28	=(SQRT(C16*C16-400)-SQRT(P15*P15-400))	=(SQRT(D16*D16-400)-SQRT(Q15*Q15-400))
17	7.28	79.04	80.09	80.5	=(SQRT(C17*C17-400)-SQRT(P16*P16-400))	=(SQRT(D17*D17-400)-SQRT(Q16*Q16-400))
18	7.3	78.72	80.1	80.68	=(SQRT(C18*C18-400)-SQRT(P17*P17-400))	=(SQRT(D18*D18-400)-SQRT(Q17*Q17-400))
19	7.1	78.38	79.83	81.1	=(SQRT(C19*C19-400)-SQRT(P18*P18-400))	=(SQRT(D19*D19-400)-SQRT(Q18*Q18-400))
20	5.6	78.28	79.97	80.98	=(SQRT(C20*C20-400)-SQRT(P19*P19-400))	=(SQRT(D20*D20-400)-SQRT(Q19*Q19-400))
21	4.6	78.25	79.87	81.66	=(SQRT(C21*C21-400)-SQRT(P20*P20-400))	=(SQRT(D21*D21-400)-SQRT(Q20*Q20-400))
22	3.5	77.7	80.36	82.08	=(SQRT(C22*C22-400)-SQRT(P21*P21-400))	=(SQRT(D22*D22-400)-SQRT(Q21*Q21-400))
23	2.3	77.34	80.34	82.99	=(SQRT(C23*C23-400)-SQRT(P22*P22-400))	=(SQRT(D23*D23-400)-SQRT(Q22*Q22-400))
24	1.7	77.19	80.6	84.06	=(SQRT(C24*C24-400)-SQRT(P23*P23-400))	=(SQRT(D24*D24-400)-SQRT(Q23*Q23-400))
25	1.36	77.01	81.7	84.56	=(SQRT(C25*C25-400)-SQRT(P24*P24-400))	=(SQRT(D25*D25-400)-SQRT(Q24*Q24-400))

TEMPLATE FOR SPEC 6 (TEST #1)

H	I	J	K	L	M
U3 (mm)	Theta (12)	Theta (23)	Theta (Avg)	M/MI	1/(M/MI)
0	0	0	0	0	0
=(SQRT(E7*E7-400)-SQRT(R6*R6-400))	=(G7-F7)/S6	=(H7-G7)/S6	=(I7+J7)/2	=(B7/T6)	=1/L7
=(SQRT(E8*E8-400)-SQRT(R7*R7-400))	=(G8-F8)/S7	=(H8-G8)/S7	=(I8+J8)/2	=(B8/T7)	=1/L8
=(SQRT(E9*E9-400)-SQRT(R8*R8-400))	=(G9-F9)/S8	=(H9-G9)/S8	=(I9+J9)/2	=(B9/T8)	=1/L9
=(SQRT(E10*E10-400)-SQRT(R9*R9-400))	=(G10-F10)/S9	=(H10-G10)/S9	=(I10+J10)/2	=(B10/T9)	=1/L10
=(SQRT(E11*E11-400)-SQRT(R10*R10-400))	=(G11-F11)/S10	=(H11-G11)/S10	=(I11+J11)/2	=(B11/T10)	=1/L11
=(SQRT(E12*E12-400)-SQRT(R11*R11-400))	=(G12-F12)/S11	=(H12-G12)/S11	=(I12+J12)/2	=(B12/T11)	=1/L12
=(SQRT(E13*E13-400)-SQRT(R12*R12-400))	=(G13-F13)/S12	=(H13-G13)/S12	=(I13+J13)/2	=(B13/T12)	=1/L13
=(SQRT(E14*E14-400)-SQRT(R13*R13-400))	=(G14-F14)/S13	=(H14-G14)/S13	=(I14+J14)/2	=(B14/T13)	=1/L14
=(SQRT(E15*E15-400)-SQRT(R14*R14-400))	=(G15-F15)/S14	=(H15-G15)/S14	=(I15+J15)/2	=(B15/T14)	=1/L15
=(SQRT(E16*E16-400)-SQRT(R15*R15-400))	=(G16-F16)/S15	=(H16-G16)/S15	=(I16+J16)/2	=(B16/T15)	=1/L16
=(SQRT(E17*E17-400)-SQRT(R16*R16-400))	=(G17-F17)/S16	=(H17-G17)/S16	=(I17+J17)/2	=(B17/T16)	=1/L17
=(SQRT(E18*E18-400)-SQRT(R17*R17-400))	=(G18-F18)/S17	=(H18-G18)/S17	=(I18+J18)/2	=(B18/T17)	=1/L18
=(SQRT(E19*E19-400)-SQRT(R18*R18-400))	=(G19-F19)/S18	=(H19-G19)/S18	=(I19+J19)/2	=(B19/T18)	=1/L19
=(SQRT(E20*E20-400)-SQRT(R19*R19-400))	=(G20-F20)/S19	=(H20-G20)/S19	=(I20+J20)/2	=(B20/T19)	=1/L20
=(SQRT(E21*E21-400)-SQRT(R20*R20-400))	=(G21-F21)/S20	=(H21-G21)/S20	=(I21+J21)/2	=(B21/T20)	=1/L21
=(SQRT(E22*E22-400)-SQRT(R21*R21-400))	=(G22-F22)/S21	=(H22-G22)/S21	=(I22+J22)/2	=(B22/T21)	=1/L22
=(SQRT(E23*E23-400)-SQRT(R22*R22-400))	=(G23-F23)/S22	=(H23-G23)/S22	=(I23+J23)/2	=(B23/T22)	=1/L23
=(SQRT(E24*E24-400)-SQRT(R23*R23-400))	=(G24-F24)/S23	=(H24-G24)/S23	=(I24+J24)/2	=(B24/T23)	=1/L24
=(SQRT(E25*E25-400)-SQRT(R24*R24-400))	=(G25-F25)/S24	=(H25-G25)/S24	=(I25+J25)/2	=(B25/T24)	=1/L25

TEMPLATE (CONTINUED)

XC01	XC02	XC03	Delta Z	Pmax
=C6	=D6	=E6	63.5	7.32
79.66	80.01	80.15	63.5	7.32
79.66	80.01	80.15	63.5	7.32
79.66	80.01	80.15	63.5	7.32
79.66	80.01	80.15	63.5	7.32
79.66	80.01	80.15	63.5	7.32
79.66	80.01	80.15	63.5	7.32
79.66	80.01	80.15	63.5	7.32
79.66	80.01	80.15	63.5	7.32
79.66	80.01	80.15	63.5	7.32
79.66	80.01	80.15	63.5	7.32
79.66	80.01	80.15	63.5	7.32
79.66	80.01	80.15	63.5	7.32
79.66	80.01	80.15	63.5	7.32
79.66	80.01	80.15	63.5	7.32
79.66	80.01	80.15	63.5	7.32
79.66	80.01	80.15	63.5	7.32
79.66	80.01	80.15	63.5	7.32
79.66	80.01	80.15	63.5	7.32
79.66	80.01	80.15	63.5	7.32
79.66	80.01	80.15	63.5	7.32

TEMPLATE CONTINUED

Data Analysis For Test # 1 (Specimen # 6, 6 mm x 6 mm weld)

P(load)-Volts	X1 (mm)	X2 (mm)	X3 (mm)	U1 (mm)	U2 (mm)	U3 (mm)	Theta (12)	Theta (23)	Theta (Avg)	M/MI	1/(M/MI)
0	7.97E+01	8.00E+01	8.02E+01	0.00E+00	0.00E+00	0.00E+00	0.00E+00	0.00E+00	0.00E+00	0.00E+00	0.00E+00
3	8.02E+01	8.00E+01	8.01E+01	5.37E-01	3.10E-02	-2.07E-02	-7.97E-03	-8.13E-04	-4.39E-03	4.10E-01	2.44E+00
4	7.95E+01	8.02E+01	8.03E+01	-2.17E-01	1.55E-01	1.55E-01	5.86E-03	-2.83E-07	2.93E-03	5.46E-01	1.83E+00
4.52	7.95E+01	8.04E+01	8.03E+01	-1.45E-01	3.51E-01	1.96E-01	7.81E-03	-2.44E-03	2.68E-03	6.17E-01	1.62E+00
5	7.97E+01	8.01E+01	8.02E+01	6.20E-02	1.34E-01	6.20E-02	1.14E-03	-1.14E-03	-2.00E-07	6.83E-01	1.46E+00
5.49	7.95E+01	8.02E+01	8.00E+01	-1.96E-01	2.17E-01	-1.14E-01	6.51E-03	-5.20E-03	6.51E-04	7.50E-01	1.33E+00
5.91	7.97E+01	8.00E+01	8.02E+01	5.17E-02	-5.16E-02	7.23E-02	-1.63E-03	1.95E-03	1.62E-04	8.07E-01	1.24E+00
6.4	7.94E+01	8.01E+01	8.02E+01	-3.10E-01	5.16E-02	9.29E-02	5.69E-03	6.50E-04	3.17E-03	8.74E-01	1.14E+00
6.6	7.96E+01	8.05E+01	8.05E+01	-8.27E-02	5.27E-01	3.30E-01	9.59E-03	-3.09E-03	3.25E-03	9.02E-01	1.11E+00
6.8	8.00E+01	8.02E+01	8.02E+01	3.51E-01	1.06E-01	1.03E-02	-2.44E-03	-2.93E-03	-2.68E-03	9.29E-01	1.08E+00
7.1	7.94E+01	8.00E+01	8.03E+01	-2.58E-01	-1.03E-02	1.34E-01	3.91E-03	2.28E-03	3.09E-03	9.70E-01	1.03E+00
7.28	7.90E+01	8.01E+01	8.05E+01	-6.41E-01	8.26E-02	3.61E-01	1.14E-02	4.39E-03	7.89E-03	9.95E-01	1.01E+00
7.3	7.87E+01	8.01E+01	8.07E+01	-9.71E-01	9.29E-02	5.27E-01	1.68E-02	6.83E-03	1.18E-02	9.97E-01	1.00E+00
7.1	7.84E+01	7.98E+01	8.11E+01	-1.32E+00	-1.86E-01	9.81E-01	1.79E-02	1.84E-02	1.81E-02	9.70E-01	1.03E+00
5.6	7.83E+01	8.00E+01	8.10E+01	-1.45E+00	-4.13E-02	8.57E-01	2.21E-02	1.41E-02	1.81E-02	7.65E-01	1.31E+00
4.6	7.83E+01	7.99E+01	8.17E+01	-1.46E+00	-1.45E-01	1.56E+00	2.07E-02	2.68E-02	2.37E-02	6.28E-01	1.59E+00
3.5	7.77E+01	8.04E+01	8.21E+01	-2.03E+00	3.01E-01	1.99E+00	3.76E-02	2.57E-02	3.18E-02	4.78E-01	2.09E+00
2.3	7.73E+01	8.03E+01	8.30E+01	-2.40E+00	3.41E-01	2.93E+00	4.31E-02	4.08E-02	4.20E-02	3.14E-01	3.18E+00
1.7	7.72E+01	8.06E+01	8.41E+01	-2.55E+00	6.09E-01	4.05E+00	4.98E-02	5.42E-02	5.20E-02	2.32E-01	4.31E+00
1.36	7.70E+01	8.17E+01	8.46E+01	-2.74E+00	1.74E+00	4.55E+00	7.06E-02	4.41E-02	5.74E-02	1.86E-01	5.38E+00

Data Analysis For Test # 2 (Specimen # 5, 6 mm x 6 mm weld)

P(load)-Volts	X1 (mm)	X2 (mm)	X3 (mm)	U1 (mm)	U2 (mm)	U3 (mm)	Theta (12)	Theta (23)	Theta (Avg)	M/MI	1/(M/MI)
0	8.22E+01	8.20E+01	8.07E+01	0.00E+00	0.00E+00	0.00E+00	0.00E+00	0.00E+00	0.00E+00	0.00E+00	0.00E+00
3.5	8.22E+01	8.20E+01	8.12E+01	1.03E-02	-3.09E-02	4.54E-01	-6.50E-04	7.64E-03	3.49E-03	4.64E-01	2.15E+00
4.5	8.23E+01	8.20E+01	8.11E+01	1.13E-01	6.19E-02	3.51E-01	-8.12E-04	4.55E-03	1.87E-03	5.97E-01	1.68E+00
5.5	8.20E+01	8.19E+01	8.10E+01	-1.44E-01	-9.28E-02	2.48E-01	8.12E-04	5.36E-03	3.09E-03	7.29E-01	1.37E+00
6.5	8.21E+01	8.22E+01	8.10E+01	-1.24E-01	2.47E-01	3.30E-01	5.85E-03	1.30E-03	3.57E-03	8.62E-01	1.16E+00
7.07	8.22E+01	8.21E+01	8.14E+01	0.00E+00	1.03E-01	6.50E-01	1.62E-03	8.61E-03	5.12E-03	9.38E-01	1.07E+00
7.54	8.18E+01	8.21E+01	8.15E+01	-3.71E-01	1.44E-01	8.36E-01	8.12E-03	1.09E-02	9.50E-03	1.00E+00	1.00E+00
6.5	8.14E+01	8.21E+01	8.19E+01	-7.84E-01	1.55E-01	1.21E+00	1.48E-02	1.66E-02	1.57E-02	8.62E-01	1.16E+00
4.25	8.13E+01	8.22E+01	8.26E+01	-8.87E-01	2.06E-01	1.98E+00	1.72E-02	2.79E-02	2.26E-02	5.64E-01	1.77E+00
2.44	8.08E+01	8.26E+01	8.39E+01	-1.39E+00	6.49E-01	3.24E+00	3.22E-02	4.08E-02	3.65E-02	3.24E-01	3.09E+00
2.1	8.07E+01	8.28E+01	8.40E+01	-1.50E+00	8.66E-01	3.38E+00	3.72E-02	3.96E-02	3.84E-02	2.79E-01	3.59E+00

Data Analysis For Test # 4 (Specimen #7, 6 mm x 6 mm weld)

P(load)-Volts	X1 (mm)	X2 (mm)	X3 (mm)	U1 (mm)	U2 (mm)	U3 (mm)	Theta (12)	Theta (23)	Theta (Avg)	M/MI	1/(M/MI)
0	8.03E+01	8.08E+01	8.10E+01	0.00E+00	0.00E+00	0.00E+00	0.00E+00	0.00E+00	0.00E+00	0.00E+00	0.00E+00
3.25	8.00E+01	8.09E+01	8.10E+01	-2.48E-01	1.03E-01	1.03E-02	5.53E-03	-1.46E-03	2.03E-03	4.06E-01	2.46E+00
4.5	8.01E+01	8.06E+01	8.11E+01	-1.86E-01	-2.37E-01	7.22E-02	-8.11E-04	4.88E-03	2.03E-03	5.63E-01	1.78E+00
5.5	8.02E+01	8.07E+01	8.12E+01	-3.10E-02	-1.55E-01	2.37E-01	-1.95E-03	6.18E-03	2.11E-03	6.88E-01	1.45E+00
6	8.01E+01	8.08E+01	8.12E+01	-2.17E-01	-7.22E-02	2.06E-01	2.28E-03	4.39E-03	3.33E-03	7.50E-01	1.33E+00
7	8.01E+01	8.06E+01	8.11E+01	-1.55E-01	-2.27E-01	1.24E-01	-1.14E-03	5.53E-03	2.19E-03	8.75E-01	1.14E+00
8	7.94E+01	8.06E+01	8.16E+01	-9.19E-01	-2.58E-01	6.50E-01	1.04E-02	1.43E-02	1.24E-02	1.00E+00	1.00E+00
7.8	7.95E+01	8.06E+01	8.16E+01	-8.47E-01	-2.68E-01	5.88E-01	9.11E-03	1.35E-02	1.13E-02	9.75E-01	1.03E+00
5.63	8.10E+01	8.07E+01	8.22E+01	7.02E-01	-1.96E-01	1.29E+00	-1.41E-02	2.34E-02	4.62E-03	7.04E-01	1.42E+00
3.4	7.85E+01	8.07E+01	8.23E+01	-1.83E+00	-1.45E-01	1.33E+00	2.65E-02	2.32E-02	2.49E-02	4.25E-01	2.35E+00
2.03	7.80E+01	8.10E+01	8.38E+01	-2.32E+00	1.44E-01	2.86E+00	3.87E-02	4.27E-02	4.07E-02	2.54E-01	3.94E+00

Data Analysis For Test # 5 (Specimen # 2, 6 mm x 9 mm weld)

P(load)-Volts	X1 (mm)	X2 (mm)	X3 (mm)	U1 (mm)	U2 (mm)	U3 (mm)	Theta (12)	Theta (23)	Theta (Avg)	M/MI	1/(M/MI)
0	8.16E+01	8.15E+01	8.25E+01	0.00E+00	0.00E+00	0.00E+00	0.00E+00	0.00E+00	0.00E+00	0.00E+00	0.00E+00
2.35	8.16E+01	8.16E+01	8.25E+01	-4.13E-02	8.25E-02	4.12E-02	1.95E-03	-6.50E-04	6.50E-04	3.13E-01	3.20E+00
3.5	8.16E+01	8.16E+01	8.26E+01	-8.25E-02	8.25E-02	1.03E-01	2.60E-03	3.24E-04	1.46E-03	4.65E-01	2.15E+00
4.5	8.15E+01	8.16E+01	8.25E+01	-1.75E-01	5.16E-02	4.12E-02	3.57E-03	-1.63E-04	1.71E-03	5.98E-01	1.67E+00
6.2	8.12E+01	8.15E+01	8.28E+01	-4.95E-01	0.00E+00	3.50E-01	7.80E-03	5.52E-03	6.66E-03	8.24E-01	1.21E+00
6.85	8.10E+01	8.15E+01	8.29E+01	-7.02E-01	-4.13E-02	4.23E-01	1.04E-02	7.30E-03	8.85E-03	9.11E-01	1.10E+00
7.25	8.07E+01	8.16E+01	8.30E+01	-9.70E-01	1.03E-01	5.15E-01	1.69E-02	6.49E-03	1.17E-02	9.64E-01	1.04E+00
7.5	8.05E+01	8.14E+01	8.30E+01	-1.18E+00	-1.03E-01	5.98E-01	1.69E-02	1.10E-02	1.40E-02	9.97E-01	1.00E+00
5	8.04E+01	8.14E+01	8.39E+01	-1.30E+00	-8.25E-02	1.45E+00	1.92E-02	2.42E-02	2.17E-02	6.65E-01	1.50E+00
3.98	8.02E+01	8.15E+01	8.44E+01	-1.51E+00	2.06E-02	1.98E+00	2.41E-02	3.08E-02	2.74E-02	5.29E-01	1.89E+00
1.6	8.11E+01	8.16E+01	8.43E+01	-5.78E-01	1.24E-01	1.90E+00	1.10E-02	2.79E-02	1.95E-02	2.13E-01	4.70E+00

Data Analysis For Test # 6 (Specimen # 1, 6 mm x 6 mm weld)

P(load)-Volts	X1 (mm)	X2 (mm)	X3 (mm)	U1 (mm)	U2 (mm)	U3 (mm)	Theta (12)	Theta (23)	Theta (Avg)	M/MI	1/(M/MI)
0	8.16E+01	8.16E+01	8.15E+01	0.00E+00	0.00E+00	0.00E+00	0.00E+00	0.00E+00	0.00E+00	0.00E+00	0.00E+00
2.5	8.14E+01	8.15E+01	8.13E+01	-2.89E-01	-1.75E-01	-1.44E-01	1.79E-03	4.87E-04	1.14E-03	3.21E-01	3.11E+00
3.5	8.13E+01	8.17E+01	8.15E+01	-3.51E-01	5.16E-02	4.13E-02	6.34E-03	-1.62E-04	3.09E-03	4.50E-01	2.22E+00
4.5	8.13E+01	8.16E+01	8.16E+01	-3.51E-01	2.06E-02	1.03E-01	5.85E-03	1.30E-03	3.57E-03	5.78E-01	1.73E+00
5	8.13E+01	8.15E+01	8.15E+01	-3.30E-01	-1.24E-01	-1.03E-02	3.25E-03	1.79E-03	2.52E-03	6.43E-01	1.56E+00
6	8.11E+01	8.16E+01	8.17E+01	-5.57E-01	-1.03E-02	2.58E-01	8.61E-03	4.22E-03	6.42E-03	7.71E-01	1.30E+00
7	8.11E+01	8.17E+01	8.18E+01	-5.36E-01	4.13E-02	2.99E-01	9.10E-03	4.06E-03	6.58E-03	9.00E-01	1.11E+00
7.46	8.03E+01	8.14E+01	8.22E+01	-1.35E+00	-2.48E-01	7.73E-01	1.74E-02	1.61E-02	1.67E-02	9.59E-01	1.04E+00
5.6	8.01E+01	8.16E+01	8.29E+01	-1.61E+00	0.00E+00	1.52E+00	2.54E-02	2.39E-02	2.46E-02	7.20E-01	1.39E+00
4	8.00E+01	8.19E+01	8.31E+01	-1.74E+00	3.09E-01	1.72E+00	3.23E-02	2.22E-02	2.73E-02	5.14E-01	1.95E+00
3.4	7.99E+01	8.19E+01	8.37E+01	-1.78E+00	2.37E-01	2.26E+00	3.17E-02	3.18E-02	3.18E-02	4.37E-01	2.29E+00
1.98	7.97E+01	8.27E+01	8.50E+01	-1.98E+00	1.06E+00	3.62E+00	4.79E-02	4.02E-02	4.41E-02	2.54E-01	3.93E+00

Data Analysis For Test # 7 (Specimen # 4, 9 mm x 9 mm weld)

P(load)-Volts	X1 (mm)	X2 (mm)	X3 (mm)	U1 (mm)	U2 (mm)	U3 (mm)	Theta (12)	Theta (23)	Theta (Avg)	M/MI	1/(M/MI)
0	1.05E+02	1.05E+02	1.06E+02	0.00E+00	0.00E+00	0.00E+00	0.00E+00	0.00E+00	0.00E+00	0.00E+00	0.00E+00
1.35	1.05E+02	1.05E+02	1.06E+02	-1.02E-01	5.09E-02	1.63E-01	5.09E-03	3.73E-03	4.41E-03	4.13E-01	2.42E+00
2.5	1.05E+02	1.05E+02	1.06E+02	-2.24E-01	4.07E-02	3.26E-01	8.83E-03	9.50E-03	9.17E-03	7.65E-01	1.31E+00
2.86	1.05E+02	1.05E+02	1.06E+02	-3.77E-01	-2.04E-02	3.87E-01	1.19E-02	1.36E-02	1.27E-02	8.75E-01	1.14E+00
3	1.05E+02	1.05E+02	1.06E+02	-4.58E-01	-3.06E-02	4.99E-01	1.43E-02	1.77E-02	1.60E-02	9.17E-01	1.09E+00
3.2	1.05E+02	1.05E+02	1.06E+02	-8.45E-01	-1.53E-01	7.13E-01	2.31E-02	2.99E-02	2.60E-02	9.79E-01	1.02E+00
3.27	1.04E+02	1.04E+02	1.06E+02	-1.72E+00	-4.58E-01	9.88E-01	4.21E-02	4.82E-02	4.52E-02	1.00E+00	1.00E+00
3.05	1.03E+02	1.04E+02	1.07E+02	-2.18E+00	-6.01E-01	1.08E+00	5.26E-02	5.60E-02	5.43E-02	9.33E-01	1.07E+00
2.85	1.03E+02	1.04E+02	1.07E+02	-2.53E+00	-7.54E-01	1.15E+00	5.91E-02	6.35E-02	6.13E-02	8.72E-01	1.15E+00
2.5	1.03E+02	1.04E+02	1.07E+02	-2.81E+00	-8.46E-01	1.20E+00	6.56E-02	6.82E-02	6.69E-02	7.65E-01	1.31E+00
2.15	1.02E+02	1.04E+02	1.07E+02	-3.20E+00	-9.68E-01	1.25E+00	7.44E-02	7.40E-02	7.42E-02	6.57E-01	1.52E+00
1.92	1.02E+02	1.04E+02	1.07E+02	-3.65E+00	-1.13E+00	1.38E+00	8.39E-02	8.39E-02	8.39E-02	5.87E-01	1.70E+00

Data Analysis For Test # 8 (Specimen # 3, 9 mm x 9 mm weld)

P(load)-Volts	X1 (mm)	X2 (mm)	X3 (mm)	U1 (mm)	U2 (mm)	U3 (mm)	Theta (12)	Theta (23)	Theta (Avg)	M/MI	1/(M/MI)
0	1.06E+02	1.07E+02	1.06E+02	0.00E+00	0.00E+00	0.00E+00	0.00E+00	0.00E+00	0.00E+00	0.00E+00	0.00E+00
1.5	1.06E+02	1.06E+02	1.06E+02	-4.07E-02	-4.07E-02	9.17E-02	3.30E-07	4.41E-03	2.21E-03	4.76E-01	2.10E+00
2.5	1.05E+02	1.06E+02	1.06E+02	-3.26E-01	-4.07E-02	1.22E-01	9.51E-03	5.43E-03	7.47E-03	7.94E-01	1.26E+00
2.8	1.05E+02	1.06E+02	1.06E+02	-4.58E-01	-1.83E-01	1.32E-01	9.17E-03	1.05E-02	9.84E-03	8.89E-01	1.13E+00
2.9	1.05E+02	1.06E+02	1.06E+02	-5.60E-01	-1.53E-01	3.36E-01	1.36E-02	1.63E-02	1.49E-02	9.21E-01	1.09E+00
3	1.05E+02	1.06E+02	1.06E+02	-7.84E-01	-1.53E-01	4.68E-01	2.11E-02	2.07E-02	2.09E-02	9.52E-01	1.05E+00
3.05	1.05E+02	1.06E+02	1.06E+02	-8.35E-01	-3.05E-01	5.09E-01	1.77E-02	2.72E-02	2.24E-02	9.68E-01	1.03E+00
3.1	1.05E+02	1.06E+02	1.06E+02	-1.01E+00	-4.07E-01	5.19E-01	2.00E-02	3.09E-02	2.55E-02	9.84E-01	1.02E+00
3.13	1.04E+02	1.06E+02	1.06E+02	-1.41E+00	-4.28E-01	7.03E-01	3.26E-02	3.77E-02	3.51E-02	9.94E-01	1.01E+00
3.14	1.04E+02	1.06E+02	1.07E+02	-1.67E+00	-4.58E-01	8.96E-01	4.04E-02	4.51E-02	4.28E-02	9.97E-01	1.00E+00
3.03	1.04E+02	1.06E+02	1.07E+02	-2.24E+00	-6.11E-01	1.04E+00	5.43E-02	5.50E-02	5.47E-02	9.62E-01	1.04E+00
2.85	1.04E+02	1.06E+02	1.07E+02	-2.33E+00	-6.31E-01	1.25E+00	5.67E-02	6.28E-02	5.98E-02	9.05E-01	1.11E+00
2.6	1.03E+02	1.06E+02	1.07E+02	-2.63E+00	-6.82E-01	1.42E+00	6.49E-02	6.99E-02	6.74E-02	8.25E-01	1.21E+00
2.3	1.03E+02	1.06E+02	1.07E+02	-2.74E+00	-7.43E-01	1.61E+00	6.66E-02	7.84E-02	7.25E-02	7.30E-01	1.37E+00
2	1.03E+02	1.06E+02	1.08E+02	-2.93E+00	-7.43E-01	1.90E+00	7.30E-02	8.82E-02	8.06E-02	6.35E-01	1.58E+00
1.6	1.03E+02	1.06E+02	1.08E+02	-3.02E+00	-5.50E-01	2.10E+00	8.22E-02	8.82E-02	8.52E-02	5.08E-01	1.97E+00

APPENDIX C

"WELDCOSTMDL" Spreadsheet Outline

Control Module (New Costs $ Million)

Tanker Characteristics

Tanker dwt	Single Skin	Double Skin
30 000 dwt	35	40.25
80 000 dwt	55	63.25
120 000 dwt	62	71.3
250 000 dwt	91	104.65

Cost Differential Frcn:	0.15		

B	C	D	E	F	G
2	Control Module (New Costs !				
3					
4					
5	Tanker Characteristics				
6					
7	Tanker dwt		Single Skin		Double Skin
8	30 000 dwt		35		=+E8*(1+E13)
9	80 000 dwt		55		=+E9*(1+E13)
10	120 000 dwt		62		=+E10*(1+E13)
11	250 000 dwt		91		=+E11*(1+E13)
12					
13	Cost Differential Frcn:		0.15		

Welding Characteristics Module

Weld Geometry, Welding Time, & Cost implications

		Increasing Rate of Total Ship Cost (R) (R1-K4)
6mm x 6mm		
	SMAW(Single-Pass)	0
	SMAW(Multi-Pass)	0
	CO2(Flux Cored Wire)	0
	CO2(Solid Wire)	0
7mm x 7mm		
	SMAW(Single-Pass)	0
	SMAW(Multi-Pass)	0.00315
	CO2(Flux Cored Wire)	0.00315
	CO2(Solid Wire)	0.00435
8mm x 8mm		
	SMAW(Single-Pass)	0
	SMAW(Multi-Pass)	0.0069
	CO2(Flux Cored Wire)	0.0069
	CO2(Solid Wire)	0.0086
9mm x 9mm		
	SMAW(Single-Pass)	0
	SMAW(Multi-Pass)	0.0086
	CO2(Flux Cored Wire)	0.0101
	CO2(Solid Wire)	0.0131
10mm x10mm		
	SMAW(Single-Pass)	0
	SMAW(Multi-Pass)	0.0101
	CO2(Flux Cored Wire)	0.0143
	CO2(Solid Wire)	0.0189
11mm x 11mm		
	SMAW(Single-Pass)	0
	SMAW(Multi-Pass)	0.0135
	CO2(Flux Cored Wire)	0.0194
	CO2(Solid Wire)	0
12mm x 12mm		
	SMAW(Single-Pass)	0
	SMAW(Multi-Pass)	0.018
	CO2(Flux Cored Wire)	0.0252
	CO2(Solid Wire)	0
13mm x 13mm		
	SMAW(Single-Pass)	0
	SMAW(Multi-Pass)	0.024
	CO2(Flux Cored Wire)	0
	CO2(Solid Wire)	0

Production Cost Breakdown Module

Hull Construction Cost Fraction (HC):	0.3
Welding Cost Fraction (WC):	0.075
Welding Cost Fraction (WCBHS):	0.015
K1	0.3
K2	0.25
K3	0.2

	B	C	D	E	F	G
		Production Cost Breakdow				
83	Hull Construction Cost Fracti				=+C89	
84						
85	Welding Cost Fraction (WC):				=C90*F83	
86						
87	Welding Cost Fraction (WCBI				=C91*F85	
88						
89	K1	0.3				
90	K2	0.25				
91	K3	0.2				
92						

Costs Display Module

UNIT1: SMAW WELDING PROCESS(One Pass)

TABLE 1A

Production Costs (6mm x 6mm welds-Entire Structure - $ Million)

	Single Skin	Double Skin
Total Ship Cost (C):		
30 000 dwt	35	40.25
80 000 dwt	55	63.25
120 000 dwt	62	71.3
250 000 dwt	91	104.65
Hull Construction Cost (HC): (Including Pipe Fitting)		
30 000 dwt	10.5	12.075
80 000 dwt	16.5	18.975
120 000 dwt	18.6	21.39
250 000 dwt	27.3	31.395
Total Welding Costs (WC):		
30 000 dwt	2.625	3.01875
80 000 dwt	4.125	4.74375
120 000 dwt	4.65	5.3475
250 000 dwt	6.825	7.84875
Welding Costs Bottom Hull Structure (WCBHS):		
30 000 dwt	0.525	0.60375
80 000 dwt	0.825	0.94875
120 000 dwt	0.93	1.0695
250 000 dwt	1.365	1.56975

	B	C	D	E	F	G	H
		Costs Display Module					
	UNIT1 : SMAW WELDING PP						
	TABLE 1A						
		Production Costs (Basis = data					
				Single Skin		Double Skin	
	Total Ship Cost (C):						
110		30 000 dwt		=+E8		=+G8	
111		80 000 dwt		=+E9		=+G9	
112		120 000 dwt		=+E10		=+G10	
113		250 000 dwt		=+E11		=+G11	
	Hull Construction Cost (HC): (including Pipe Fitting)						
117		30 000 dwt		=+F83*E110		=+F83*G110	
118		80 000 dwt		=+F83*E111		=+F83*G111	
119		120 000 dwt		=+F83*E112		=+F83*G112	
120		250 000 dwt		=+F83*E113		=+F83*G113	
	Total Welding Costs (WC):						
123		30 000 dwt		=+F85*E110		=+F85*G110	
124		80 000 dwt		=+F85*E111		=+F85*G111	
125		120 000 dwt		=+F85*E112		=+F85*G112	
126		250 000 dwt		=+F85*E113		=+F85*G113	
	Welding Costs Bottom Hull Str						
130		30 000 dwt	=$D$123:$D$1	=+F87*E110		=+F87*G110	
131		80 000 dwt	=$D$123:$D$1	=+F87*E111		=+F87*G111	
132		120 000 dwt	=$D$123:$D$1	=+F87*E112		=+F87*G112	
133		250 000 dwt	=$D$123:$D$1	=+F87*E113		=+F87*G113	

APPENDIX D

LIMIT LOADS FOR NON SYMMETRIC WELDS

EVALUATION OF LIMIT LOAD (LOWER LIMIT) FOR NON-SYMMETRIC WELDS USING WORK EQUILIBRIUM (T-JOINTS)

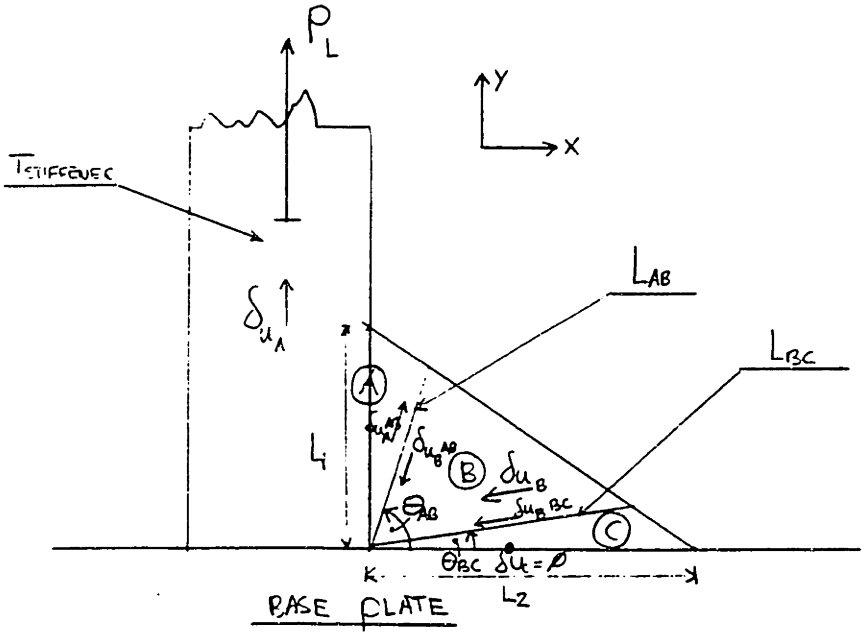

FIGURE 1.

=> WORK EQUILIBRIUM (BALANCE) EQUATION:

(1) $$P_L \, \delta u_A = K \, L_{AB} \left[| \delta U_{A(AB)} | + | \delta U_{B(AB)} | \right] + K' L_{BC} \, \delta_{U_{B(BC)}}$$

(δU_{AB})

where: P_L = LIMIT LOAD PER UNIT LENGTH OF JOINT

δU_A = VERTICAL DISPLACEMENT OF STIFFENER DUE TO P_L (STIFFENER + WELD MATERIAL (A))

δU_B = MOTION OF WELDMENT WEDGE (B) AS IT SLIDES IN TO FILL GAP RESULTING FROM δU_A acting up fine direction of L_{BC}

$\delta U_C = \emptyset$ = MOTION OF BASE PLATE & REMAINING WELD MATERIAL

$\delta u_{A(AB)}$ = Component of δu_A along Slip Line LAB (Between bodies A & B)

$\delta u_{B(AB)}$ = Component of δu_B along Slip Line L_{AB}

$\delta u_{B(BC)}$ = Component of δu_B along Line (slip) L_{BC}.

K = Shear Strength of Material = 0.75 T.S (Tensile Strength)

$\Rightarrow$ Hodograph (Velocity) $\Rightarrow \left(\delta u_i / \delta t\right)$; $i = A, B, C$

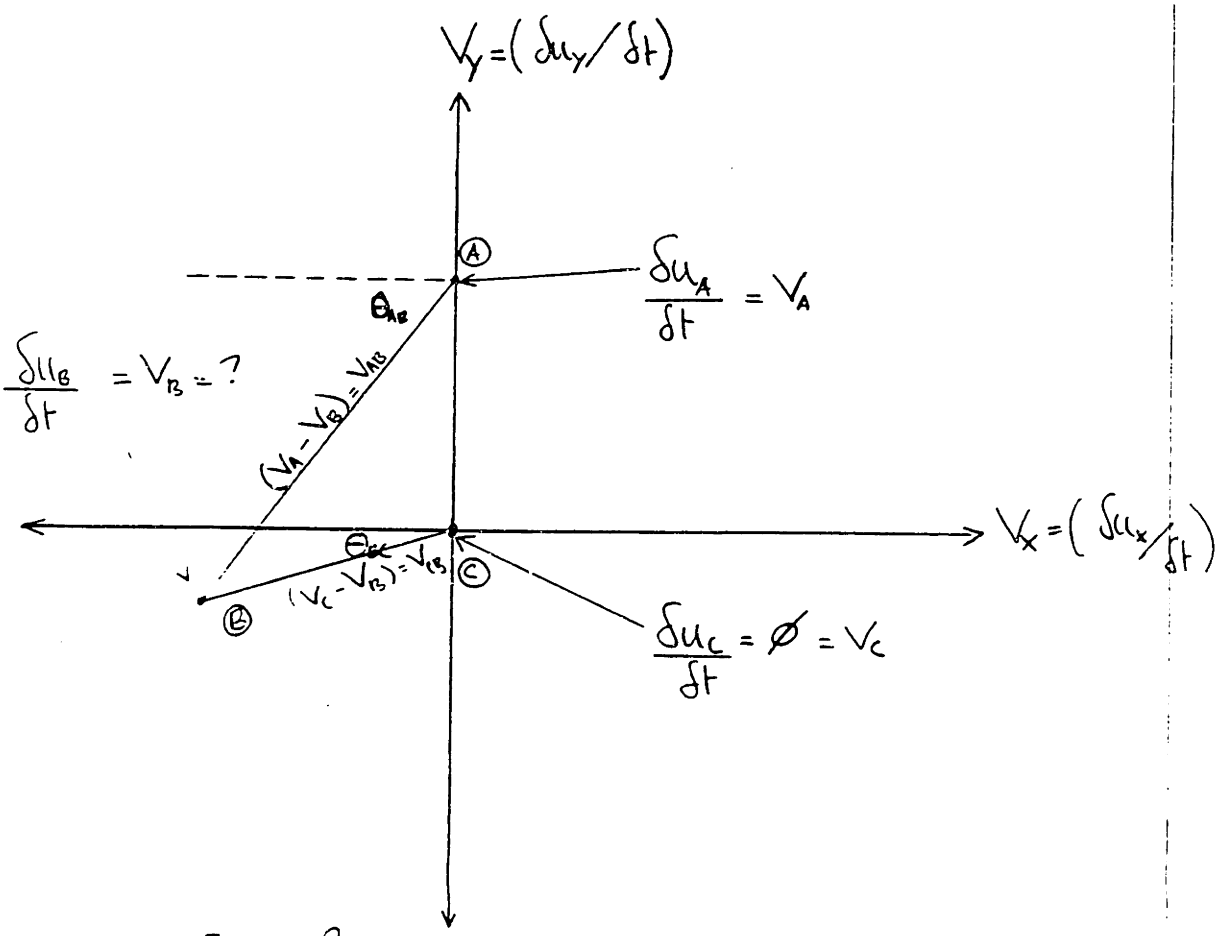

FIGURE 2:

Note: $V_{AB} = \frac{\delta u_{AB}}{\delta t}$

$V_{BC} = \frac{\delta u_{B(BC)}}{\delta t}$

} For the purposes of further analysis on the following page, the δt terms are disregarded.

INTERPRETATION OF HODOGRAPH :

1] Solving for $\delta u_{B(BC)}$:
From Graph we get the following Two relation ships.

a] $\delta u_{AB} \cos(\theta_{AB}) = \delta u_{B(BC)} \cos(\theta_{BC})$

b] $\delta u_{AB} \sin(\theta_{AB}) = \delta u_A + \delta u_{B(BC)} \sin(\theta_{BC})$

} 2 EQUATIONS IN 2 UNKNOWNS

shifting terms in b]: $\delta u_{B(BC)} = \dfrac{\delta u_{AB} \sin(\theta_{AB}) - \delta u_A}{\sin(\theta_{BC})}$ [b']

from [A]: $\delta u_{AB} = \delta u_{B(BC)} \dfrac{\cos(\theta_{BC})}{\cos(\theta_{AB})}$ m to [b']

we get: $\delta u_{B(BC)} = \dfrac{\delta u_{B(BC)} \dfrac{\cos(\theta_{BC})}{\cos(\theta_{AB})} \sin(\theta_{AB}) - \delta u_A}{\sin(\theta_{BC})}$

collecting terms with Respect to $\delta u_{B(BC)}$

$$\delta u_{B(BC)} = \frac{-\delta u_A}{\left[1 - \dfrac{\sin(\theta_{AB})}{\cos(\theta_{AB})} \cdot \dfrac{\cos(\theta_{BC})}{\sin(\theta_{BC})}\right] \cdot \sin(\theta_{BC})}$$

$$= \frac{-\delta u_A}{\left[\dfrac{\sin(\theta_{BC})\cos(\theta_{AB}) - \sin(\theta_{AB})\cos(\theta_{BC})}{\cos(\theta_{AB})\sin(\theta_{BC})}\right] \cdot \cancel{\sin(\theta_{BC})}}$$

@1 $$\boxed{\delta u_{B(BC)} = -\frac{\delta u_A \cos(\theta_{AB})}{\sin(\theta_{BC} - \theta_{AB})}} \quad (2)$$

2] Solving for δu_{AB}

Using the same identities obtained from the Hodograph and depicted in Equations [a] and [b] on page ③:

$$b] \quad \delta u_{AB}\ sin(\theta_{AB}) = \delta u_A + \delta u_{B(BC)}\ sin(\theta_{BC})$$

and substituting from [A]: $\delta u_{B(BC)} = \delta u_{AB} \dfrac{cos(\theta_{AB})}{cos(\theta_{BC})}$

we get;

$$\delta u_{AB}\ sin(\theta_{AB}) = \delta u_A + \delta u_{AB} \frac{cos(\theta_{AB})}{cos(\theta_{BC})}\ sin(\theta_{BC})$$

collecting Terms with respect to δu_{AB}:

$$\delta u_{AB} \left[sin(\theta_{AB}) - \frac{cos(\theta_{AB})}{cos(\theta_{BC})}\ sin(\theta_{BC}) \right] = \delta u_A$$

further simplifying:

$$\delta u_{AB} = \frac{\delta u_A}{\left[\dfrac{sin(\theta_{AB})cos(\theta_{BC}) - cos(\theta_{AB})sin(\theta_{BC})}{cos(\theta_{BC})} \right]}$$

or $$\boxed{\delta u_{AB} = \frac{\delta u_A\ cos(\theta_{BC})}{sin(\theta_{AB} - \theta_{BC})}} \quad (3)$$

$\Rightarrow$ We Must Also Express L_{AB} and L_{BC} in Terms of L_1 & L_2 which are The Given Weld Geometry Parameters

i]

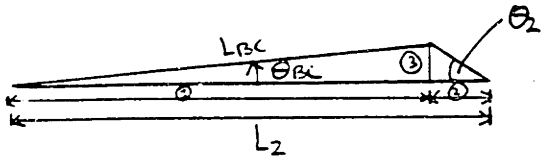

FIGURE 3.

$① = L_{BC}\cos(\theta_{BC})$

$② = L_2 - L_{BC}\cos(\theta_{BC})$

$③ = L_{BC}\sin(\theta_{BC})$

$\tan\theta_2 = \frac{L_1}{L_2}$ (Similar Triangles)

$\therefore L_1 = L_{BC}\left[\frac{L_1}{L_2}\cos(\theta_{BC}) + \sin(\theta_{BC})\right]$

$$\therefore L_{BC} = \frac{L_1}{\left[\left(\frac{L_1}{L_2}\right)\cos(\theta_{BC}) + \sin(\theta_{BC})\right]} \quad (4)$$

ii]

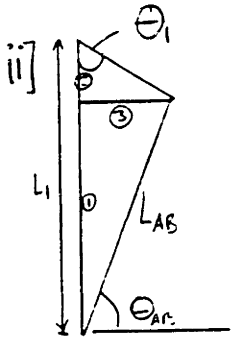

FIGURE 4.

$① = L_{AB}\sin(\theta_{AB})$

$② = L_1 - L_{AB}\sin(\theta_{AB})$

$③ = L_{AB}\cos(\theta_{AB})$

$\tan\theta_1 = \frac{L_2}{L_1}$

$L_2 = L_{AB}\left[\left(\frac{L_2}{L_1}\right)\sin(\theta_{AB}) + \cos(\theta_{AB})\right]$

$$\therefore L_{AB} = \frac{L_2}{\left[\left(\frac{L_2}{L_1}\right)\sin(\theta_{AB}) + \cos(\theta_{AB})\right]} \quad (5)$$

Incorporating Equations (2) and (3) into (1), we have:

$$P_L \cancel{\delta\alpha_A} = K L_{AB} \cdot \frac{\cancel{\delta\alpha_A} \cos(\theta_{BC})}{\sin(\theta_{AB} - \theta_{BC})} - K L_{BC} \frac{\cancel{\delta\alpha_A} \cos(\theta_{AB})}{\sin(\theta_{BC} - \theta_{AB})}$$ (2)

① $\sin(\theta_{BC} - \theta_{AB}) = -\sin(\theta_{AB} - \theta_{BC})$

$$\boxed{P_L = \frac{K}{\sin(\theta_{AB} - \theta_{BC})} \left(L_{AB} \cos(\theta_{BC}) + L_{BC} \cos(\theta_{AB}) \right)} \quad (6)$$

Incorporating Equations (4) and (5) into (6) we have:

$$\boxed{P_L = \frac{K}{\sin(\theta_{AB} - \theta_{BC})} \left(\frac{L_2 \cos(\theta_{BC})}{\left[\left(\frac{L_2}{L_1} \right) \sin(\theta_{AB}) + \cos(\theta_{AB}) \right]} + \frac{L_1 \cos(\theta_{AB})}{\left[\left(\frac{L_1}{L_2} \right) \cos(\theta_{BC}) + \sin(\theta_{BC}) \right]} \right]} \quad (7)$$

TI-74 PROGRAM (BASIC)

```
90  INPUT  X
100 INPUT  Y
110 L1=0.236
120 L2=0.354
200 LBC = L1 / ( (L1/L2) * COS(Y) + SIN(Y))
300 LAB = L2 / ( (L2/L1) * SIN(X) + COS(X))
400 K = 70 000
500 C1 = 1 / SIN(X-Y)
510 C2 = COS(X)
520 C3 = COS(Y)
550 PL = K*C1*(LAB*C3 + LBC*C2)
600 PRINT "LAB IS"; LAB: PAUSE
610 PRINT "LBC IS"; LBC: PAUSE
620 PRINT "PL IS"; PL: PAUSE
```

NOTE: $X = \theta_{AB}$
$Y = \theta_{BC}$

ITERATION ACCOUNT

θ_{AB} (x)°	θ_{BC} (y)°	L_{AB} (m")	L_{BC} (m")	P_{LIMIT} (lb/inch weld)
90	0	0·236	0·354	16520
80	0	0·214	0·354	19611
60	0	0·197	0·354	30211
40	0	0·205	0·354	51812
20	0	0·243	0·354	117955
90	10	0·236	0·284	16520
90	20	0·236	0·244	16520
90	30	0·236	0·219	16520
90	40	0·236	0·205	16520
90	60	0·236	0·197	16520
80	10	0·214	0·284	19408
80	20	0·214	0·244	19707
80	60	0·214	0·197	28936
70	10	0·202	0·284	23947

$\Rightarrow$ Lowest Limit Load Iterated = 16520 lb/m for one weld

$\therefore$ for both welds of the T Joint: $P_{LIMIT} = 2 \times 16520 \text{ lb/m}$

$$P_{LIMIT} = 33040 \text{ lb/m}$$

EXPERIMENTALLY RECORDED LIMIT LOAD: $P_{exp} = 32\,000 \text{ lb/m}$

$$\% \text{ variation of data} = \left| P_{exp} / P_{LIMIT} - 1 \right| \times 100$$

$$= 3.15\ \%$$

APPENDIX E

THEORY OF LIMIT LOAD AND TEARING WORK

Finding the Critical Displacement for Through-Cracking, u_c, and the Work per Unit Crack Growth, R, from Bending Moment and Bend Angle Measurements in the Fillet Weld Bend Test

Appendix to

Fully Plastic Fracture Mechanics for Welded T-Joints

by Frank. A. McClintock

Joint MIT-Industry Project on Tanker Safety

4th Steering Commmittee Meeting

January 26-27, 1994

Objectives. Consider a bend test of a fillet weld in the lap-joint configuration of Fig. 1. In order that a fully plastic weld will fracture before the single lapped plate yields, the tearing strength per unit length of the combined welds must be less than the yield strength per unit length of the single plate of base metal. Take the shear strength k of the weld parallel to the x-z plane to depend on its tensile strength from the welding literature, and in turn take the tensile strength to be 0.3 times the Knoop hardness (in consistent units, as derived from hardness conversion tables and supported by approximate limit analysis) Then

$$k = 0.75\ TS = 0.225\ HK\ . \qquad (A1)$$

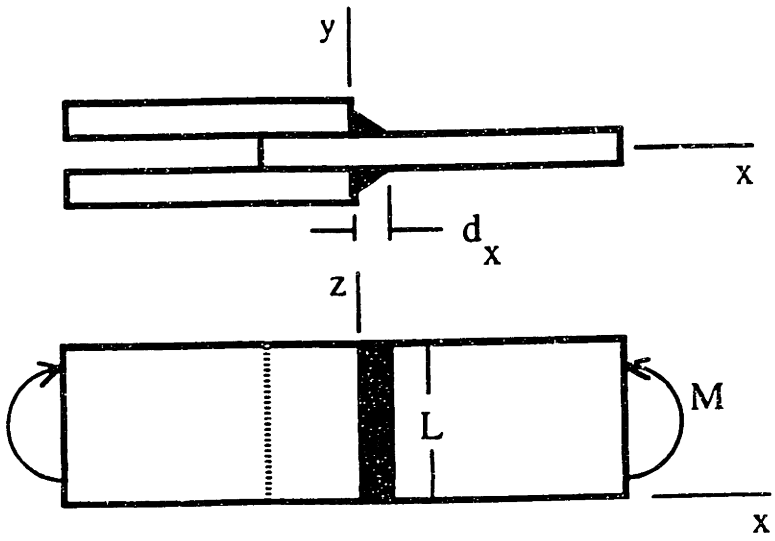

Fig. 1 A lap joint in bending to simulate a T-weld in tension

The first two parameters of interest are the maximum transverse (web) tearing strength per unit length P and the corresponding tearing work per unit length R. As the displacement across the weld, u, is increased, the tearing strength per unit length P increases elastically and, after a small displacement becomes constant at the limit load P_L. Cracking in the weld decreases P gradually to 0. The integral of P with respect to u gives the tearing work per unit length R.

For a preliminary analysis, approximate the P vs. u curve for a joint as a square wave. Further, take the force per unit original area of the fillet weld to be constant at a shear strength k until a critical displacement u_c has been reached. Assume that the strength then drops abruptly to zero. This corresponds to a crack growing instantaneously across the weld when the displacement u_c has been reached. Here initiation and growth will apply to such a through-weld crack. The tearing work (resistance) per unit length of a pair of evenly matched fillet welds with leg length in the x-direction d_x would then be

$$R = 2ku_cd_x \quad . \tag{A2}$$

With the shear strength from (A1), the tearing work R can be estimated as that giving in some sense the best fit of u_c to experimental data for bending moment vs. bend angle, for the specimen of Fig. 1. If it appears worthwhile, an improved analysis could be carried out using a trapezoidal shape for the force-displacement relation for the weld.

Limit moment and bend angle of the beam for initiation of a transverse crack. Assume no crack growth on the compressive side of the beam. This assumption is made for simplicity, and because the tensile stress on one side of a shear crack makes it deviate by 10-25° from the mean slip direction for strain hardening with exponents of $n = 0.12$ - 0.23 (see Table 5 of Kardomateas and McClintock 1987 and, schematically, Fig. 35 of McDonald 1993). On the compressive side, such a deviation will put any crack in compression and slow it down.

With crack growth through the weld on the tensile side only, by an amount a from that end of the weld, the fully plastic limit moment of a pair of fillet welds of leg distance d_x and weld length L, is given by equilibrium:

$$M = 2kd_x(L-a)^2/4 \quad . \tag{A3}$$

The critical bend angle in the beam, at initial through-cracking ($a = 0$), is

$$\theta_c = u_c/(L/2) \quad . \tag{A4}$$

The relation of crack length a to bend angle θ. For a crack of length a, the neutral axis measured from the tensile side of the bend specimen is at $y = (L + a)/2$, and the displacement increment at y is

$$du = [(L+a)/2 - y]\, d\theta \quad . \tag{A5}$$

The crack growth will be the displacement increment at the tip $y = a$ from (3), divided by the negative of the current slope at the crack tip found from the plot of displacement vs. y, $(du/dy)_{tip}$:

$$da = -(L - a)d\theta / [2(du/dy)_{tip}] \quad . \tag{A6}$$

The increments in slope due to an increment in bend angle are found by differentating (A5) with respect to y. They turn out to be the same all along the weld and just the negative of the increment in bend angle:

$$d(du/dy) = -d\theta \quad . \tag{A7}$$

Integrating (A7) from the start of bending shows the slope of the displacement-y curve (for $\theta << 1$) is just θ. Introducing this into (A6) gives the differential equation for crack growth:

$$da/(L - a) = (1/2)\, d\theta/\theta \quad . \tag{A8}$$

Logarithmic integration of (L - a) gives

$$[L/(L - a)]^2 = \theta/\theta_c \quad \text{or} \quad a/L = 1 - \sqrt{(\theta_c/\theta)} \quad \text{for } \theta \geq \theta_c \quad . \tag{A9}$$

Equation A9 shows the crack length constant at $a/L = 0$ until $\theta = \theta_c$, after which it increases, with an initial slope of $d(a/L) / d(\theta/\theta_c) = 1/2$, asymptotically to 1 as $\theta \rightarrow \infty$.

The relation of bending moment M to bend angle θ. Use (A9) to eliminate a/L in the moment relation (A3). When this is normalized in terms of the uncracked limit moment, also from (A3),

$$M_L = kd_x L^2/2 \quad , \tag{A10}$$

the result is

$$M/M_L = \theta_c/\theta \quad \text{for } \theta \geq \theta_c \quad . \tag{A11}$$

The critical displacement for through-cracking, u_c, and the tearing work per unit length, R. From the introduction, for a double fillet weld the tearing work per unit length is found from the critical displacement to fracture u_c, which is in turn found from the beam bend angle at initiation through (A4):

$$R = 2kd_x u_c = kd_x L\theta_c \, . \tag{A12}$$

The bend angle to initial through-cracking, θ_c, is likely to be affected by elasticity and end effects (including lack of constraint, strain hardening, and deformation of the weld). Therefore the value of θ_c $(= u_c/(L/2))$ from (A4) found from the break in the M - θ

relation (A11) at initial through-cracking may be either high or low compared to that for later quasi-stready cracking. Consequently the bend angles in (A11) should be replaced by effective angles $\theta_{eff} = \theta - \theta_0$, where θ_0 is either positive or negative:

$$M/M_L = \theta_{c\,eff} / (\theta - \theta_0) \quad \text{for } \theta \geq \theta_{c\,eff} + \theta_0 \ . \tag{A13}$$

Rearrange (A13) so that $\theta_{c\,eff}$ can be found by a linear regression analysis:

$$\theta = \theta_0 + \theta_{c\,eff} / (M/M_L) \ . \tag{A14}$$

As shown in Fig. 2, $\theta_{c\,eff}$ is the slope of the plot of bend angle vs. the reciprocal of the normalized limit load.

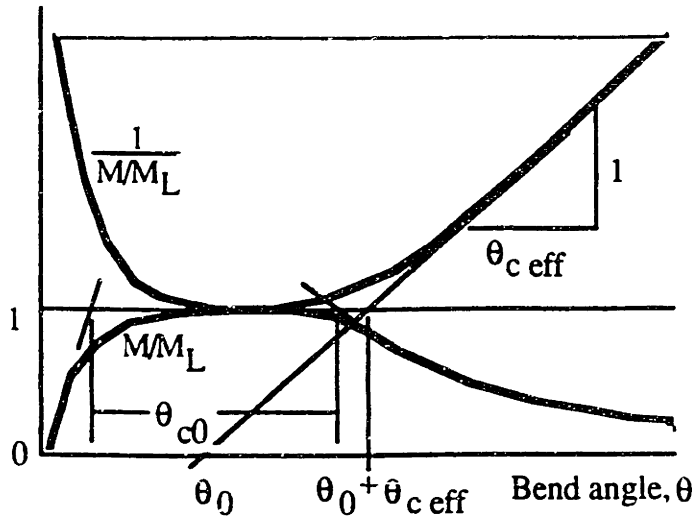

Fig. 2 Reciprocal moment vs. bend angle to determine effective bend angle at initiation

$\theta_{c\,eff}$ may be greater or less than the value for initial through-cracking, θ_{c0} from Fig. 2. From these two, the critical displacements for initial through-cracking and for steady-state growth of through-cracks can be found from (A4):

$$u_{c0} = \theta_{c0} L/2 \ , \ u_{css} = \theta_{c\,eff} L/2 \ . \tag{A15}$$

If the growing crack causes damage ahead of the current tip, or if tunnelling develops, the crack growth may accelerate. This would be shown in Fig. 2 by decreasing $\theta_{c\,eff}$, with the upper curve on the right becoming steeper, so that $u_c = u_c(a)$. Likewise, it would be interesting to see how u_c depended on the size of the weld d_x and on the thickness of the gap between web and base-plate left by incomplete penetration.

The work per unit crack growth can now be found from (A12), with u_{css}. At the same time it may be desirable to eliminate the shear strength k in terms of the limit

moment with (A3). For a double fillet weld, the tearing work per unit crack growth is then

$$R = M_L u_{css} / (L/2)^2 \ . \qquad (A16)$$

References

Kardomateas, G. A. and McClintock, F. A. 1987 "Tests and Interpretation of Mixed Mode I and II Fully Plastic Fracture from Simulated Weld Defects", Int. J. Fracture v35, 103-124

McDonald, H. A. 1993 "Required Strength and Tear Resistance for Fillet Welds in Ships Exposed to Grounding or Collision Loads", M. S. Thesis, M. I. T. Department of Ocean Engineering, May, 1993. See also Report 14, Joint MIT-Industry Program on Tanker Safety.

This appendix evolved from

McClintock, F. A. and McDonald, H. A. 1993 "Finding the Critical Displacement for Through-Cracking, u_c ,and the Work per Unit Crack Growth, R ,from Bending Moment and Bend Angle Measurements in the Fillet Weld Bend Test" Appendix at 3rd Steering Committee Meeting, Joint MIT-Industry Program on Tanker Safety, J une 9-10 1993